EPA-650/2-74-016

December 1973

Environmental Protection Technology Series

SAMPLING INTERFACE FOR QUANTITATIVE TRANSPORT OF AEROSOLS

Office of Research and Development
U.S. Environmental Protection Agency
Washington, DC 20460

EPA-650/2-74-016

SAMPLING INTERFACE FOR QUANTITATIVE TRANSPORT OF AEROSOLS

by

Madhav B. Ranade

IIT Research Institute
10 West 35th Street
Chicago, Illinois 60616

Contract No. 68-02-0579
Project No. 26AAM
Program Element No. 1AA010

EPA Project Officer: Dr. Kenneth T. Knapp

Chemistry and Physics Laboratory
National Environmental Research Center
Research Triangle Park, North Carolina 27711

Prepared for

OFFICE OF RESEARCH AND DEVELOPMENT
U.S. ENVIRONMENTAL PROTECTION AGENCY
WASHINGTON, D.C. 20460

December 1973

This report has been reviewed by the Environmental Protection Agency and approved for publication. Approval does not signify that the contents necessarily reflect the views and policies of the Agency, nor does mention of trade names or commercial products constitute endorsement or recommendation for use.

SAMPLING INTERFACE FOR QUANTITATIVE TRANSPORT OF AEROSOLS

ABSTRACT

A sampling probe was designed, fabricated, and evaluated for quantitative transport of aerosols through a conduit from a source to a sensor. The probe consists of a porous metal tube encased in a manifold through which transpiration air was passed inward to provide a moving clean air sheath that minimized particle deposition on the walls. In Phase I, the quantitative mass transport of aerosols was investigated, and in Phase II, the preservation of size distribution of the transported aerosol was studied. The 178 cm (70 in.) long by 1.27 cm (½ in.) ID probe required only 14.2 lpm (0.5 cfm) of transpiration air to virtually eliminate deposition of particles in the 0.05 to 15 μm size range. Particles as large as 70 μm required as much as 283 lpm (10 cfm) to prevent deposition losses at low sample flow rates. A statistical analysis of the data conclusively demonstrates the effectiveness of the porous probe sampling concept. Tests at selected conditions show that the porous probe is effective in the preservation of size distribution.

Optimization of the sample and transpiration flow ratio is necessary for a given size range to obtain the most effective use of the porous probe concept.

TABLE OF CONTENTS

LIST OF FIGURES

LIST OF FIGURES (continued)

LIST OF FIGURES (continued)

LIST OF TABLES

ACKNOWLEDGMENTS

This report was prepared by the Fine Particles Research Section of the Chemistry Division at IIT Research Institute, Chicago, Illinois, under EPA Contract No. 68-02-0579.

The work was divided into two phases. Phase I involves fabrication and demonstration of a sampling interface for quantitative mass transport of aerosols from a source to a sensor. Mr. Don Werle served as the project director for Phase I. Dr. Fred Bock designed the factorial test plan and made the statistical analysis of the data. Flame emission analyses were performed by Ms. G. Marks. K. Walanski and L. Martin assisted in some of the tests conducted under Phase I.

Phase II of this contract involves preservation of size distribution in the sampling interface. Dr. Madhav Ranade served as the project director for Phase II. Dr. Earl Knutson direct the use of mobility analyzer for the Phase II tests. George Yamate and Jean Graf assisted in the tests. Dr. Ken Knapp acted as the EPA project officer.

SAMPLING INTERFACE FOR QUANTITATIVE TRANSPORT OF AEROSOLS

1. INTRODUCTION

Conventional stack sampling probes used to transport particulate material from a source through a conduit to a collector or sensor can easily result in biased measurements due to particulate deposition on and/or interaction with the probe walls. Such interaction and deposition can result in a significant loss of particle mass and alteration of the particulate size distribution, especially as measured by continuous monitors. The goal of this research program is to develop and demonstrate through controlled laboratory tests a sampling interface system which will prevent or minimize aerosol deposition. The system selected is based on the use of a porous walled probe through which clean filtered air passes radially inward to provide a boundary layer of particle free air.

The program is divided into two phases. Phase I is concerned with the mass transport of source aerosols. Phase II is concerned with the preservation of the source aerosol size distribution during transport to a sensor. The sampling interface requirements call for the following:

1. Accommodate aerosol concentrations from at least 10^2 particles/cm^3 to at least 10^8 particles/cm^3.
2. Accommodate aerosols from 0.05 μm to 50 μm as a minimum size range.
3. Sample rate of from 7.1 alpm (0.25 acfm) to 28.3 alpm (1.0 acfm).
4. Permit dilution of the aerosol with a clean air stream where the dilution ratio is at least 10:1.

The following tasks are involved in Phase I:

Task (A) Prepare detailed design and engineering specifications for a sampling interface to meet the requirements for quantitative transport.

Task (B) Fabricate the system according to the design and specifications agreed upon with the Project Officer.

Task (C) Design and conduct laboratory tests to demonstrate the effectiveness of the sampling interface in achieving the above stated goals for Phase I.

Task (D) Prepare detailed report on Phase I including operating and maintenance instructions. Review with Project Officer before proceeding to Phase II.

Phase II is concerned with the preservation of source aerosol size distribution during transport to a sensor. The technical effort under Phase II consists of the following tasks.

Task (E) Develop design and engineering specifications for the sampling interface to meet the requirements for preservation of particle size distribution as well as quantitative transport.

Task (F) Fabricate the system according to the designs and specifications agreed upon with the Project Officer.

Task (G) Design and conduct laboratory tests to demonstrate the effectiveness of the sampling interface in achieving the above stated goals for Phase II.

Task (H) Prepare a detailed Phase II interim report including operating instructions and maintenance manuals.

The sampling interface designed and tested under Phase I was considered to be adequate for Phase II. A test plan with various particles representing a wide size range was suggested to EPA and was executed.

This report describes the technical effort under both Phase I and Phase II of the contract.

PHASE I

SAMPLING INTERFACE FOR QUANTITATIVE MASS TRANSPORT OF AEROSOLS

2. SAMPLING PROBE DESIGN AND OPERATION

The sampling interface conduit utilized in the Phase I experiments consists of 178 cm (70 in.) long by 2.54 cm (1 in.) ID straight stainless steel porous tube obtained from the Mott Metallurgical Corporation of Farmington, Connecticut. While a tube with a 90° bend at the inlet end was originally ordered, the manufacturer encountered fabrication problems which delayed the order and it became expedient to delete the bending operation to obtain a reasonable delivery. The design philosophy of the prototype interface hardware was necessarily oriented toward conduct of the laboratory tests to demonstrate the effectiveness of the hardware. Therefore, quick disassembly and assembly of the prototype was given priority to facilitate the analytical requirements of the experimental program. The hardware as it is now fabricated is not intended for direct use in stack sampling since it has temperature sensitive components (rubber O-ring seals, lead solder connections, and epoxy seals) not compatible with hot stack gases. The lack of a 90° inlet bend is also not compatible with most stack sampling operations, but the straight configuration was ideal for rapid disassembly of the interface and interpretation of the test results. Thus, the hardware must be considered as the first prototype model to demonstrate feasibility and effectiveness rather than a prototype ready for limited production for field use.

2.1 Prototype Design

2.1.1 The Porous Tube

Originally a porous ceramic tube was considered for the sampling interface. However examination of several ceramic specimens revealed two serious disadvantages in the proposed application. First, a long small ID ceramic tube would be very susceptible to breakage. Second, the firing process used to sinter green ceramic compacts often leaves a rough surface

where ceramic dust droppings fuse to the surface. A rough surface would introduce objectionable boundary layer flow disparities which are antagonistic to the goal of minimizing wall losses.

A porous type 316 stainless steel tube of 2 μm nominal porosity and 1.27 cm (½ in.) ID by 1.9 cm (3/4 in.) long was ordered and obtained from the Mott Metallurigical Corporation. Inspection of the tube interior on delivery revealed some surface roughness as well as a shallow bend. The internal surface roughness was readily corrected by lightly polishing with a 240 grit aluminum oxide abrasive cloth, and the bend was easily straightened. The actual OD is close to 2 cm (13/16 in.) and the length is actually 177.6 cm (69-15/16 in.) rather than the nominal 1.9 cm (3/4 in.) and 178 cm (70 in.) dimensions, respectively. The ID at the ends is within 0.0013 cm (0.0005 in.) of 1.27 cm (½ in.). The opening at the forward end is centered within ± 0.008 cm (0.003 in.) while the opening at the downstream end is noticeably eccentric. The wall thickness at the downstream end varied from a minimum of 0.325 cm (0.128 in.) to a maximum of 0.406 cm (0.160 in.).

2.1.2 The Sampling Probe Assembly

The details of the transpiration air manifold for admission of the boundary layer air to the porous tube are given in Figure 1. A two-stage manifold is used to minimize the incoming air velocity and objectionable jetting which could prevent a balanced distribution of the air. The penetration of the inlet air jet through the porous wall opposite the jet had been a problem in diffusion experiments conducted earlier by Dr. Wasan's graduate students. Thus, the inlet air is first introduced into an outer 5.08 cm (2 in.) diameter copper pipe before passage through the second inner manifold. The inner manifold has a series of twenty 1.27 cm (½ in.) diameter holes in a 23 cm (9 in.) long section near the center of the probe. Not shown in the drawing are two pressure

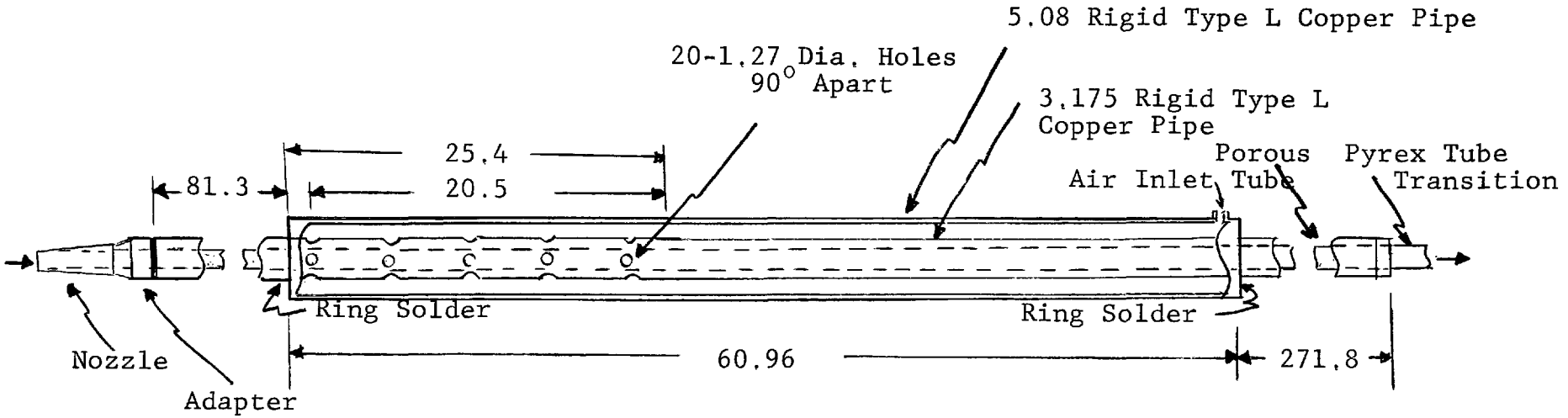

All Dimensions in Centimeters

Figure 1. Sampling Probe Transpiration Air Manifold Details

taps for measuring the air pressure in the center of the manifold and at the extreme downstream end of the manifold. At all flow conditions used identical pressures were observed at these two locations.

The details of the sampling nozzle construction and assembly are shown in Figure 2. The 45° sampling nozzle shown was fabricated but was not used in the Phase I tests due to the non-ideal shape for isokinetic sampling. Instead a 1.27 cm (½ in.) ID Western Precipitation standard nozzle was modified for attachment to the porous sampling probe and was used in all of the Phase I tests.

The transition from the downstream end of the porous sampling probe to the collection filter is detailed in Figure 3. A 1.27 cm (½ in.) ID glass tube in the transition allows visual observation of the aerosol passage and in many cases revealed the existence of the particle-free boundary layer immediately after the porous tube. Turbulent breakup of the aerosol stream is minimized or prevented by bringing the glass tube to within 0.63 cm (¼ in.) of the filter surface with the result that the filter became a witness plate for the existence or absence of a particle-free air sheath.

2.1.3 The Test Layout

A flow schematic of the test layout is shown in Figure 4. Three aerosol generators, described in Section 3.1, produced any of three test aerosols in the desired size and concentration. Instead of running the tests in a wind tunnel as originally proposed, a much more suitable system was developed, which in effect reduced the size of the wind tunnel to the ID of the sampling probe so that a 100% aliquot was taken of the aerosol flow. Thus, the aerosol mass sampled by the porous probe was determined directly by adding the amount collected on the downstream filter to the amount deposited on the porous tube -- an exact and direct measurement of the aerosol mass sampled as well as the amount deposited upstream of the filter.

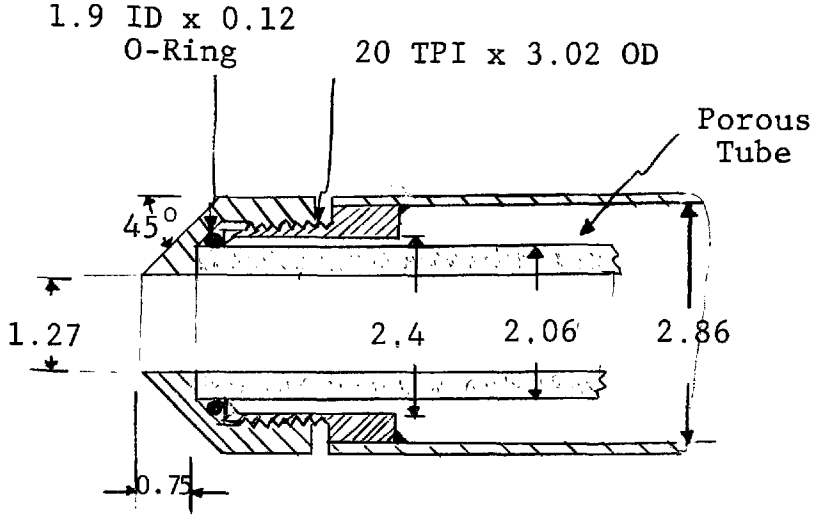

45° Sampling Nozzle Attachment

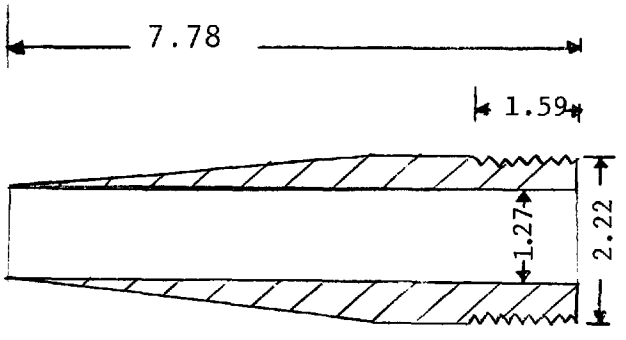

Interchangeable Standard Nozzle
(Western Precipitation, Modified)

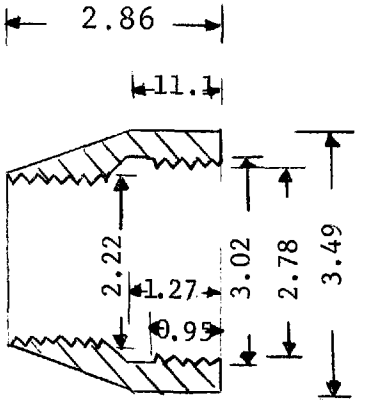

Mating Collar Adapter

All Dimensions in Centimeters.

Figure 2. Sampling Nozzle Details

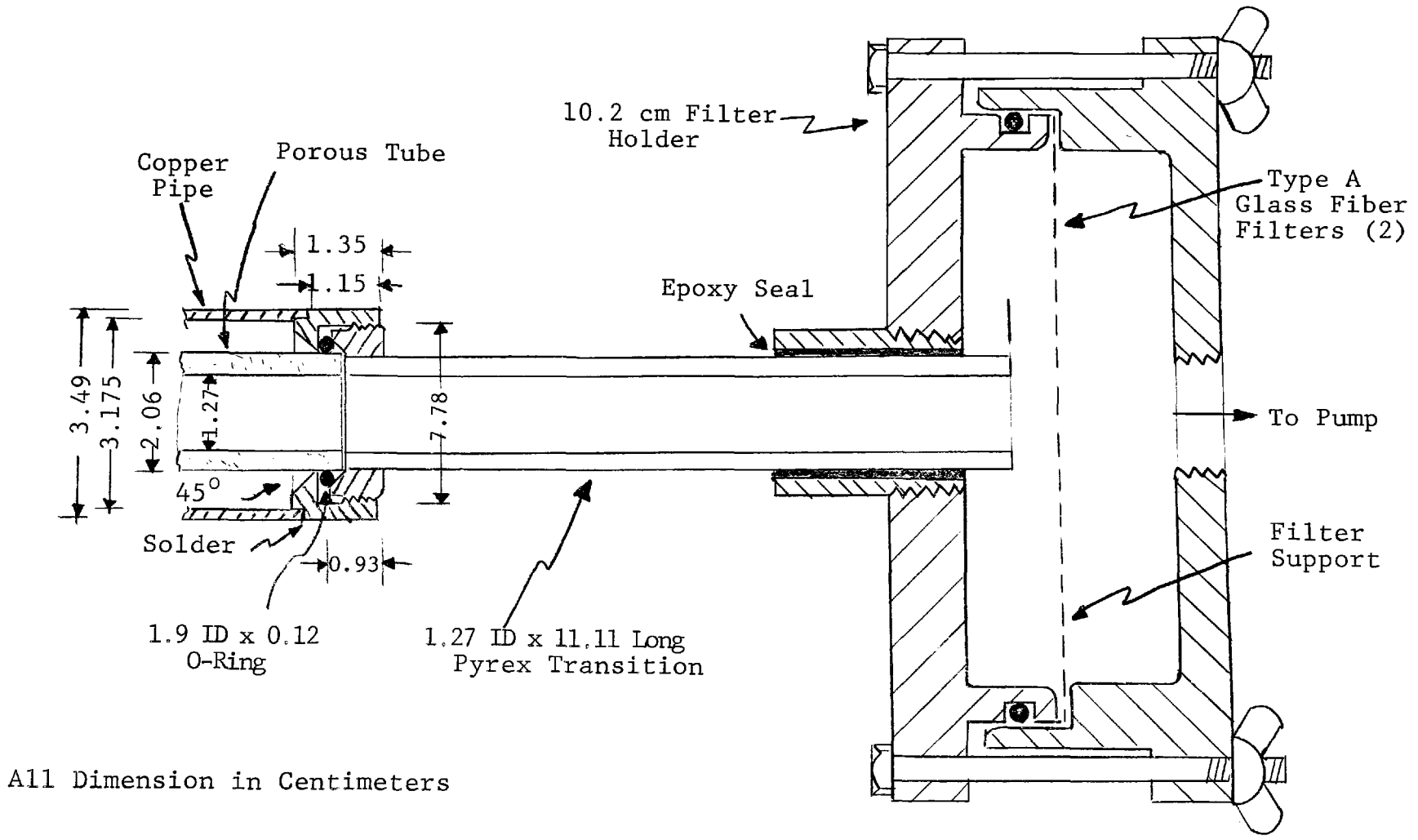

Figure 3. Downstream Probe Seal and Filter Housing Transition Details

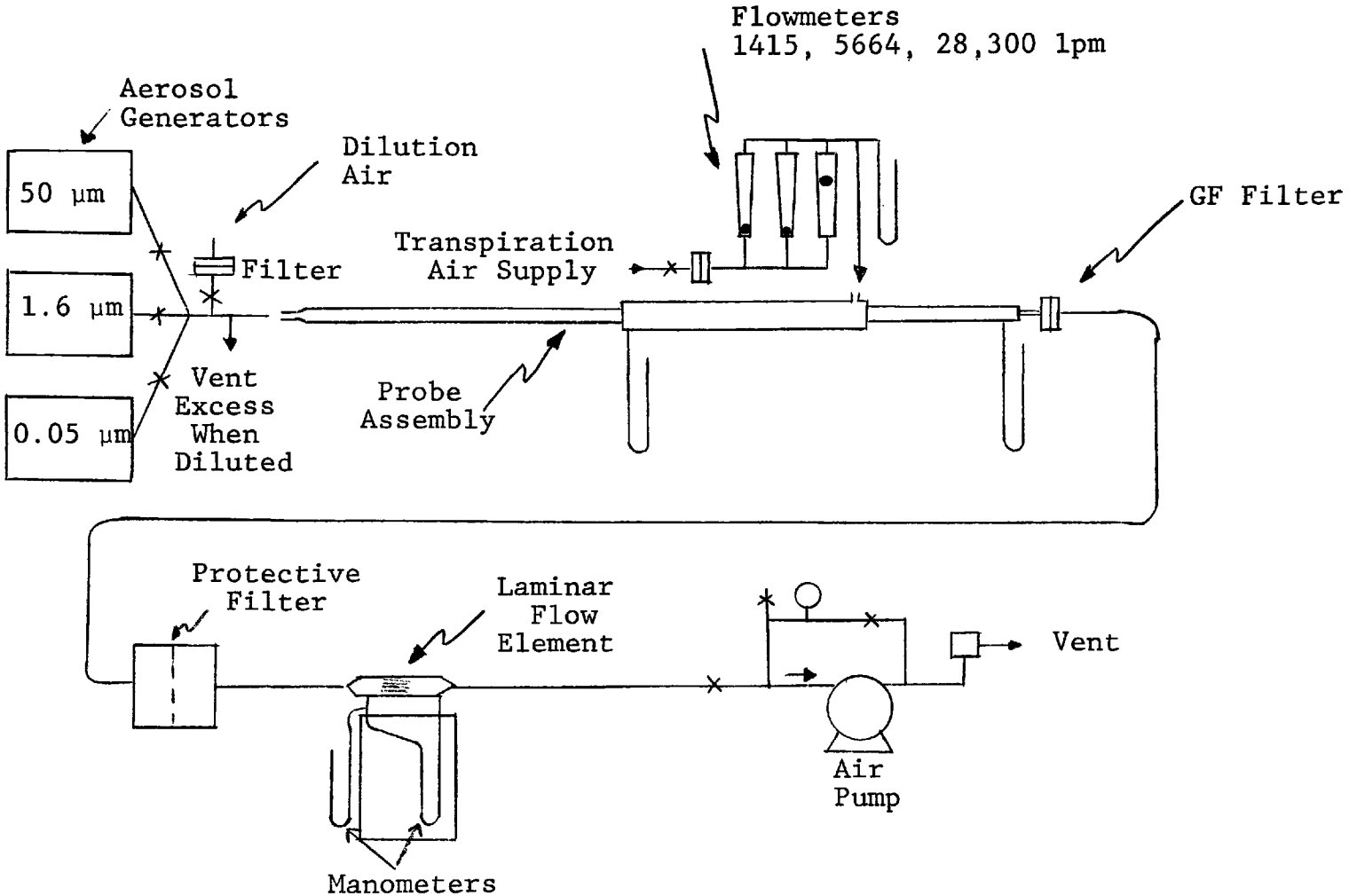

Figure 4. Flow Schematic of Porous Probe Sampler as Evaluated for Mass Transport of 0.05-50 μm Aerosols

The filtered transpiration air supply is metered by three panel-mounted Dwyer flowmeters with 23, 90, and 470 lpm (0.8, 3.2, and 16.6 cfm) capacities. A flexible hose connects the filter holder to a Cambridge absolute filter (#F-599), which protects the Meriam 50MW20-1-½ laminar flow element. The pressure drop across the laminar flow element is proportional to velocity. The pressure drop is monitored by a Dwyer Model No. 421-10 single column manometer. A 566 lpm (20 cfm) Leiman #195-2 Type G vacuum pump with 1½ HP, 230 volt, 3 phase, direct drive pulls the required air plus sample volume through the interface. The Leiman pump is provided with a by-pass and appropirate valves for easy manual control of the interface flow rate.

A composite photograph of the laboratory test facility used is shown in Figure 5. The entire facility is mounted in a 5 meter long laboratory fume hood. The aerosol generators and the interface sampling nozzle are located in the far left hood compartment. The main body of the sampling interface is in the center left hood and extends partially into the third compartment. Also located in the third compartment are the glass fiber filter collector, the protective absolute filter, and the laminar flow element. The vacuum pump is on the far right.

2.2 Sampling Probe Operation

The operation of the sampling probe is relatively simple. The basic difference compared with a conventional stack sampling probe is that there are two flows which must be monitored and that the sample flow rate (SFR) is not measured directly but is the net difference between the exhaust flow rate (EFR) and the transpiration air flow rate (TAFR),

$$SFR = EFR - TAFR$$

The exhaust flow rate is monitored by means of the Meriam laminar flow element. The transpiration air rotameters were

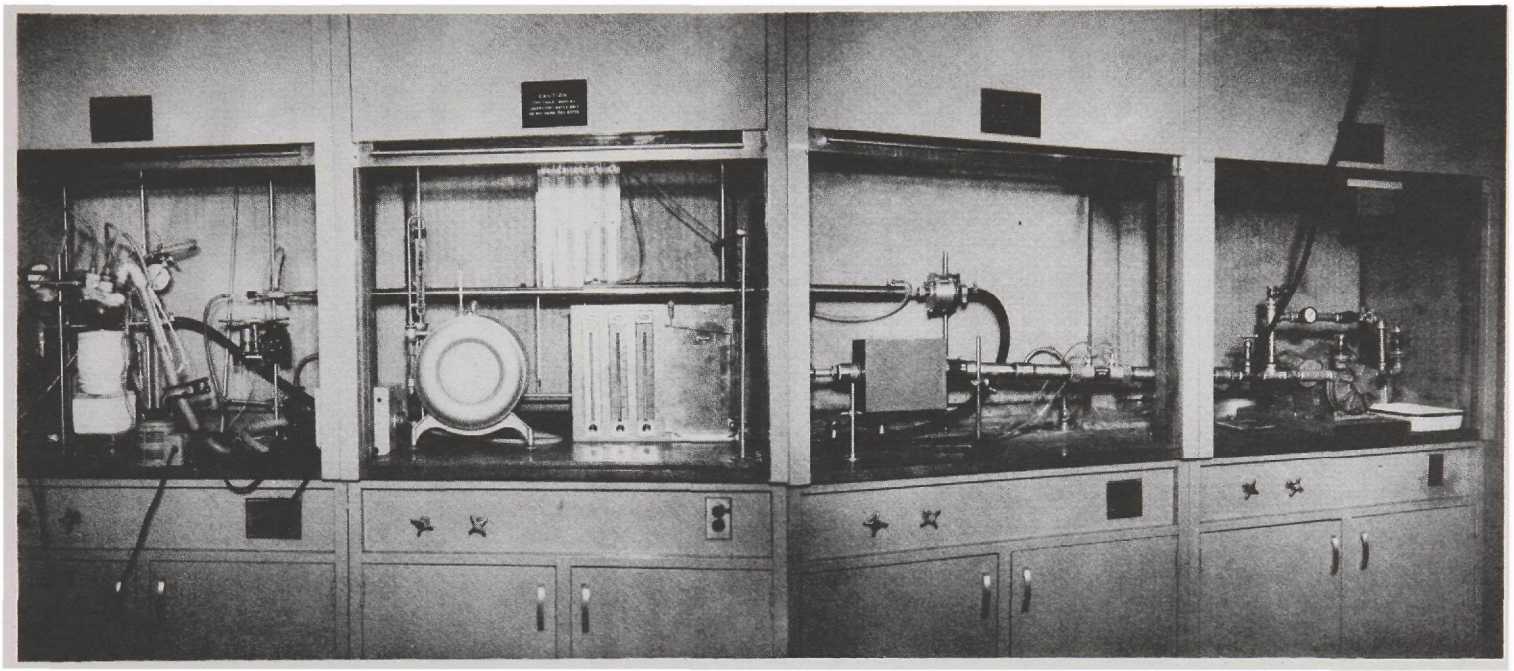

Figure 5. The Sampling Interface Test Facility

calibrated with the laminar flow element. The actual flow rate was found to agree with the manufacturers indicated settings. Since the rotameters are factory calibrated for standard conditions, a correction must be applied to the observed flowmeter reading (FR in lpm) to obtain either the standard or absolute volume at the flow conditions, e.g.,

$$slpm = FR\sqrt{\frac{P_1}{P_s} \times \frac{T_s}{T_1}}$$

where P_s and T_s are the standard pressure and temperature, and P_1 and T_1 are the actual pressure and temperature, respectively. It was found convenient to first set the exhaust flow to the proper level as indicated by the laminar flow ΔP. Next, the transpiration air (TA) flow was adjusted to the desired value for the volume of TA desired. Then the laminar flow level, if disturbed by the TA, was readjusted to the target setting. The sample flow rate (SFR) was then confirmed by wet-test meter attached directly to the sample nozzle. Fine tuning of the SFR, if needed, was obtained with a slight adjustment of the total exhaust flow. Once the flow-rate was properly adjusted, the wet-test meter was disconnected and aerosol was then introduced into the sampling nozzle entrance.

For all of the test flow conditions used in the Phase I tests, the axial pressure drop inside the porous tube was determined as a function of distance from the entrance shown in Figure 6.

Since the flow rate of transpiration air will vary in proportion to the radial ΔP across the porous tube, it is important to know the radial driving force at all points along the length of the porous tube. Obviously, we could not tolerate a situation where the transpiration air supply pressure would be less than the pressure on the sample air side of the porous tube. This situation could occur near the

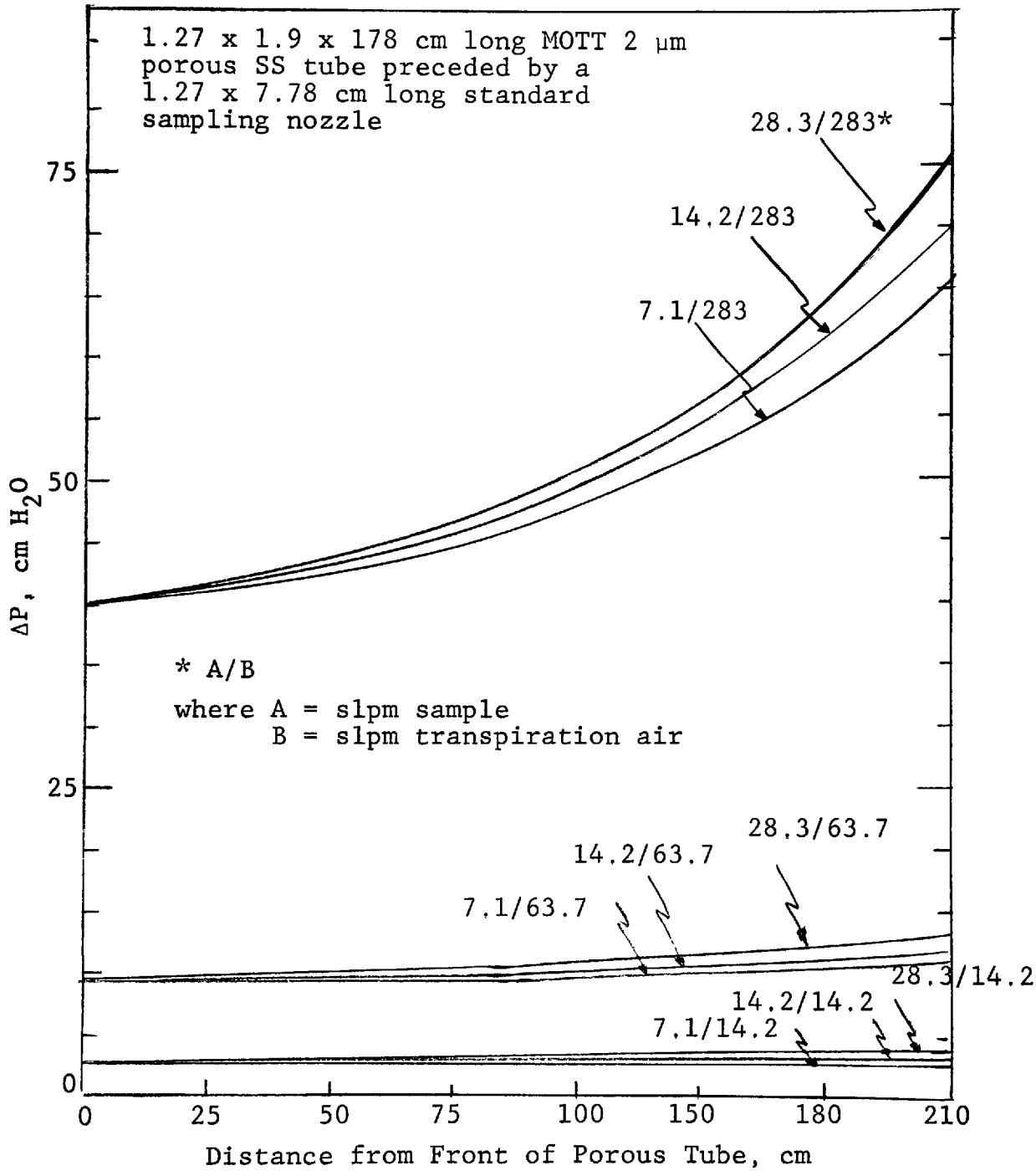

Figure 6. Transpiration Air Pressure Drop Across the Porous Tube Wall

entrance of the probe at high sample flow rates and low transpiration air flow rates if the porous tube is too permeable. In such a situation, some of the sample could by-pass the inside bore in following a path of least resistance and reenter the porous tube further downstream. Such a reverse flow would defeat the purpose of the porous tube. The use of a low permeability porous tube avoids this undesirable situation by requiring an air supply pressure considerably greater than the pressure at the inside upstream end of the porous tube. An added advantage is a more even distribution of transpiration air.

In all of the flow tests the transpiration air pressures at the middle of the manifold and at the extreme downstream end of the manifold were essentially identical, indicating negligible pressure drop over the length of the transpiration air manifold. Also, at all the parametric levels selected for the experimental design, the air pressure in the transpiration air manifold was positive, indicating reverse flow through the porous tube could not occur at these conditions. Figure 6 shows the radial ΔP for the transpiration air passing through the wall of the porous tube as a function of the axial distance from the upstream end of the porous tube. Note that the porous tube was preceded by a 7.78 cm (3-1/16 in.) long by 1.27 cm (½ in.) ID sampling nozzle.

The pressure drop was invariably lowest at the upstream end of the porous tube and highest at the downstream end. The greatest percent change (nearly twice the ΔP at the downstream end compared to the upstream end) in the radial ΔP occurred when the highest transpiration air flow rate of 283 slpm (10 scfm) was used.

3. EXPERIMENTAL PROCEDURES FOR PHASE I

Dependable aerosol generation in the desired concentration and size range was a vital part of the tests conducted on the sampling interface. This section describes the methods of aerosol generation, the aerosols produced, and the experimental and analytical procedures.

3.1 Aerosol Generation

The experimental design of Phase I called for 0.05 μm, 1.6 μm and 50 μm aerosols. Accurate measurement of minute amounts of aerosol deposition on the porous sampling probe suggested the use of soluble aerosols which could be solvent extracted from the porous tube and quantitatively analyzed with a sensitive analytical test. KCl was ultimately selected for the generation of the 0.05 μm aerosols, 1-methylaminoanthraquinone (1-MAAQ) for the 1.6 μm aerosols, and sodium fluorescein (uranine) for the 50 μm aerosols. Flame emission, colorimetric absorption, and fluorescence analytical techniques were used to assess the extracts and samples.

3.1.1 KCl Aerosol, 0.05 μm

The KCl aerosol generator was selected as the alternate choice over the $MgCl_2$ aerosol generator initially attempted when it was found that the magnesium salt was much too susceptible to hydrolysis and erratic output. In contrast, the KCl aerosol generator proved to be quite stable and predictable over test periods which ran as long as six days of continuous operation. The KCl aerosol generator operates by vaporization from a plug of the salt in an electrically heated nichrome coil. At an air flow of 7.1 lpm (0.25 cfm) and a voltage of 21.8 volts across the 5 ohm coil (#12 BWG Nichrome V wire), a satisfactory test aerosol was generated. The condensation nuclei counter showed a concentration greater than 10^7 particles/cc while illumination of the aerosol in an intense beam of light showed no light scattering despite

the high concentration. A sample collected with the TSI Electrostatic Aerosol Sampler (Model 3100, Thermosystem Incorporated, St. Paul, Minn.) was examined and sized in the electron microscope (EM). An approximate size distribution from a limited number of particles showed that the aerosol was in the desired size range with a count median diameter (CMD) of 0.038 μm and a σ_g of 1.63. The size distribution of the KCl aerosol as measured by EM examination was confirmed in particle electrical mobility tests with an aerosol analyzer similar to the Whitby Aerosol Analyzer sold by TSI (Appendix A). Dr. Earl Knutson, a former student of Dr. Whitby, made the measurements and reported a CMD of 0.032 μm, Figure 7.

Flame emission measurements of the potassium concentration was used to analyze the samples in the sampling interface tests with the KCl aerosols.

3.1.2 1-MAAQ Aerosol, 1.6 μm

The 1.6 μm aerosol was readily generated by controlled vaporization and condensation of the 1-MAAQ. Figure 8A is a photograph of the combined KCl and 1-MAAQ aerosol generator which is operated at a reduced voltage (18 volts) to generate the condensation nuclei needed for controlled condensation of the 1-MAAQ vapor. The KCl-nucleated air stream at 0.25 cfm passes into a second three-necked flask with the 1-MAAQ above a hot glycerine bath. A lab jack raises the bath and immerses the flask whenever aerosol generation is desired. The vapor-laden air stream then passes through a heated glass tube followed by the condensation tube. A portion of the aerosol formed in the condensation tube was sampled by the interface probe. The aerosol was sampled by an IITRI moving slide impactor and sized from photomicrographs, Figures 9 and 10.

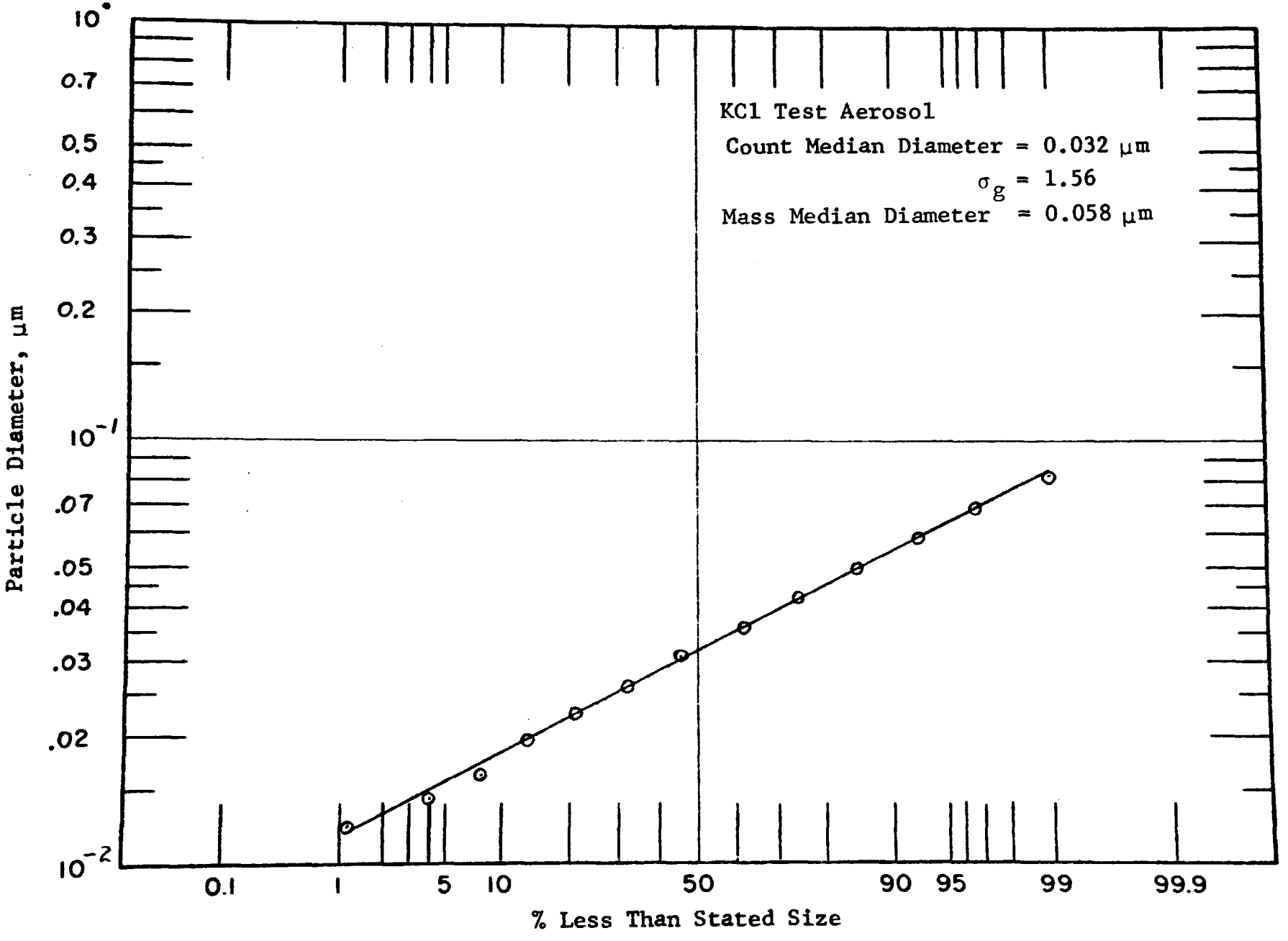

Figure 7. Test Aerosol Size Distribution from Electrical Mobility Data

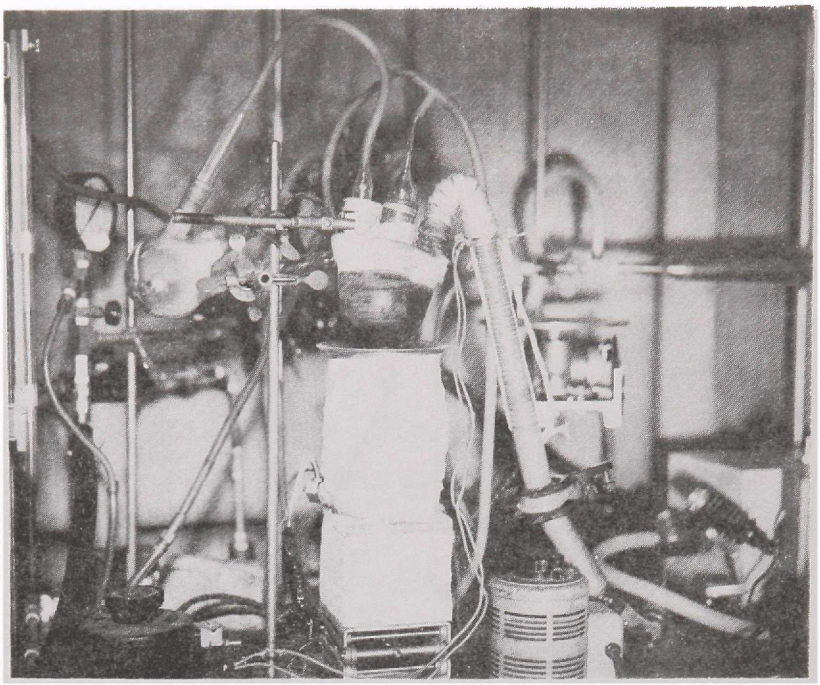

A. The combined KCl and 1-MAAQ aerosol generators for 0.05 μm KCl or 1.6 μm 1-MAAQ aerosols.

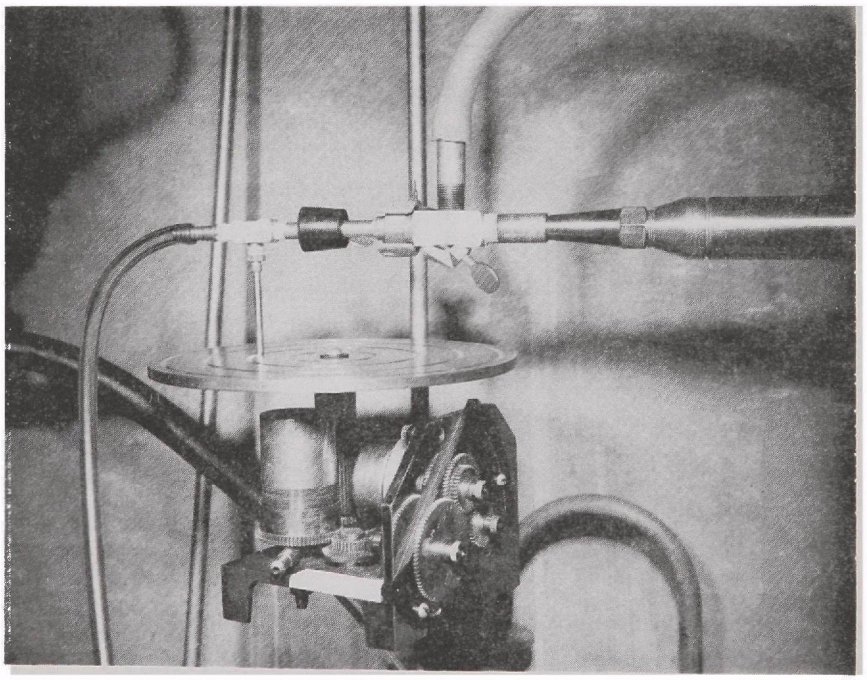

B. The miniature venturi dust feeder for 50 μm uranine aerosol generation.

Figure 8. Photographs of the Aerosol Generators

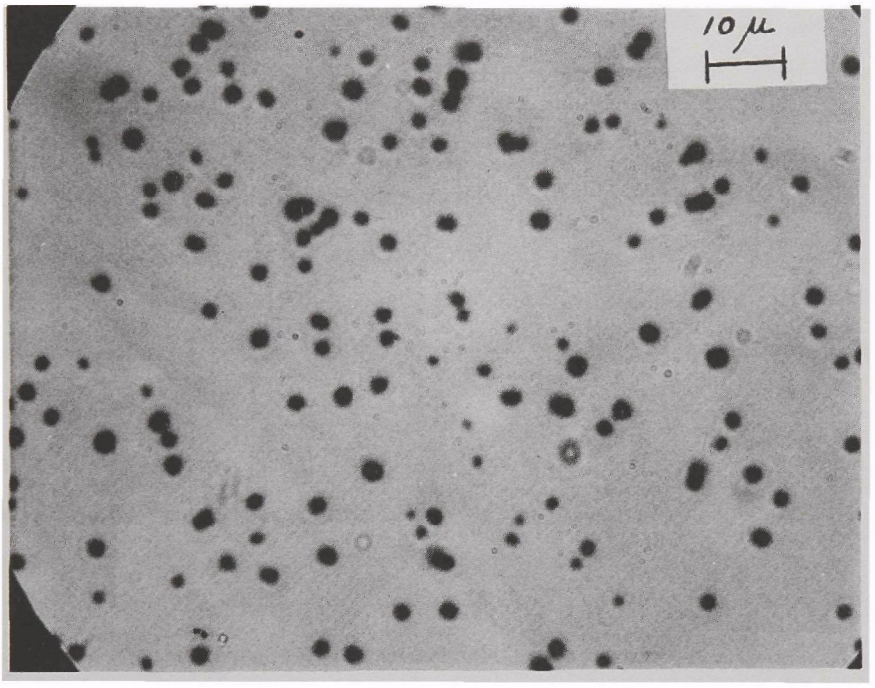

Figure 9. Photomicrograph of the 1-MAAQ Test Aerosol

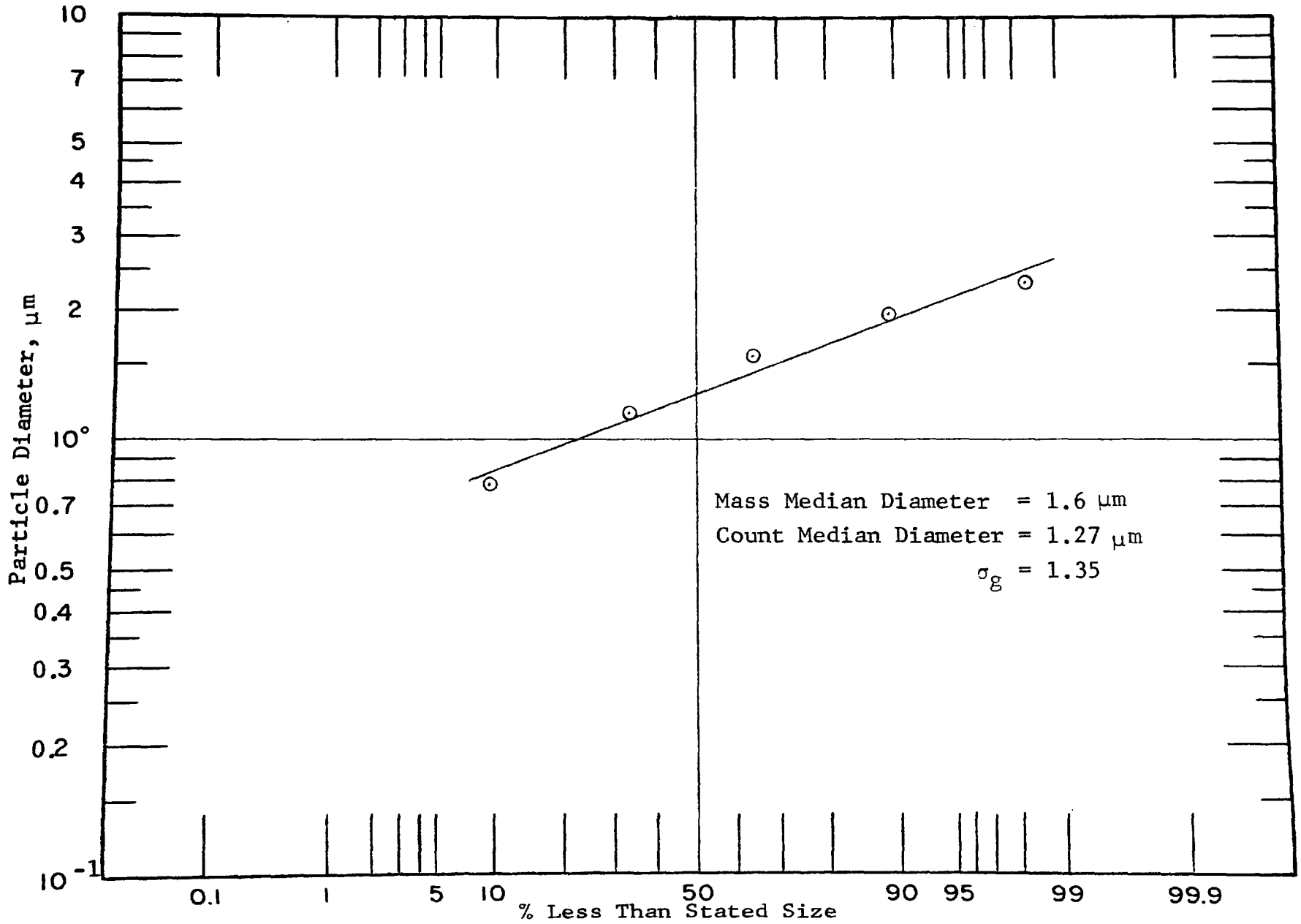
Particle Diameter, μm
10
7
5
4
3
2
10°
0.7
0.5
0.4
0.3
0.2
10⁻¹
0.1
1
5
10
50
90
95
99
99.9
% Less Than Stated Size
Mass Median Diameter = 1.6 μm
Count Median Diameter = 1.27 μm
σg = 1.35

3.1.3 Uranine Aerosol, 50 μm

The uranine aerosol generator utilized the motorized gear drive mechanism of a Wright dust feeder to rotate a grooved aluminum plate. Four V-shaped grooves at 1, 2, 3, and 4 in. radii are machined in the face of the aluminum plate. Interchangeable gears also provide the capability for changing the dust feed rate. The 270 to 325 mesh fraction of uranine particles was freshly sieved before each test and 250 mg of the powder was placed in one of the grooves. The powder was subsequently aspirated into the venturi dispenser as the groove rotated past the aspiration tube. The venturi dispenser is miniaturized so that it operates efficiently at a total output (primary and aspirated air) of less than 7.1 lpm (0.25 cfm) the smallest sample volume used in the statistical tests. The system, Figure 8B, works very well with the easily deagglomerated large uranine particles.

The electrostatic charge distribution on the uranine aerosol particles was determined by collection in a modified Wesix Ion Spectrometer operated vertically at 500 volts. The charge from the collected particles was collected on a capacitor and the voltage increase was monitored with a Keithly electrometer. The average uranine particle carried 1.4×10^4 negative charges and 6.5×10^3 positive charges. Kunkel (1) found charges as high as 3×10^4 on air dispersed particles in the size range 0.5 to 30 μm. He also noted that asymmetric charging occurred in a heterogenous system with negative bias for the large particles. Our measurements agree with Kunkel's. He also observed that humidity did not affect charging. Thus, differences in charging due to humidity changes of different days during the test series should not be a significant factor. Charge measurements were not made on the KCl and 1-MAAQ condensation aerosols because of the insignificant charge levels known to exist on such condensation aerosols. The

---

(1) Kunkel, W. B., J. Appl. Physics, 21, 820 (1950).

effect of the presence of charged particles in the deposition on conduit walls tends to increase with the charge level

Figure 11 shows a photomicrograph and Figure 12 shows the size distribution of the sieved uranine powder. The particles, while irregular in shape, are narrowly sized and dispersed readily as single particles with few associated fines. Some attrition and fines formation undoubtedly occurs during aerosol generation and transport, but the collected aerosol samples show less than ~2% of the mass as fines

3.2 Test Procedure

The following procedure was followed in the Phase I tests:

(1) Two Gelman Type A glass fiber filters were inserted in the filter holder (as shown in Figure 3) prior to assembly in the sampling interface. Double filters were used to establish whether quantitative collection was obtained on the first filter, a concern in the tests with the 0.05 μm aerosol.

(2) The solvent-extracted clean porous tube was partly inserted in the probe sheath from the rear. Rubber gloves were used during all handling operations to avoid potassium contamination from perspiration. The rear O-ring was placed on the end of the porous tube and the tube was then inserted the rest of the way. The downstream filter unit (as shown in Figure 3) was then screwed tightly with the spanner wrench into the probe sheath, automatically positioning the porous tube. The forward O-ring was then placed on the porous tube and the mating collar adapter was tightly fastened before the standard nozzle was attached (Figure 2)

(3) The transpiration air and exhaust air flows were turned on and adjusted to the desired levels as described previously in Section 2.2. During these adjustments, a protective inlet filter prevented contamination of the porous probe interface.

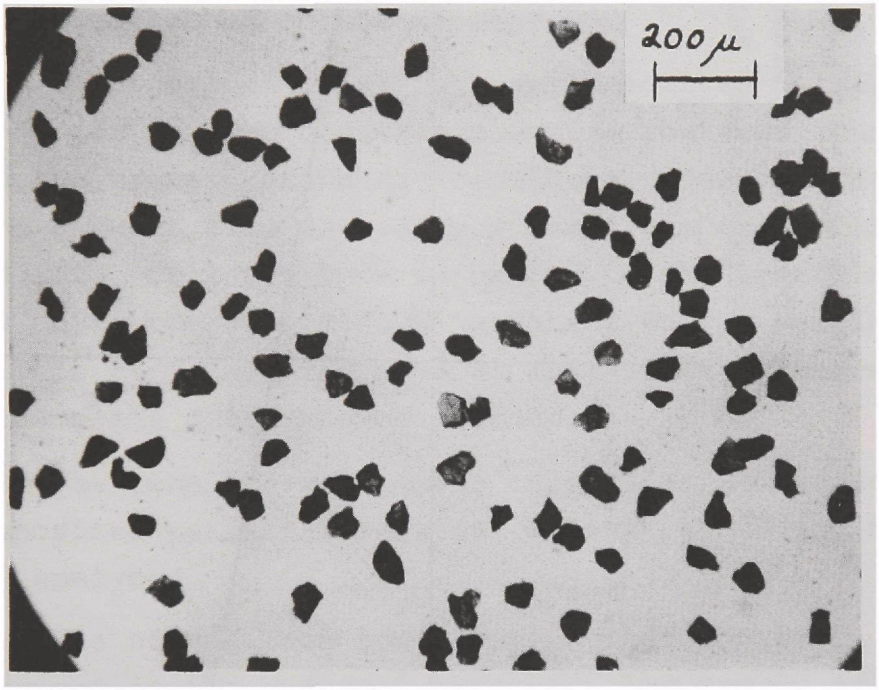

Figure 11. Photomicrograph of the 55 μm Uranine Test Powder

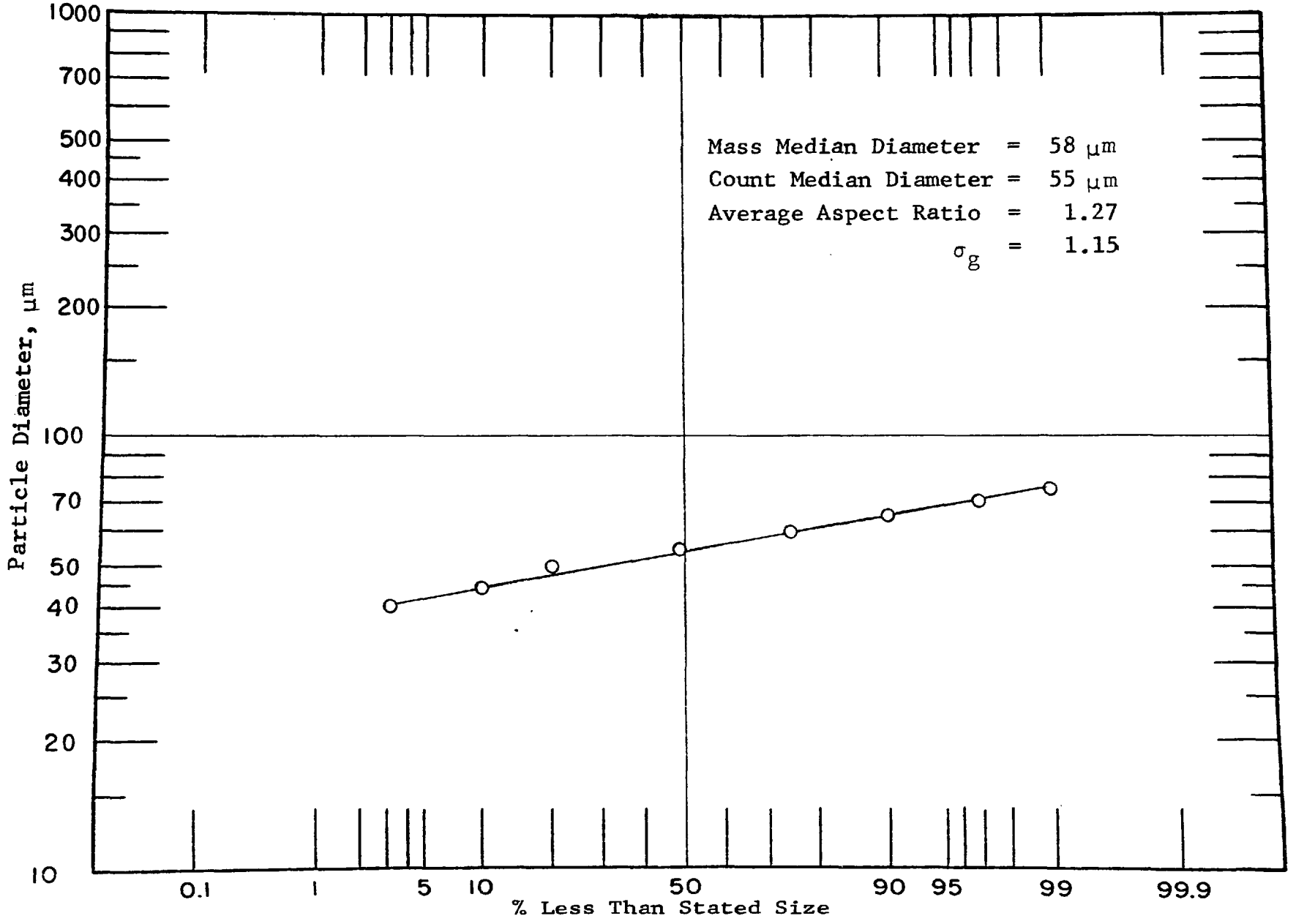
Mass Median Diameter = 58 μm
Count Median Diameter = 55 μm
Average Aspect Ratio = 1.27
σ_g = 1.15
Particle Diameter, μm
1000
700
500
400
300
200
100
70
50
40
30
20
10
0.1
1
5
10
50
90
95
99
99.9
% Less Than Stated Size

(4) When the aerosol generator was ready for the initiation of the test, the protective inlet filter was removed from the nozzle and the aerosol was injected directly into the sampling nozzle for a test period which for the series ranged from 1½ minutes to as long as six days.

(5) At the end of the test the aerosol generator was detached from the sampling nozzle and the protective inlet filter was reattached to the nozzle.

(6) In order not to disturb any deposited particles by sudden changes in flow conditions during shutdown, the exhaust flow and the transpiration air flow were reduced by steps, i.e., the exhaust flow was reduced until the sample flow approached zero, followed by a reduction in the transpiration air flow until the sample flow increased to the original test value. This cycle was repeated as many times as necessary until a complete shutdown was reached.

(7) The sampling nozzle was carefully removed and internally deposited particles were solvent extracted and quantitatively analyzed.

(8) The porous tube was removed after insertion of a small stopper in the upstream opening. The porous tube with stopper was inserted in a pyrex extraction column with the stoppered end down. Again, rubber gloves were used since skin fluids were found to be a significant source of potassium at the trace levels that were measured.

(9) The appropriate solvent (distilled water for KCl or uranine and acetone for 1-MAAQ) was poured inside the porous tube so that the solvent passed through the tube walls. Quantitative extraction was achieved with 1-3 liters of solvent. The porous tube extract was quantitatively analyzed.

(10) The glass fiber collection filter was photographed, solvent extracted, and quantitatively analyzed.

(11) The porous tube was washed with an additional 4 liters of solvent, followed by a final acetone rinse before air drying in preparation for the next test.

3.3 Chemical Analysis

Uranine was analyzed by colorimetric and fluorometric techniques. A Bausch and Lomb Spectronic 20 Colorimeter was used to measure uranine solution optical density at 485 nm and a Turner Model 111 Fluorometer was used for more sensitive detection at trace levels.

1-MAAQ was analyzed colorimetrically at 500 nm. Solutions were concentrated when necessary to obtain measureable levels of optical density.

Potassium was analyzed by flame emission with a Jarrell Ash Model 82-528 Atomic Absorption/Flame Emission Spectrophotometer. Most of the porous tube extracts were concentrated 10/1 but, because of the low mass concentration of the 0.05 μm test aerosol and the very low deposition, many of the deposition levels are reported as upper limits. The actual amounts deposited could be less than the reported levels.

4. TEST DESIGN, DATA, AND OBSERVATIONS

4.1 Test Design

A balanced ½ replicate of a 2 x 3^3 factorial experiment in which sample flow rate, transpiration flow rate, and particle size each have three levels and particle concentration has two levels was designed. Seven added combinations were subsequently added to the design to show comparative results with the equivalent of a standard EPA stack sampling probe with a 1.27 cm (½ in.) ID pyrex tube in place of the porous metal tube. The experiment design is described in greater detail in Section 5 of this report.

4.2 Test Data and Observations

4.2.1 Tabular and Graphic Data

Table 1 summarizes the test data obtained. The percent probe deposition was calculated independently of the nozzle deposition since the standard nozzle used for these tests would not be used in a final prototype interface. Thus, the percent probe deposition in Table 1 is for the porous tube only. The aerosol concentration could not be fixed at precise levels in the experiment design but was either "high" or "low" on a relative basis for a given size aerosol. The number concentration of the test aerosols ranged from a low of 1.7/cc for the 50 μm uranine to a high of 8 x 10^7/cc for the 0.05 μm KCl. The mass concentration varied from a low of 0.08 mg/m^3 for the KCl to a high of 5,120 mg/m^3 for the uranine aerosol.

The percent deposition on the porous tube as a function of transpiration air flow and sample flow rate are shown in Figures 13-15. The points are plotted with an adjacent + or - sign to indicate the experiment design and concentration of high or low, respectively. Concentration was expected to have a very low order effect on deposition (confirmed in the statistical analysis of Section 5 in this report), allowing a realistic graphic representation of the experimental data which was a fractional design with respect to concentration.

Table 1. AEROSOL MASS TRANSPORT TEST DATA FOR PHASE I EXPERIMENTS WITH THE IITRI BOUNDARY LAYER SAMPLING PROBE

Test Sequence	1	1B	2	3	3B	4	5	5B	6	7	8	9
Combination	27	-	21	7	-	19	3	-	9	1	25	18
Sample, lpm	28.3	28.3	28.3	7.1	7.1	28.3	7.1	7.1	7.1	7.1	28.3	14.2
Transpiration, lpm	283.0	0	14.2	283.0	0	14.2	14.2	0	283.0	14.2	283.0	283.0
Particle Size, μm	44-55	44-53	44-53	0.05	0.05	0.05	44-53	44-53	44-53	0.05	0.05	44-53
Concentration	High	High	Low	High	High	High	High	High	Low	Low	Low	Low
Probe	2 μm SS	Pyrex	2 μm SS	2 μm SS	Pyrex	2 μm SS	2 μm SS	Pyrex	2 μm SS	2 μm SS	2 μm SS	2 μm SS
Aerosol Samples (Filter + Probe), mg	212.1	199.9	211.0	2.33	2.18	1.33	97.8	31.0	57.4	2.18	2.02	191.1
Aerosol Concentration,* mg/m^3	5120.0	4840.0	975.0	0.76	0.53	0.08	2300.0	749.0	272.0	0.23	0.08	795.0
Aerosol Concentration, Particles/cc	51.2	48.4	9.8	5.9×10^7	8.0×10^7	5.9×10^6	23.0	7.5	2.7	1.8×10^7	5.9×10^6	8.0
Aerosol Deposited on Probe, mg	0.120	0.112	0.0362	<0.004	0.050	<0.004	96.4	29.9	0.0248	<0.004	0.114	0.0671
Aerosol Deposited on Nozzle, mg	0.012	0.009	0.010	0.02	0.02	<0.02	70.7	109.7	98.7	<0.02	<0.02	0.036
Probe Deposition,** %	0.057	0.056	0.017	<0.2	2.3	<0.3	98.9	96.5	0.043	<0.2	5.7	0.035
Clean Air Sheath Noted	No	No	No	Yes	NV	NV	Yes***	No	No	Yes	NV	No
Filter Deposit Dia., cm	9.5	9.5	9.5	2.5	-	-	6.0	9.5	9.5	6.2	-	9.5

(continued)

Table 1 (continued). AEROSOL MASS TRANSPORT TEST DATA FOR PHASE I EXPERIMENTS WITH THE IITRI BOUNDARY LAYER SAMPLING PROBE

Test Sequence	10	10B	11	12	13	14	15	16	17	18	19
Combination	12		6	5	16	22	24	23	4	11	14
Sample, lpm	14.2	14.2	63.7	7.1	14.2	28.3	28.3	28.3	7.1	14.2	14.2
Transpiration, lpm	14.2	0	63.7	63.7	63.7	283.0	63.7	63.7	63.7	14.2	63.7
Particle Size, μm	44.53	44-53	44-53	1.6	0.05	0.05	44-53	1.6	0.05	1.6	1.6
Concentration	High	High	Low	Low	High	Low	High	High	High	High	Low
Probe	2 μm SS	Pyrex	2 μm SS	2 μm SS	2 μm SS	2 μm SS	2 μm SS	2 μm SS	2 μm SS	2 μm SS	2 μm SS
Aerosol Samples (Filter + Probe), mg	156.9	30.0	39.1	28.4	3.68	2.48	177.0	176.5	3.74	85.7	38.3
Aerosol Concentration,* mg/m^3	2750.0	689.0	173.0	91.2	0.23	0.08	3950.0	160.0	0.50	276.0	90.2
Aerosol Concentration, Particles/cc	27.5	6.9	1.7	3.0×10^4	1.8×10^7	5.9×10^6	39.5	5.2×10^7	3.8×10^7	9.1×10^4	3.0×10^4
Aerosol Deposited on Probe, mg	155.0	29.4	37.5	0.0168	~0.020	<0.010	0.0195	0.0335	<0.008	0.0252	0.0158
Aerosol Deposited on Nozzle, mg	19.7	22.0	95.4	0.024	<0.01	<0.02	0.004	0.020	0.002	0.016	0.009
Probe Deposition,** %	98.8	97.9	96.0	0.059	0.5	<0.4	0.011	0.019	<0.02	0.029	0.041
Clean Air Sheath Noted	Yes	No	Yes	Yes	Yes	NV	No	Yes	Yes	Yes	Yes
Filter Deposit Dia., cm	6.8	9.5	2.8	2.9	NM	-	9.5	~5.0****	5.0	7.3	3.9

(continued)

Table 1 (continued). AEROSOL MASS TRANSPORT TEST DATA FOR PHASE I EXPERIMENTS WITH THE IITRI BOUNDARY LAYER SAMPLING PROBE

Test Sequence	20	21	22	23	24	25	26	27	27B	18B	21B
Combination	17	20	13	10	26	15	8	2	-	-	-
Sample, lpm	14.2	28.3	14.2	14.2	28.3	14.2	7.1	7.1	7.1	14.2	28.3
Transpiration, lpm	283.0	14.2	283.0	14.2	283.0	63.7	283.0	14.2	0	0	0
Particle Size, μm	1.6	1.6	0.05	0.05	1.6	44-53	1.6	1.6	1.6	1.6	1.6
Concentration	Low	High	Low	Low	Low	High	High	Low	High	High	High
Probe	2 μm SS	2 μm SS	2 μm SS	2 μm SS	2 μm SS	2 μm SS	2 μm SS	2 μm SS	Pyrex	Pyrex	Pyrex
Aerosol Samples (Filter + Probe), mg	34.2	80.7	1.37	9.07	25.7	134.9	14.0	9.91	32.6	87.6	90.9
Aerosol Concentration,* mg/m^3	78.0	168.0	0.09	0.08	47.1	3090.0	198.0	56.1	219.0	193.0	117.0
Aerosol Concentration, Particles/cc	$2.6x10^4$	$5.5x10^4$	$7.1x10^6$	$5.9x10^6$	$1.5x10^4$	30.9	$6.5x10^4$	$1.8x10^4$	$7.2x10^4$	$6.3x10^4$	$3.8x10^4$
Aerosol Deposited on Probe, mg	0.0063	0.0567	<0.004	<0.020	0.2963	80.0	0.0032	0.0158	1.015	1.223	0.734
Aerosol Deposited on Nozzle, mg	0.018	0.024	<0.02	0.02	0.009	22.6	0.007	0.004	0.020	0.029	0.034
Probe Deposition,** %	0.018	0.070	<0.2	<0.2	1.15	59.7	0.022	0.16	3.1	1.4	0.81
Clean Air Sheath Noted	Yes	No	Yes	Yes	No	Yes	Yes	Yes	No	No	No
Filter Deposit Dia., cm	~4.0	9.5	5.0	7.6	9.5	3.0	~2.5	6.1	9.5	9.5	9.5

* At upstream end of porous tube.

** Porous tube only.

*** 0.3 μm to 12 μm fines transported with no deposition (see filter photo).

**** Not evident in photograph but estimated from visual appearance of eroded heavy deposit.

NV not visible

NM not measured

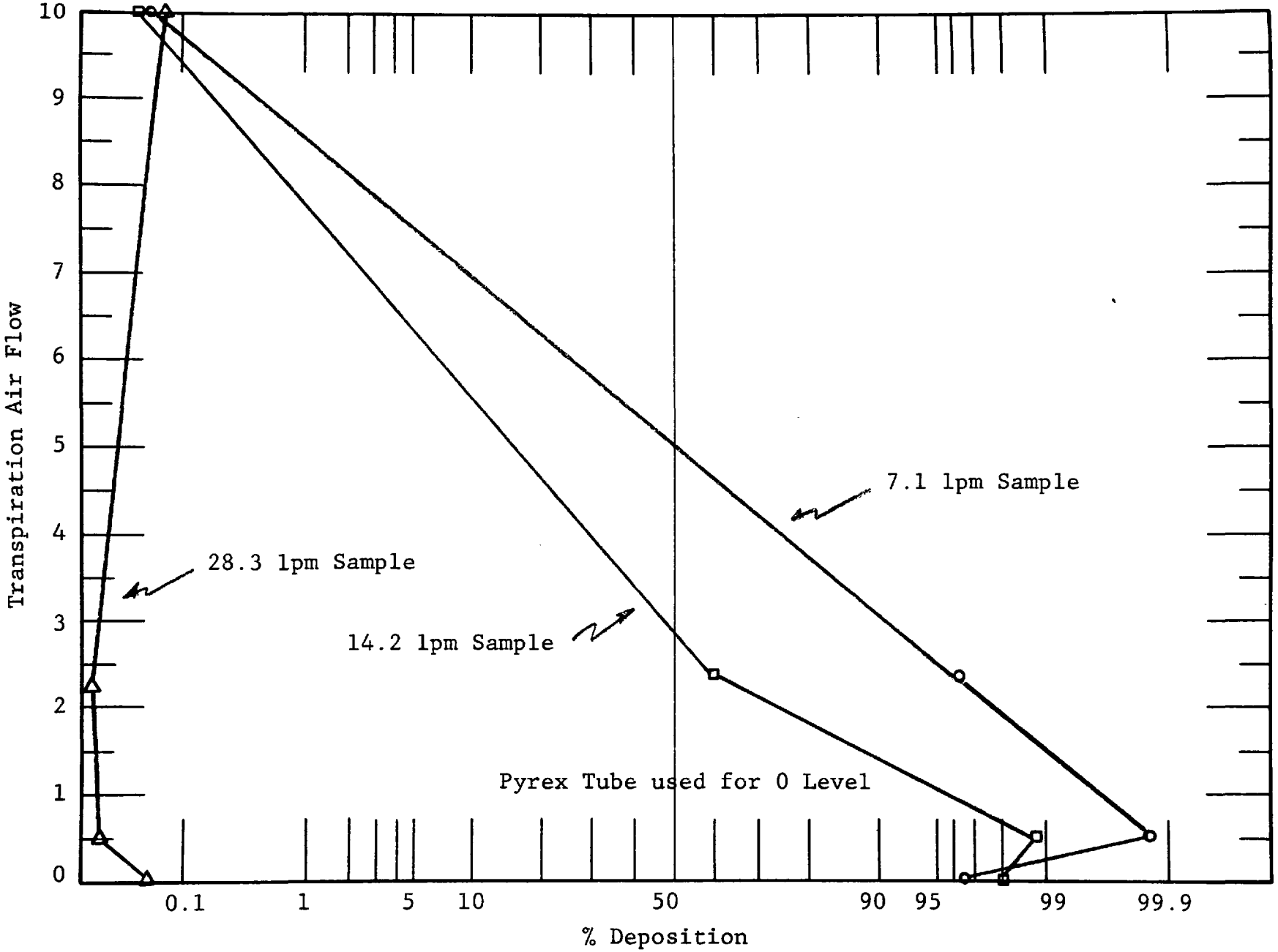

Figure 13. Deposition of 50 μm Uranine Particles in the 1.27 cm Diameter by 178 cm Long Porous Sampling Probe

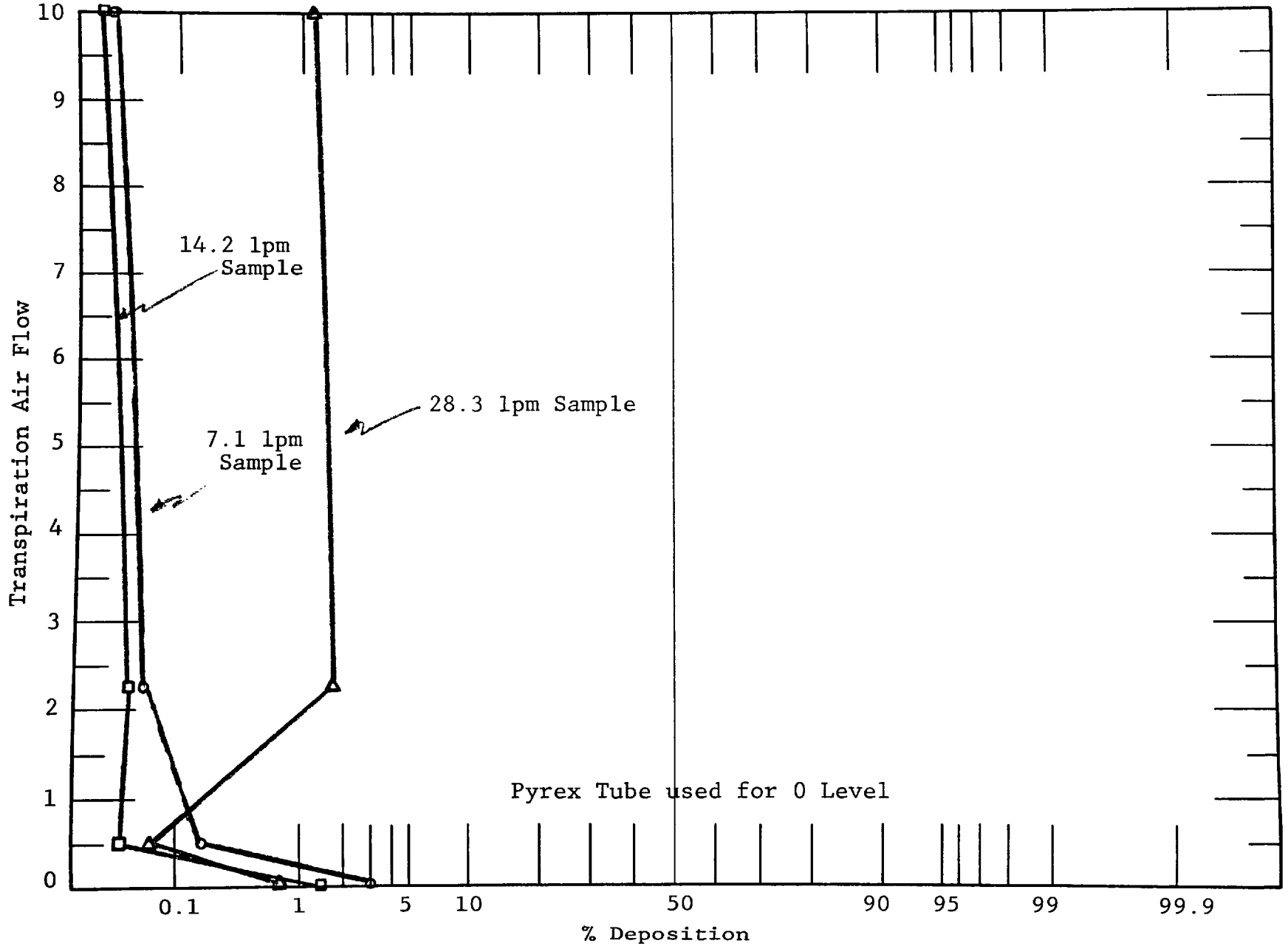

Figure 14. Deposition of 1.6 μm 1-MAAQ Particles in the 1.27 cm Diameter

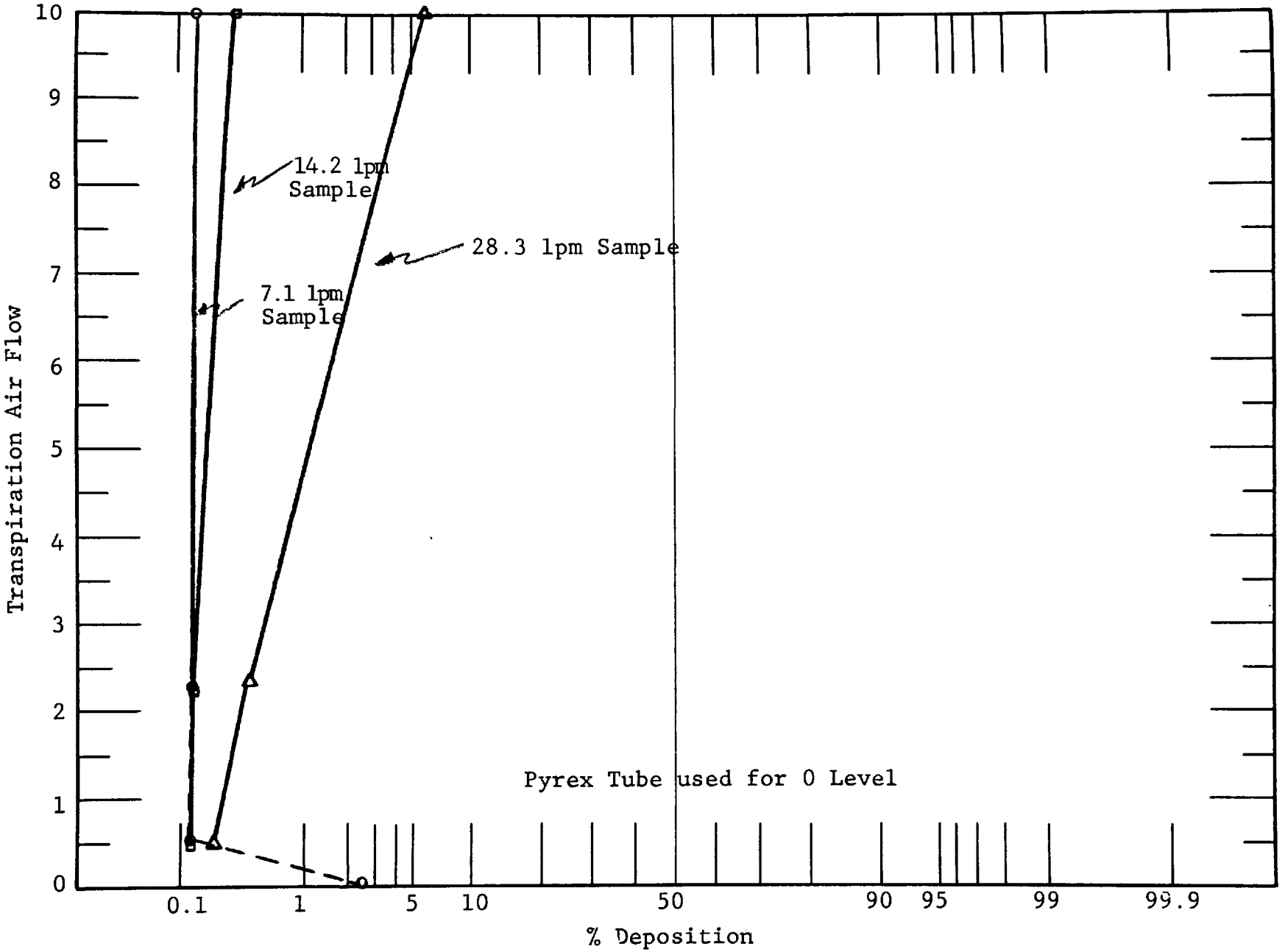

Figure 15. Deposition of 0.05 μm KCl Particles in the 1.27 cm Diameter by 178 cm Long Porous Sampling Probe

The experiments with 50 μm uranine aerosols, Figure 13, shows that when the sample flow rate is 7.1-14.2 lpm (0.25-0.50 cfm), the use of 283 lpm (10 cfm) transpiration air reduces deposition from about 98 percent to less than 0.1%. At 28.3 lpm (1 cfm) sample flow rate, deposition was less than 0.1% regardless of the amount of transpiration air used. This indicates that the greatest advantage of the porous probe interface is in the quantitative transport of these large particles when the sample flow rate is low.

The tests with the 1.6 μm 1-MAAQ aerosols, Figure 14, shows that deposition was virtually eliminated with only 14.2 lpm (0.5 cfm) of transpiration air at all sample rates. The downward deposition trend continued for the 7.1-14.2 lpm (0.25-0.50 cfm) sample rates as the transpiration air increased to 283 lpm (10 cfm). An exception to this continuing trend is noted with the 28.3 lpm (1.0 cfm) sample rate curve where after dropping 3% to 0.07% deposition at 14.2 lpm (0.5 cfm) of transpiration air, deposition increased to 1-2% with further increases in transpiration air. This phenomenon is believed to be related to the jetting action of the air as it issues from the individual micropores in the porous tube. Microturbulence certainly exists close to the tube wall before the air jets disappear and merge as a relatively smooth flow farther away from the wall. At the tube entrance the incoming aerosol is quite near the wall where microturbulent deposition can occur. As the aerosol stream progresses down the tube it tends to be squeezed inward and accelerated downstream due to the influx of transpiration air. At the higher sample flow rate, a longer distance of travel is needed to squeeze the aerosol stream away from the microturbulent region near the wall; this accounts for the higher deposition of 1.6 μm particles at the higher sample flow rate. Deposition generally appeared to be concentrated in the first foot of travel down the porous probe.

The same phenomenon occurred in the tests with the 0.05 μm KCl aerosol, Figure 15. After a virtual elimination of deposition with only 14.2 lpm (0.5 cfm) of transpiration air at all sample flow rates, the deposition at the 28.3 lpm (1 cfm) sample flow rate significantly increased to 6% with increasing transpiration air flow. At sample flows of 7.1-14.2 lpm (0.25-0.50 cfm) the deposition remained below 0.5% when the transpiration air flow was in the range of 14.2-283 lpm (0.5-10.0 cfm).

4.2.2 Photographic Proof of Effectiveness

As stated in Section 2.1.2, the glass fiber collection filter often served as a witness plate for confirmation of the existence of a particle-free air sheath surrounding the aerosol stream. Photographs were taken of the filters after tests with one of the colored aerosols, i.e., uranine or 1-MAAQ, Figures 16 and 18, and measurements were taken of the filter deposit diameter, Table 1. Photographs were not taken of the KCl deposits on the collection filters due to insufficient contrast, but in many tests with the KCl the deposit could be seen visually when viewed at a shallow angle. The KCl deposits were similar in size and shape to those in comparable tests with 1-MAAQ, confirming the similar probe deposition behavior for the two aerosols.

Examination of the glass fiber filter sample from test 5 revealed an unexpected wealth of quantitative data on the effectiveness of the porous probe at these flow conditions for particles smaller than 50 μm. Generation of the 50 μm uranine aerosol unavoidably produced a very small amount of secondary small particle aerosol associated with the coarse particle fraction. Thus, while test 5 was a failure with respect to transport of 50 μm particles, it was an unqualified success in transporting smaller particles. Figure 16 shows the fine particle deposit on the glass fiber filter completely surrounded by a particle-free clean air sheath.

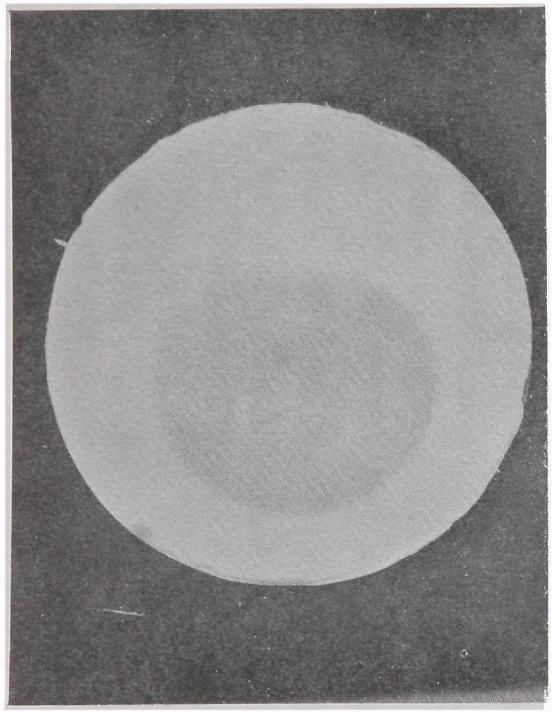

Figure 16. Particle Deposit on Glass Fiber Filter Showing Laminar Flow with Clean Air Sheath, Test 5

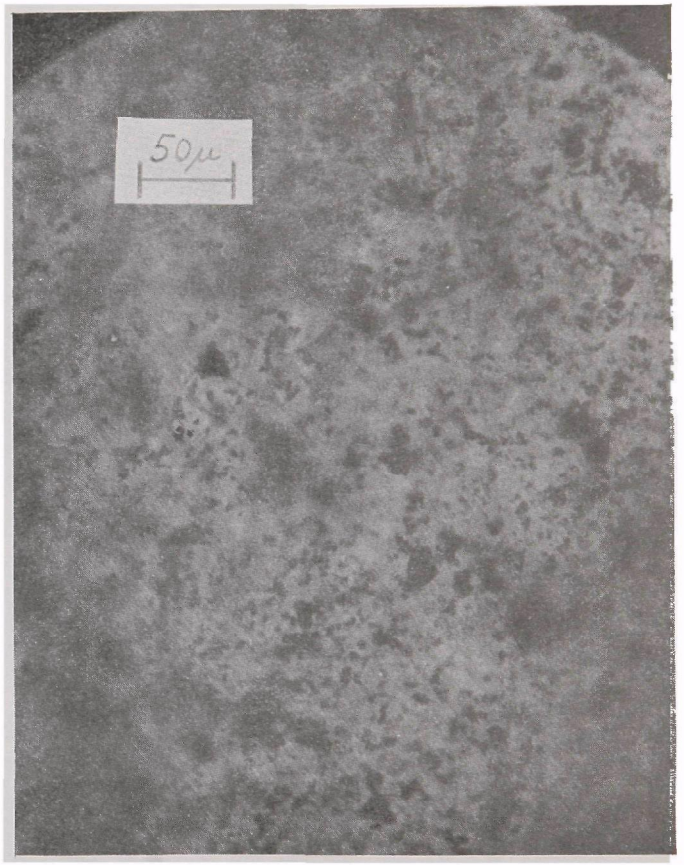

Figure 17. Photomicrograph of Particle Deposit on Glass Fiber Filter of Test 5

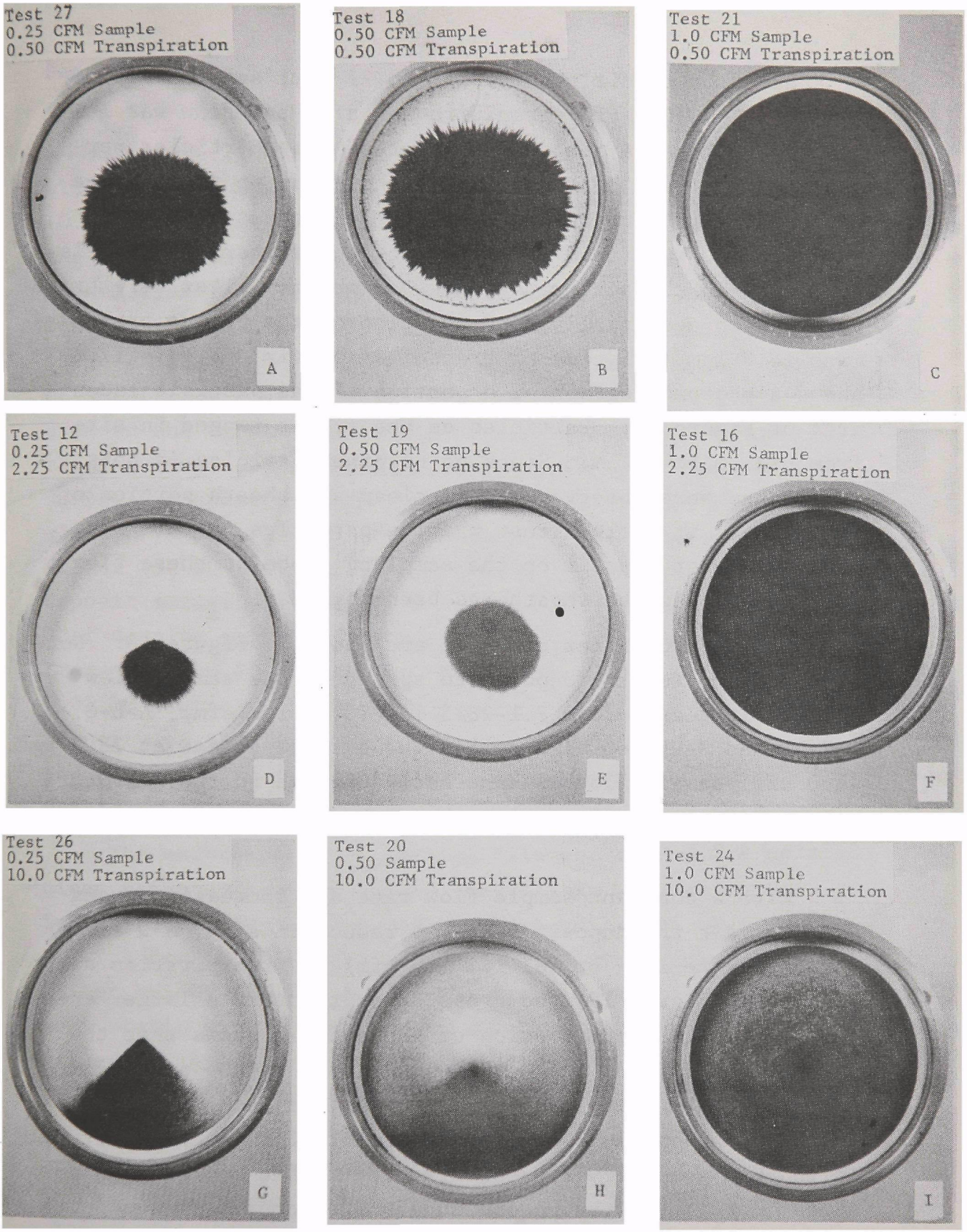

Figure 18. Photographs of Filter Deposits of 1-MAAQ Aerosols which Confirm Effectiveness of Boundary Layer Principle for Aerosol Transport

At these flow conditions 7.1 lpm (0.25 cfm) sample volume and 14.2 lpm (0.5 cfm) transpiration air, the flow was laminar such that the aerosol filament of fine particles persisted downstream of the porous probe right up to the face of the filter. The outline of the deposit was displaced slightly downward from the center of the filter. Nonetheless, particles in the size range observed on the filter were transported with essentially no deposition on the porous probe with 14.2 lpm (0.5 cfm) of transpiration air. Figure 17 shows a photomicrograph of a portion of the particle laden area of Figure 16. Particles on the filter ranged in size from 0.3 μm to 15 μm. Since no uranine particles in this size range were observed in the clean-air-sheath portion of the filter, it follows that uranine particles in this size range will not deposit on the sampling probe at these flow conditions once the sheath has been formed.

The 1-MAAQ filter deposits are shown in Figure 18. Note the tendency for the deposit to spread as the sample flow rate is increased from 7.1-28.3 lpm (0.25-1.0 cfm), A-B-C, D-E-F, and G-H-I of Figure 18. The extreme spread at 28.3 lpm (1.0 cfm) sample flow is apparently related to the microturbulent diffusion effect near the probe wall as discussed in Section 4.2.1.

With a constant sample flow rate and increasing transpiration air the deposit tends to reduce in size, A-D and B-E of Figure 18. At 283 lpm (10 cfm) of transpiration air, G and H of Figure 18, the gross deposit covers a larger area, but close visual examination of the deposit shows that the triangular shape of the deposit is caused by the axial displacement of the aerosol filament from the geometric center of the probe opening. The displacement of the aerosol stream is in turn caused by the eccentricity of the bore in the downstream portion of the porous tube. The comparable test with 0.05 μm KCl at 7.1 lpm (0.25 cfm) sample and 283 lpm (10 cfm) transpiration air revealed a deposit the size of a quarter.

Because of the low aerosol mass, the KCl deposit did not smear and was sharply outlined.

In test 23 with 0.05 μm KCl, a six day test was conducted with 14.2 lpm (0.5 cfm) of transpiration air and 14.2 lpm (0.5 cfm) of sample volume to obtain a visible deposit on the collection filter. The filter deposit from this test showed clearly that the KCl particulates were completely confined within a clean air sheath. The deposit was circular in shape with a diameter of 76 mm on the 95 mm diameter open face of the filter. At no point did the deposit come closer than 8 mm to the outside portion of the filter sealed by the retaining ring. If no diffusion of the aerosol had occurred during transport through the probe, the area of the deposit would have covered 50% of the available area of the collection filter (50-50 volume ratio of aerosol/transpiration air). The deposit actually covered 64% of the filter area, suggesting that despite some diffusion toward the probe wall a lower transpiration air flow rate would have been effective for 0.05 μm particles. At 14.2 lpm (0.5 cfm) the average face velocity of the existing TA is 3.4 mm/sec, well in excess of the actual diffusion velocity of 0.9 mm/sec for the 0.05 μm particles in this test.

The existence of an aerosol filament surrounded by a clean air sheath was observed directly in test 26 as well as in many other tests with 1-MAAQ. A pencil-lead thin red aerosol filament was clearly visible in the pyrex tube of the filter holder, Figure 3. The filament observed was invariably stable with no visible spreading over the distance observed. The existence of a stable aerosol filament at 283 lpm (10 cfm) of transpiration air flow is surprising in view of the high Reynolds Number (~32,000) and is a phenomenon restricted to a region within 1-2 mm of the center of the opening in the porous tube. Closer to the porous tube wall turbulent eddies exist, increasing in scale as the wall is approached, but the very center of flow at the tube axis appears to be laminar at least for the 10 tube diameters from the downstream end of the porous tube to the face of the collection filter.

5. STATISTICAL ANALYSIS OF PHASE I TEST DATA

The effects of four controlled variables -- sample flow rate, transpiration flow rate, particle size, and particle concentration -- on mass percent particle deposition in tubular sampling probes have been investigated experimentally with a fractional factorial design. The results of statistical analysis of the data are presented here and the principal conclusions are stated.

5.1 Definition and Coding of Variables

Dependent variable. The property (dependent variable) measured in each test is the mass percent particle deposition in the tube, denoted by PD. Prior to the statistical analysis of the data a mathematical transformation was made, yielding a working dependent variable, Y, which is functionally related to PD as follows (forward and backward transformations):

$$Y = \log_{10} (PD/(100-PD))$$

$$PD = 100\ (10^{Y})/1 + 10^{Y})$$

PD is restricted to the range of values $0<PD<100$ whereas Y has unrestricted range and is therefore more convenient computationally. This type of transformation is often employed in the statistical analysis of variables with both lower and upper bounds and in many cases serves to expand the scale of values in such a way that effects of controlled factors are more nearly additive and the variance is more nearly uniform. The end results of the analyses are readily expressed in terms of percent deposition by employing the backward transformation.

Independent variables. The four controlled experimental factors (independent variables) were tested at selected levels spanning the ranges of interest. Logarithmic spacing of the levels of the factors was considered to be appropriate in designing the experiment because of the large ratios between the largest and smallest values and the inherent non-negativity

of the values physically. The levels are expressed below both in physical units and corresponding orthogonally coded values. The coded (X) variables are especially well suited computationally for accurately estimating the effects of the controlled factors. For the three factors tested at three or four levels there are coded variables representing possible quadratic (curvilinear) effects as well as linear effects.

Sample flow rate (SFR) was tested at three levels, evenly spaced on a logarithmic scale.

	Coded Variables	
	Linear	Quadratic
SFR, lpm	X_1	X_{1Q}
7.1	-1	+1
14.2	0	-2
28.3	+1	+1

The defining formulas for X_1 and X_{1Q} are:

$$X_1 = (\log_{10}(SFR) - 1.523)/1.523$$

$$X_{1Q} = 3X_1^2 - 2$$

Transpiration flow rate (TFR) was tested at four levels.

	Coded Variables	
	Linear	Quadratic
TFR, lpm	X_2	X_{2Q}
0	-3.000	1.000
14.2	-0.933	-1.032
63.7	+0.933	-1.032
283.0	+3.000	1.000

The defining formulas for X_2 and X_{2Q} are:

$$X_2 = (\log_{10}(TFR + 4.389) - 1.5506)/0.30273$$

$$X_{2Q} = X_2^2/4 - 1.25$$

The constant K = 0.155 in the formula for X_2 was chosen so that the four values corresponding to the four levels of TFR are, after addition of K, as nearly equally spaced as possible on a logarithmic scale.

Particle size (PS) was tested at three levels, nearly evenly spaced on a logarithmic scale.

	Coded Variables	
	Linear	Quadratic
PS, μm	X_3	X_{3Q}
0.05	-1	+1
1.6	0	-2
50.0	+1	+1

The defining formulas for X_3 and X_{3Q} are:

$$X_3 = (\log_{10} (PS) - 0.204)/1.5$$

$$X_{3Q} = 3X_3^2 - 2$$

Particle concentration (PC) was tested at two levels.

PC	X_4
Low	-1
High	+1

5.2 Experiment Design

Altogether, 34 tests were made, each test specified by a unique combination of the levels of the independent variables. Combination numbers 1 through 27 (see Table 2) form a balanced ½ replicate of a 2×3^3 factorial design in which sample flow rate, transpiration flow rate, and particle size each have three levels and particle concentration has two levels. The fourth level of TFR, zero flow, was not included in the original design but occurs throughout the seven added combinations 28 through 34 Particle concentration is at the high level in these seven combinations. The 34 tests as a whole constitute slightly less

Table 2. EXPERIMENTAL DATA

Combination	SFR, lpm	TFR, lpm	PS	PC	Percent Deposition
1	7.1	14.2	0.05	Low	<0.2
2	7.1	14.2	1.6	Low	0.16
3	7.1	14.2	50.0	High	98.9
4	7.1	63.7	0.05	High	<0.2
5	7.1	63.7	1.6	Low	0.059
6	7.1	63.7	50.0	Low	96.0
7	7.1	283.0	0.05	High	<0.2
8	7.1	283.0	1.6	High	0.022
9	7.1	283.0	50.0	Low	0.043
10	14.2	14.2	0.05	Low	<0.2
11	14.2	14.2	1.6	High	0.029
12	14.2	14.2	50.0	High	98.8
13	14.2	63.7	0.05	Low	<0.2
14	14.2	63.7	1.6	Low	0.041
15	14.2	63.7	50.0	High	59.7
16	14.2	283.0	0.05	High	0.5
17	14.2	283.0	1.6	Low	0.018
18	28.3	283.0	50.0	Low	0.035
19	28.3	14.2	0.05	High	<0.3
20	28.3	14.2	1.6	High	0.07
21	28.3	14.2	50.0	Low	0.017
22	28.3	63.7	0.05	Low	<0.4
23	28.3	63.7	1.6	High	0.019
24	28.3	63.7	50.0	High	0.011
25	28.3	283.0	0.05	Low	5.7
26	28.3	283.0	1.6	Low	1.15
27	28.3	283.0	50.0	High	0.057
28	7.1	0.00	50.0	High	0.056
29	7.1	0.00	0.05	High	2.3
30	14.2	0.00	50.0	High	96.5
31	14.2	0.00	50.0	High	97.3
32	28.3	0.00	1.6	High	1.4
33	7.1	0.00	1.6	High	0.81
34		0.00	1.6	High	3.1

than a ½ replicate of a $2 \times 3^2 \times 4$ factorial consisting of 72 possible combinations of factor levels.

5.3 Data Base

The levels of the four controlled variables in each of the 34 test combinations, and the observed percent deposition, are given in Table 2. The percent deposition ranges from a low of 0.011 to a high of 98.9. In seven tests involving the smallest particle size the percent deposition could not be exactly measured; however, an upper limit for PD was established in each such test as noted in the table (combinations 1, 4, 7, 10, 13, 19, and 22).

5.4 Candidate Terms of the Multiple-Regression Performance Model

The framework for the statistical analysis of the data is provided by a model equation that incorporates a set of terms considered capable of representing the ways in which the percent particle deposition might be affected by the controlled factors of the experiment. The dependent variable of the model is Y, as defined above. The candidate independent variables of the model are given in Table 3. These are the X variables defined above together with some simply derived variables. There are 14 candidate terms altogether, including the constant term. The variable components of the linear and quadratic terms are exactly as defined above. The variable components of the six interaction terms are the pairwise products of the linear variables.

The complete model has the form

$$Y = b_0X_0 + b_1X_1 + \ldots + b_4X_4 + b_{1Q}X_{1Q} + \ldots$$
$$+ b_{3Q}X_{3Q} + b_{12}X_1X_2 + \ldots + b_{34}X_3X_4 + e$$
$$= \hat{Y} + e$$

Where Y stands for the observed values of the dependent variable, $\hat{Y}$ stands for the corresponding values of the dependent

Table 3. SET OF CANDIDATE PREDICTIVE VARIABLES FOR THE SAMPLING TUBE PERFORMANCE EQUATION

Constant Term		
1.	$X_0 = 1$	
Linear Terms		
2.	X_1	Coded sample flow rate
3.	X_2	Coded transpiration flow rate
4.	X_3	Coded particle size
5.	X_4	Coded particle concentration
Quadratic Terms		
6.	X_{1Q}	Coded sample flow rate
7.	X_{2Q}	Coded transpiration flow rate
8.	X_{3Q}	Coded particle size
Interaction Terms (Product Variables)		
9.	$(X_1)(X_2)$	
10.	$(X_1)(X_3)$	
11.	$(X_1)(X_4)$	
12.	$(X_2)(X_3)$	
13.	$(X_2)(X_4)$	
14.	$(X_3)(X_4)$	

variable computed from the expression on the right, the X's are the coded values of the independent variables, the b's are the regression coefficients to be estimated from the experimental data, and e represents the differences between observed and computed values of the dependent variable due to residual variation or "experimental error" in the observations

5.5 Methods of Data Analysis

The experimental data were analyzed by the method of least squares in accordance with the model, resulting in the actual performance equation that is presented in the next section.

The computer program used, BMD-02R, performs stepwise multiple regression -- i.e., the equation is built up, term by term, by introducing at each step that candidate term which will result in the greatest reduction in the sum of squared deviations between the observed values of the dependent variable and the values computed from the regression equation (the error sum of squares). A cutoff point for this process can be set by the user of the program through choice of a threshold "F" value. The F value associated with the coefficient of a term in a regression equation is the square of the ratio of the coefficient to its standard error. In other words, no candidate term is introduced into the equation unless the value of the coefficient of that term is a specified multiple of its standard error. This excludes from the equation terms with coefficients of a magnitude that could readily arise due merely to the inevitable background or residual variation between measurements (experimental error). In the present analysis the threshold F value was set to correspond to a probability of 10%, i.e., no term was introduced if the regression coefficient was so small as to have that probability or higher of occurring due to random variation in the data.

An elaboration of the stepwise fitting procedure was made necessary by the occurrence of the tests in which upper

limits on percent deposition were obtained instead of point values. Such outcomes are called "censored observations" in statistical terminology. An iterative method was used to obtain the least-squares estimates of the regression coefficients taking into account the limit values resulting from the censored tests in conjunction with all point values. The stepwise regression procedure was performed at each iteration.

In the initial iteration the limit values from the censored tests were treated as if they were point values. Each limit value was then compared with the corresponding value computed from the fitted equation. If the computed value was smaller than the observed limit values, a trial value smaller than the limit value was substituted for the latter, to be used in the next iteration. If the computed value was no smaller than the limit value, the latter was retained. The iterative process was continued until a solution was reached at which, 1) all limit values smaller than corresponding computed values were retained as data points, and 2) all trial values from the previous iteration were equal to the corresponding computed values from the current iteration.

Information provided as computer output in conjunction with the fitted equation includes: an overall analysis of variance with respect to the terms in the equation and the residual degrees of freedom, the residual standard deviation, the multiple correlation coefficient, the coefficient of determination, the computed value and the standard error of each regression coefficient, the F ratios for all terms in the equation and all candidate terms not in the equation, and individual residuals for all observations.

5.6 The Particle Deposition Equation

The final particle deposition equation is presented in Table 4. Of the 14 candidate terms (Table 3) nine are in the equation; the remaining five were excluded in the fitting process because of lack of statistical significance at the

Table 4. PARTICLE DEPOSITION EQUATION

Dependent Variable:	$Y = \log_{10}(PD/(100-PD))$; PD is mass percent deposition
Data Base:	All test results
Number of Tests:	34
Number of Terms in Equation:	9
Residual Degrees of Freedom:	25
Residual Standard Deviation:	1.0659
Coefficient of Determination (R^2):	0.7505

Independent Variable		Regression Coefficient b	Standard Error s_b	Variance Ratio F
Constant Term				
$X_0 = 1$		-2.2889		
Linear Terms				
X_1	Sample Flow Rate, Coded	-0 4960	0.2258	4.83
X_2	Transpiration Flow Rate, Coded	-0.2002	0.0933	4.60
X_3	Particle Size, Coded	0.8011	0.2381	11.32
X_4	Particle Concentration, Coded	0.3327	0 2105	2.50
Quadratic Term				
X_{3Q}	Particle Size, Coded	0.3246	0.1292	6.31
Interaction Terms				
$(X_1)(X_2)$		0.2941	0.1046	7.91
$(X_1)(X_3)$		-1.3172	0.2888	20.80
$(X_2)(X_3)$		-0.2355	0.1142	4.25

10% probability level. All four candidate linear terms appear (the term for particle concentration is of marginal significance). Of the three candidate quadratic terms only the term referring to particle size is present. Of the six candidate interaction terms three are present, representing interactions between 1) sample flow rate and transpiration flow rate, 2) sample flow rate and particle size, and 3) transpiration flow rate and particle size. The F values associated with all the terms in the equation except the term involving X_4 (coded particle concentration) are sufficiently large that the effects are clearly of importance in understanding and predicting particle deposition in porous or non-porous sampling tubes.

The effects represented by the individual terms of the equation can be examined separately. For instance, the linear term for particle size has a relatively large F value, indicating quite a strong effect, and the regression coefficient is positive, so that as particle size increases the rate of deposition also increases. The quadratic term for particle size is definitely significant and the coefficient is positive, so the curve associated with the quadratic effect is concave upward, and so on. To understand the net effect on particle deposition (taking into account all the terms of the equation) as the four controlled factors, or any subset, are varied, tables and families of curves can be constructed by solving the equation for specified combinations of factor levels. Curves of this nature are presented below.

5.7 Residuals

The observed and calculated values are listed in Table 5 for both the transformed dependent variable Y and the percent deposition PD. The calculated PD values were obtained by backward transformation of the calculated Y values. The Y residuals (observed minus calculated values) are also given. As noted, in five of the seven cased in which the recorded

Table 5. OBSERVED AND CALCULATED VALUES OF THE DEPENDENT VARIABLE AND RESIDUALS

Combination	Y_{OBS}	Y_{CAL}	Residual $Y_{OBS}-Y_{CAL}$	Percent Deposition PD_{OBS}	Percent Deposition PD_{CAL}
1	<-2.698	-3.678	*	<0.2	0.021
2	-2.795	-2.314	-0.482	0.160	0.483
3	1.954	1.664	0.290	98.9	97.9
4	<-2.698	-3.495	*	<0.2	0.032
5	-3.229	-3.236	0.007	0.059	0.058
6	1.380	-0.364	1.744	96.0	30.2
7	<-2.698	-4.030	*	<0.2	0.009
8	-3.657	-3.592	-0.065	0.022	0.026
9	-3.366	-1.874	-1.494	0.043	1.325
10	<-2.698	-3.131	*	<0.2	0.074
11	-3.537	-2.419	-1.119	0.029	0.380
12	1.916	-0.424	2.340	98.8	27.4
13	<-2.698	-3.065	*	<0.2	0.086
14	-3.387	-3.458	0.070	0.041	0.035
15	0.171	-1.237	1.408	59.7	5.48
16	-2.299	-2.327	0.028	0.500	0.469
17	-3.745	-3.871	0.127	0.018	0.013
18	-3.456	-2.803	-0.653	0.035	0.157
19	<-2.522	-1.919	-0.603	<0.3	1.191
20	-3.155	-3.189	0.034	0.070	0.065
21	-3.769	-3.177	-0.592	0.017	0.066
22	<-2.396	-1.970	-0.427	<0.4	1.061
23	-3.721	-3.014	-0.707	0.019	0.097
24	-3.959	-2.776	-1.183	0.011	0.167
25	-1.219	-1.289	0.070	5.70	4.89
26	-1.934	-3.485	1.551	1.15	0.033
27	-3.244	-3.069	-0.175	0.057	0.085
28	-3.252	-2.219	-1.033	0.056	0.600
29	-1.628	-2.478	0.850	2.30	0.332
30	1.440	3.172	-1.732	96.5	99.9
31	1.557	0.477	1.080	97.3	75.0
32	-1.848	-2.005	0.157	1.40	0.979
33	-2.088	-3.383	1.295	0.810	0.041
34	-1.495	-0.627	-0.868	3.10	19.11

* The observed value is an upper bound and the calculated value is less than the upper bound.

deposition is an upper bound the computed value is less than that upper bound. In these five cases there is no meaningful residual.

The estimate, s, of the standard deviation of residuals is 1.066 (Table 4). The degree of determination, R^2, is 0.75; in other wards, about 3/4 of the raw variability of Y (as measured by sum of squared deviations from the mean) is explained by the terms in the regression equation.

A plot of calculated vs. observed Y values (Figure 19) shows no extreme outliers. One of the 29 points lies somewhat outside the 2-sigma limits; this is test combination 12.

The cumulative percentage of residuals is plotted against the values of the residuals on normal probability paper in Figure 20. Considering the limited number of observations, the approach to a straight line is reasonably good.

5.8 Plots of Functional Relationships Between Particle Deposition and the Experimental Factors

Families of curves are presented (Figures 21-24), derived from the particle deposition equation, to show the net effects of changes in the experimental factors. In each figure the three separate lines represent percent deposition as a function of transpiration flow rate for particles of size 0.05, 1.6, and 50 μm diameter. In Figure 21 particle concentration is low and sample flow rate is low, 7.1 lpm (0.25 cfm). In Figures 22, 23, and 24 particle concentration is high and the sample flow rates are 7.1, 14.2, and 28.3 lpm (0.25, 0.5, and 1.0 cfm), respectively. Figure 25 shows calculated percent deposition as a function of particle size at intermediate levels of sample flow rate, transpiration flow rate, and particle concentration.

5.9 Discussion and Conclusions

From the fairly small but carefully designed set of tests that have been conducted, the major effects of sample flow

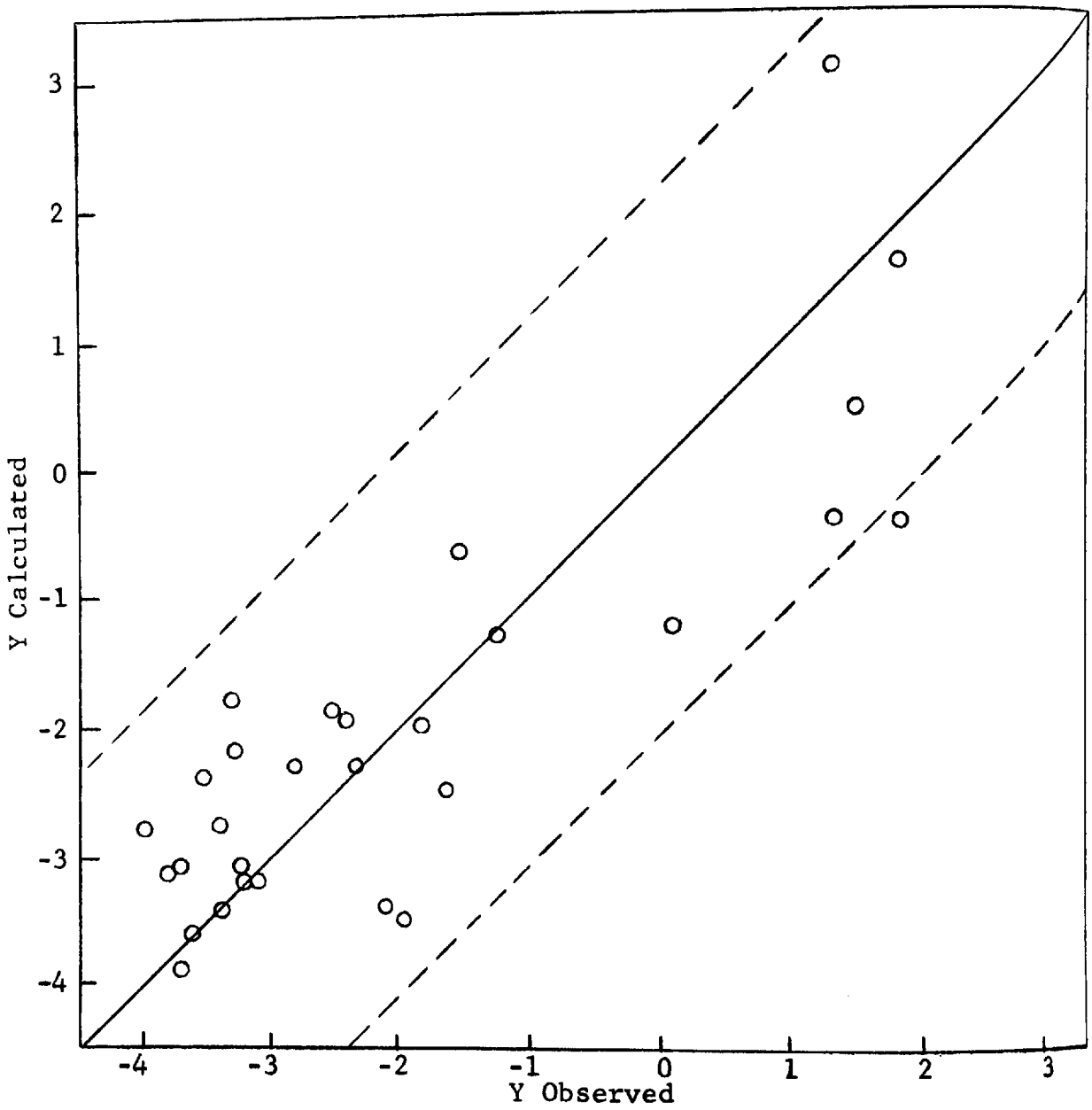

Figure 19. Plot of Observed vs. Calculated Values of the Dependent Variable Y

(The line of perfect agreement and the $\pm 2\sigma$ lines are shown.)

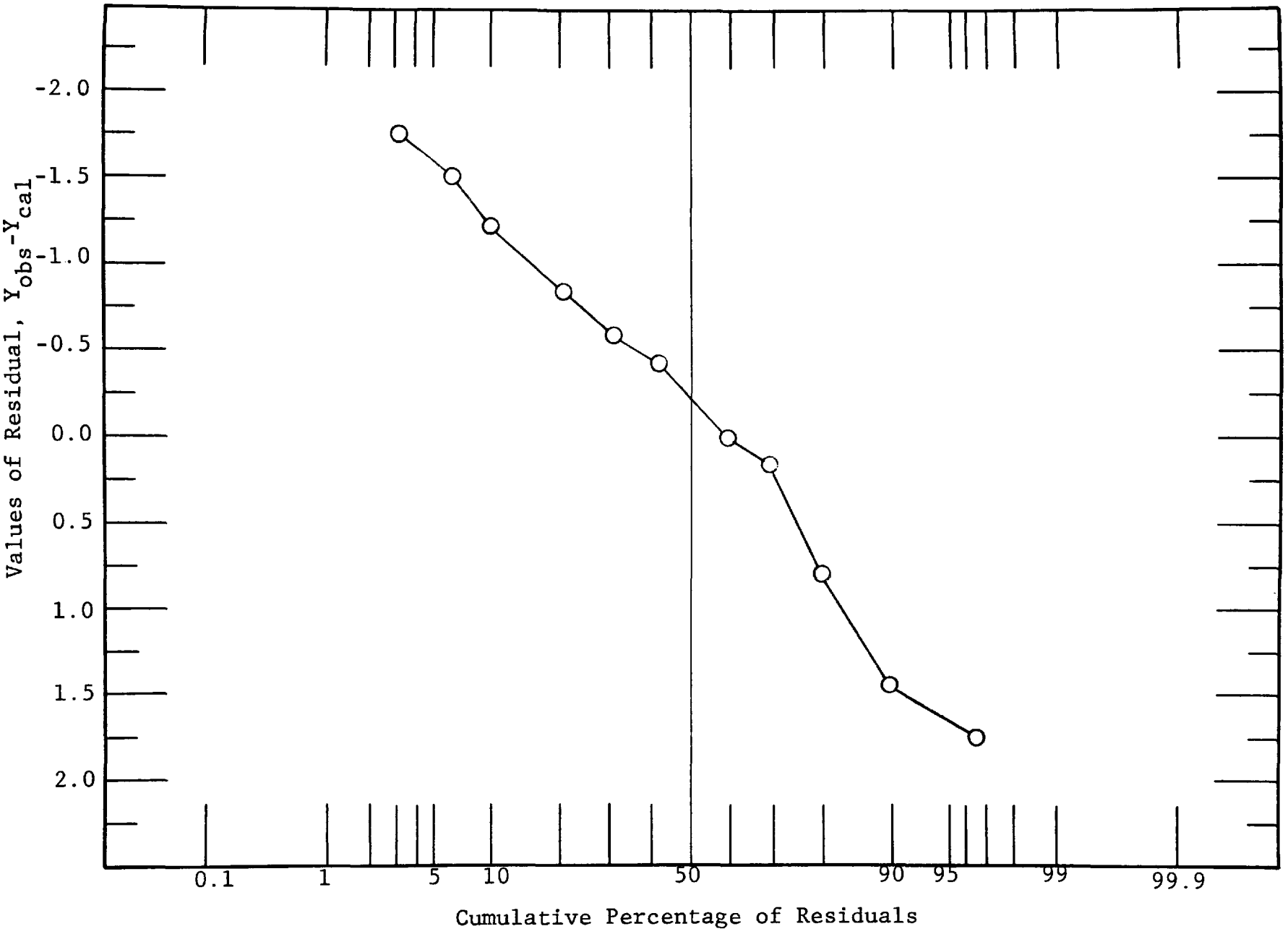

Figure 20. Plot of Cumulative Percentage of Residuals on Normal Probability Paper

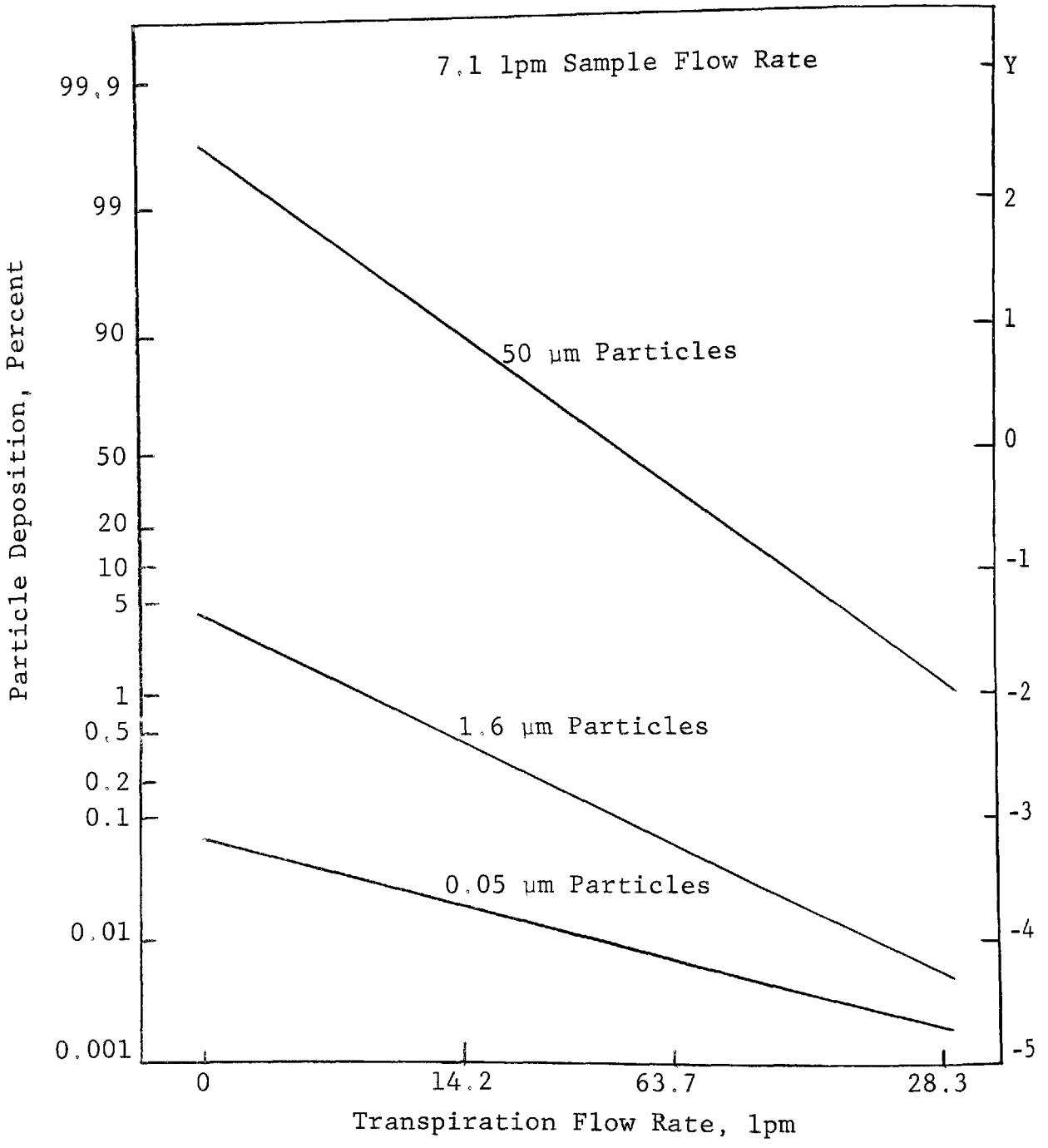

Figure 21. Deposition of Small, Medium, and Large Particles vs. Transpiration Flow Rate with Low Particle Concentration and Low Sample Flow Rate

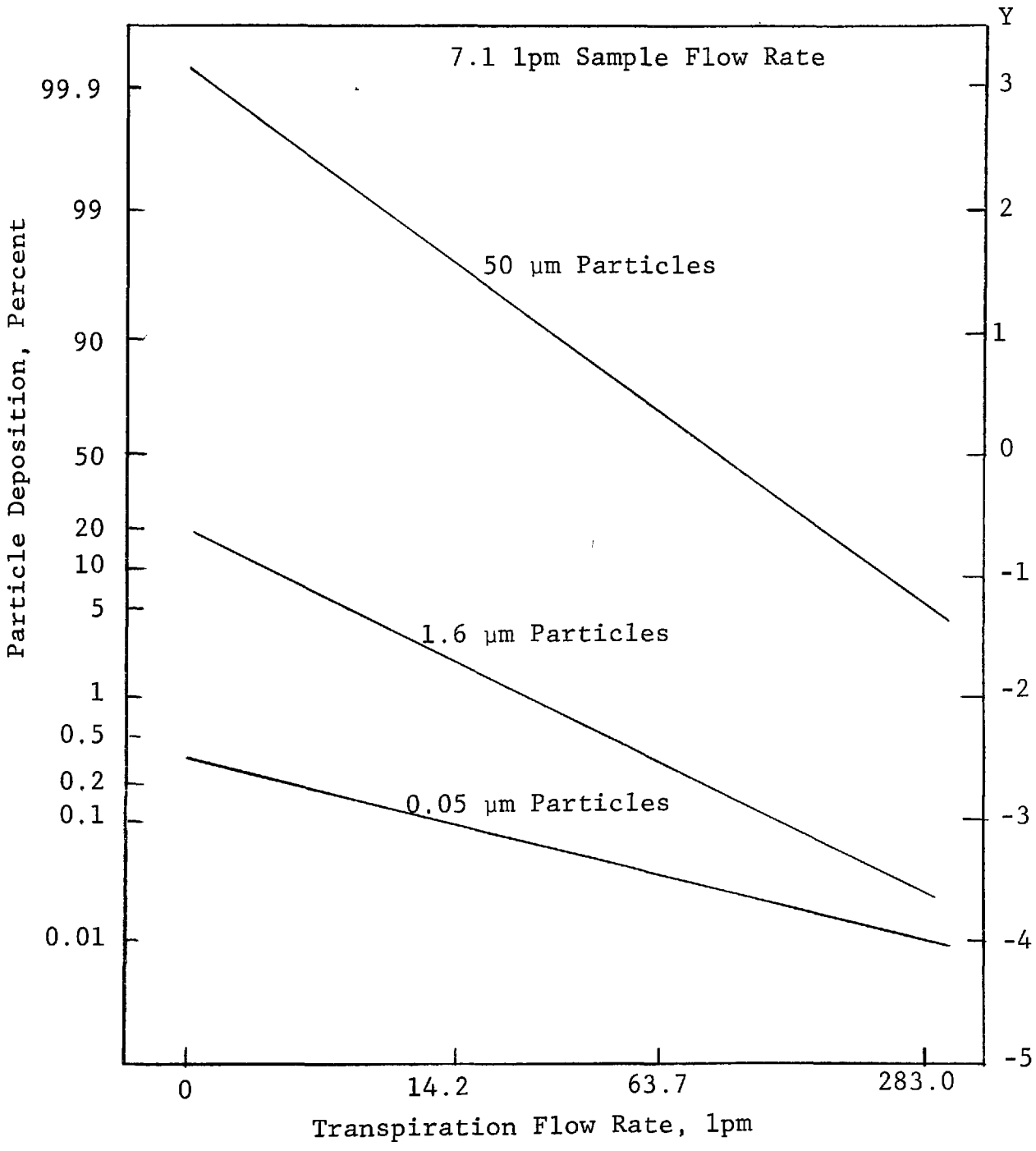

Figure 22. Deposition of Small, Medium, and Large Particles vs. Transpiration Flow Rate with High Particle Concentration and Low Sample Flow Rate

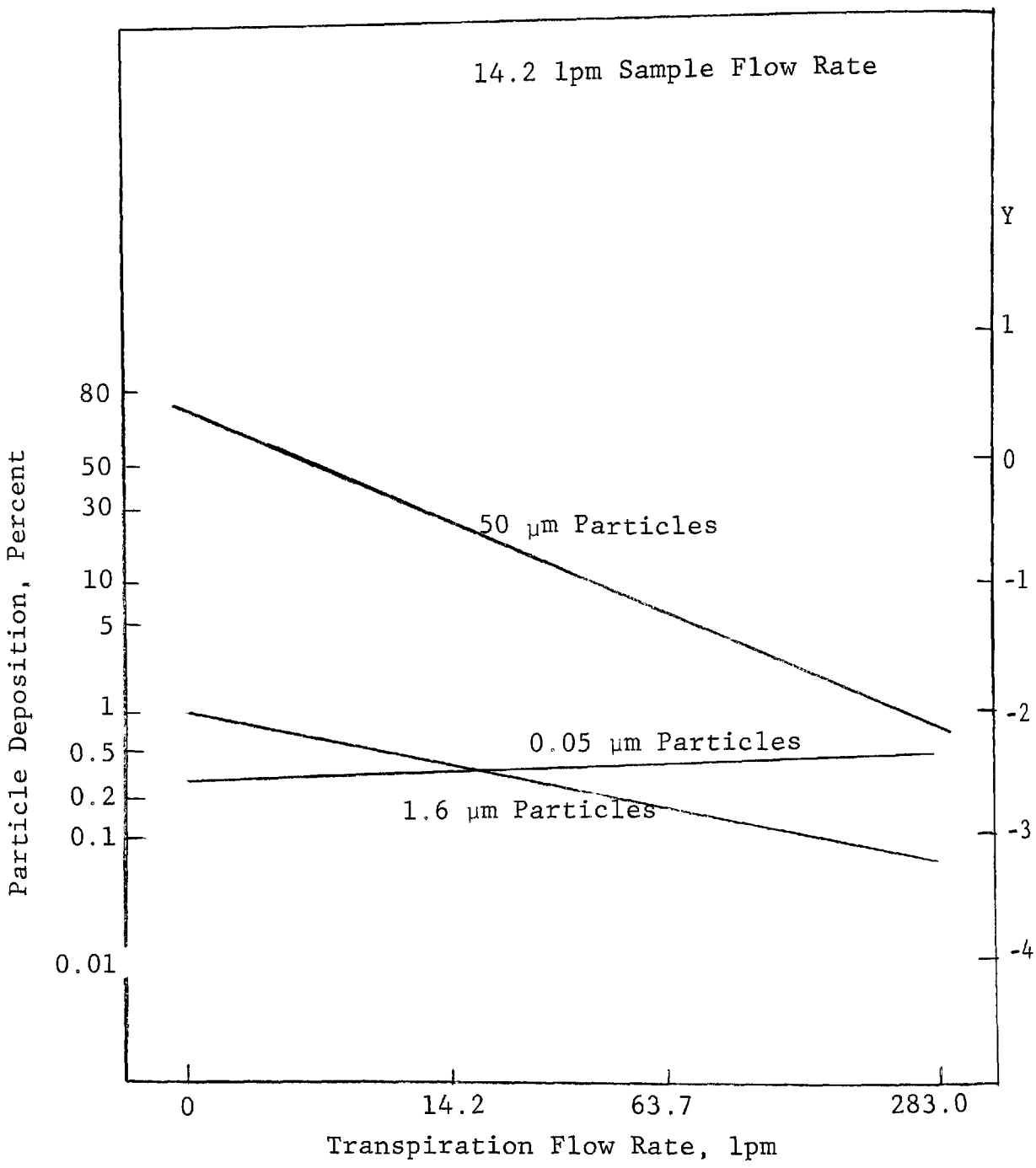

Figure 23. Deposition of Small, Medium, and Large Particles vs. Transpiration Flow Rate with High Particle Concentration and Medium Sample Flow Rate

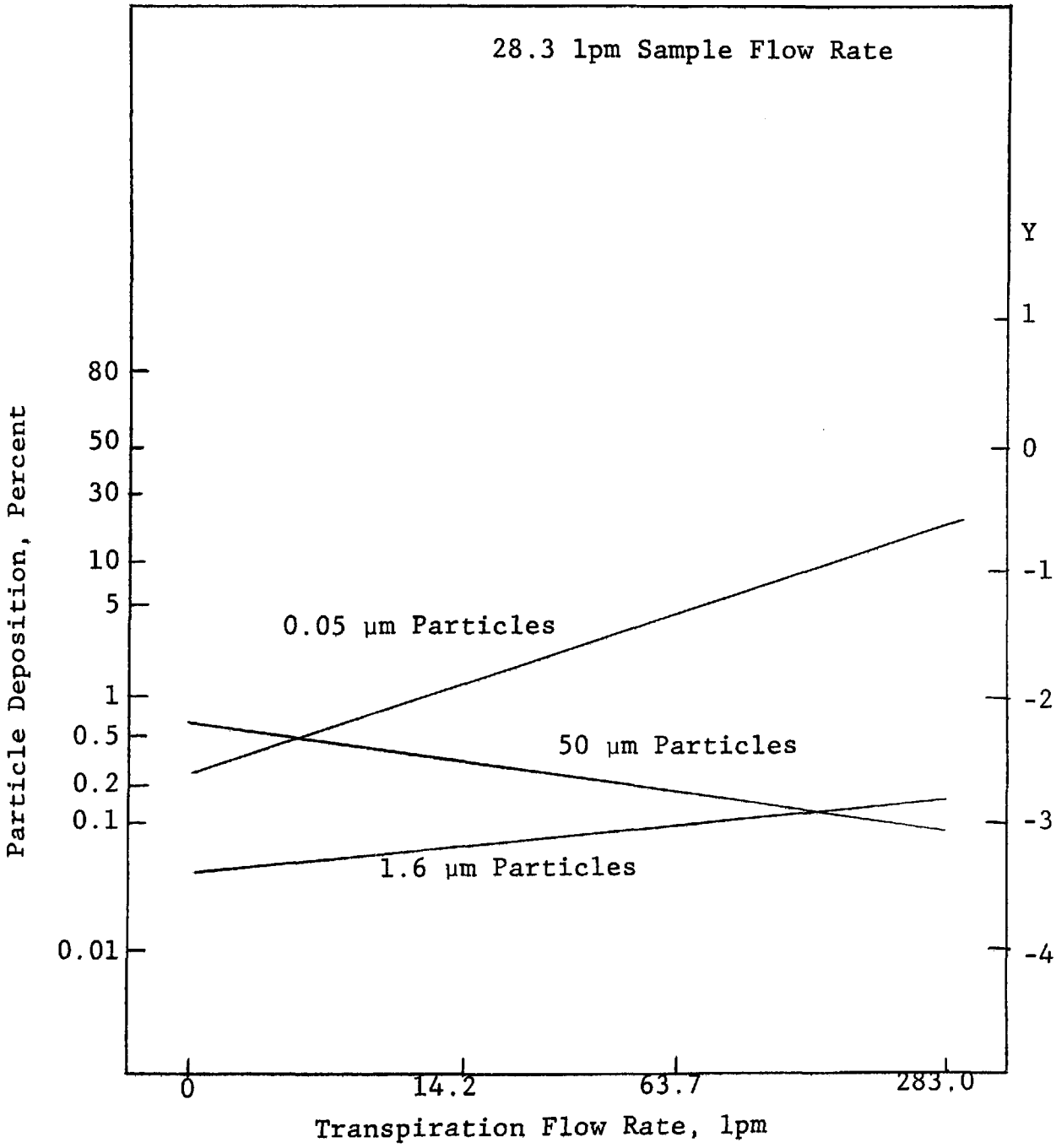

Figure 24. Deposition of Small, Medium, and Large Particles vs. Transpiration Flow Rate with High Particle Concentration and High Sample Flow Rate

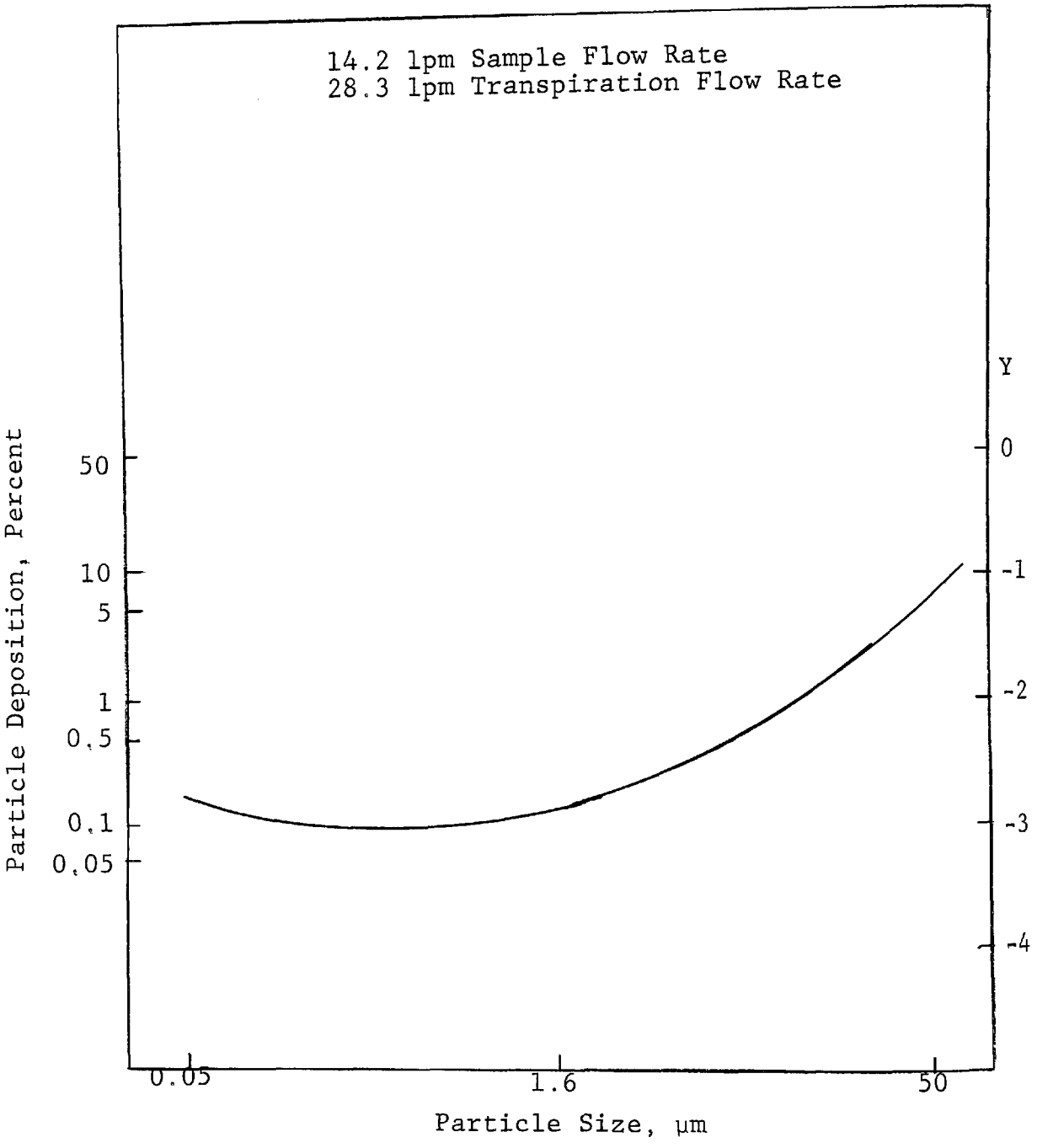

Figure 25. Deposition of Particles in Relation to Particle Size at Intermediate Levels of Particle Concentration, Sample Flow Rate, and Transpiration Flow Rate

rate (SFR), transpiration flow rate (TFR), particle size (PS), and particle concentration (PC), on the mass percent particle deposition (PD) in porous sampling tubes have been clearly brought out. A non-porous sampling tube was included as a control. A single predictive performance equation was developed from the combined data incorporating the significant relationships among the variables.

The analysis was facilitated by application of suitable mathematical transformations to the variables. The independent linear variables X_1, X_2, X_3, and X_4 are orthogonally coded logarithmic transforms of the physical variables SFR, TFR, PS, and PC, respectively, X_{1Q}, X_{2Q}, and X_{3Q} similarly are quadratic variables for SFR, TFR, and PS. The dependent variable Y, which is of the form log (p/(1-p)) where P is a proportion, expands the PD scale with endpoints of 0 and 100% to a scale with unlimited range in both directions. The transformations have the desired properties of simplifying the representation of the systematic effects of the controlled factors and providing approximate uniformity of variance for the measure of performance. Results can be readily translated back into the original scale of physical measurement.

The statistical analysis of the data has been made within the framework of a multivariate regression model. The model includes candidate terms representing all the first and second order effects, including interaction effects, of the independent variables on which the experiment furnishes evidence. The actual equation, developed from the data by a stepwise least-squares method, includes nine of the 14 candidate terms. All four controlled factors are represented in the equation. Graphs of some of the functional relationships implicit in the equation have been constructed. Other graphs and tables can be prepared if desired by solving the equation for specified combinations of values of the independent variables, including combinations not included in the experiment.

Some principal substantive conclusions are as follows:

(1) Of the four factors investigated, particle concentration has the least effect on percent deposition. The linear term in X_4, which is marginally significant statistically, has a positive regression coefficient, indicating some increase in percent deposition as particle concentration changes from low to high. The candidate quadratic term of this factor did not come into the equation, nor did any interaction term involving the factor. Comparison of Figure 22 with Figure 21 shows the contrast between high and low particle concentration, i.e., the shift upward of all three curves relating deposition to transpiration flow rate.

(2) Deposition depends strongly on the size of the particles being sampled. The equation includes both a linear term in X_3 and a quadratic term in X_{3Q} to represent the effect of this factor when the other factors are held constant at their intermediate levels, and particle size is involved in interactions with both sample flow rate (X_3 times X_1) and transpiration flow rate (X_3 times X_2). The calculated curve of percent deposition vs. particle size at intermediate levels of SFR, TFR, and PC is shown in Figure 25. The curve combines the linear effect associated with the variable X_3 and the quadratic effect associated with X_{3Q}. Very little difference between 0.05 and 1.6 μm particles is indicated. The 50 μm particles, however, have a substantially higher deposition rate: between 5 and 10% as contrasted with the range 0.1 to 0.5% for the smaller particles. The three-way interactions involving particle size, sample flow rate, and transpiration flow rate are illustrated by Figures 22, 23, and 24 and discussed below under point 5.

(3) Sample flow rate and transpiration flow rate are both important factors with respect to the proportion of the particle mass trapped in the sampling tube. The main effects of both SFR and TFR are captured in the equation by linear

terms -- in X_1 and X_2, respectively; the absence of the quadratic terms means that there is no evidence of a departure from linearity in either case when other factors are held constant. There is an interaction between SFR and TFR (term in X_1 times X_2) and an interaction of each with particle size (terms in X_1 times X_3 and X_2 times X_3). There is a certain degree of parallelism in the effects of SFR and TFR as evidenced by the similarity in the terms brought into the equation and the fact that the coefficients of like terms have the same sign.

(4) Since the sign of the term in X_1 (coded sample flow rate) is negative, the simple effect of increasing SFR, holding other factors at their intermediate settings, is to decrease the deposition. The interactions of SFR with TFR and particle size substantially modify the influence of this factor: compare Figures 22, 23, and 24, which differ due to increasing SFR. The interactions involving SFR, TFR, and PS are discussed under the following point.

(5) The effect of transpiration flow rate on percent particle deposition is represented in the equation by a linear term in X_2 and cross-product terms involving sample flow rate (X_2 times X_1) and particle size (X_2 times X_3). The coefficients of these terms are all negative. Therefore, the main effect of increasing transpiration flow from zero (non-porous tube) to the maximum level tested (10 cu ft/min), with the other factors at intermediate levels, is to reduce the proportion of the particle mass that is deposited on the walls of the sampling tube. Taking into account the interactions with sample flow rate and particle size, and also the interaction between the latter two factors, one sees a more complex picture. The relationships are shown by Figures 22, 23, and 24. At all levels of sample flow rate tested, increasing the transpiration flow rate is effective in lowering the deposition of large particles. The slope (Y vs. X_2) is steepest at the low sample flow rate and becomes progressively less

steep while remaining negative. Under conditions of a high concentration of large particles and a low sample flow rate of 7.1 lpm (0.25 cfm) the estimated effect of increasing the transpiration flow rate from zero to 283 lpm (10 cfm) is to reduce sharply the deposition, from more than 99.9% to about 5%. At the higher levels of SFR the percentage deposition of large particles is brought considerably lower than at low SFR as TFR increases from zero to 283 lpm (10 cfm), but the reference values at zero TFR are also much lower. At low SFR, the porous tube with increasing rates of transpiration flow reduces deposition over the entire range of particle sizes tested (Figure 22). At the intermediate SFR the data indicate a continued effect of transpiration on reducing deposition of medium sized particles, but little or no effect on small particles. At high SFR, the range of variation of particle deposition rate is markedly damped. Increasing the TFR is indicated to actually increase the rate of deposition of intermediate sized, and especially small, particles.

PHASE II

PRESERVATION OF SIZE DISTRIBUTION OF AEROSOL IN TRANSPORT THROUGH THE SAMPLING INTERFACE

6 EXPERIMENTAL PROGRAM FOR PHASE II

Phase II is concerned with the preservation of aerosol size distribution. The experimental program included a series of tests with aerosols covering particle size range of 0.05-50 μm. Originally, the three aerosols KCl, 1-MAAQ and Uranine used in the Phase I were to be used for these tests. On suggestion by EPA, another aerosol, flyash, was added to the experimental plan. Sample flow rates of 7.1 lpm (0.25 cfm) and 28.3 lpm (1 cfm) were used. The transpiration flow rate also varied from 14.2 lpm (0.5 cfm) to 283 lpm (10 cfm). In addition, on suggestion by EPA, tests with a 1.27 cm (½") diameter pyrex tube were also planned. The experimental plan is presented in Table 6.

6.1 Tests with KCl Aerosol

Two aerosols were used to cover the nominal size ranges of 0.01-0.1 μm. For the 0.01-0.1 μm aerosol the generator used on Phase I was used. It operates by vaporization from a plug of salt in an electrically heated nichrome coil. At an air flow of 7.1 lpm (0.25 cfm) and a voltage of 31 volts across the 5 ohm coil, a satisfactory test aerosol was obtained.

In test K-1, the aerosol was directly transferred to the porous-probe at a rate of 7.1 lpm (0.25 cfm). A transpiration flow rate of 14.2 lpm (0.5 cfm) was used. In test K-2, the sample flow rate was increased to 28.3 lpm (1 cfm) by adding clean air to the aerosol. The transpiration flow rate was maintained at 14.2 lpm (0.5 cfm). Size distribution at the inlet to the porous probe and at the outlet were measured with an electric mobility analyzer. The principle and operation of this device is described in Appendix A.

For test K-3 and K-4, the nebulizer shown in Figure 26 was used to cover particle size range of 0.1-1.0 μm.

Table 6. PHASE II EXPERIMENTAL PROGRAM

Test No.	Aerosol	Sample Flow Rate (lpm)	Transpiration (lpm)	Probe	Size Assessment Technique
K-1	0.01-0.10 μm KCl	7.1	14.2	Porous	Electrical mobility
K-2	" " "	28.3	14.2	"	"
K-3	0.10-1.0 μm KCl	7.1	14.2	Porous	"
K-4	" " "	28.3	14.2	"	"
K-5	0.01-1.0 μm KCl	7.1	0	Pyrex	"
U-1	1-50 μm Uranine	7.1	141.0	Porous	Imanco Quantimet 720
U-2	" "	28.3	141.0	"	" " "
U-3	" "	7.1	283.0	"	" " "
U-4	" "	28.3	14.2	"	" " "
U-5	" "	7.1	0	Pyrex	" " "
F-1	1-50 μm Flyash	7.1	141.0	Porous	Optical microscopy
F-2	" "	28.3	141.0	"	" "
F-3	" "	7.1	283.0	"	" "
F-4	" "	28.3	14.2	"	" "
F-5	" "	7.1	0	Pyrex	" "
M-1	1.6 μm 1-MAAQ	28.3	14.2	Porous	" "
M-2	" "	7.1	14.2	"	" "
M-3	" "	28.3	63.7	"	" "
M-4	" "	7.1	63.7	"	" "
M-5	" "	7.1	0	Pyrex	" "

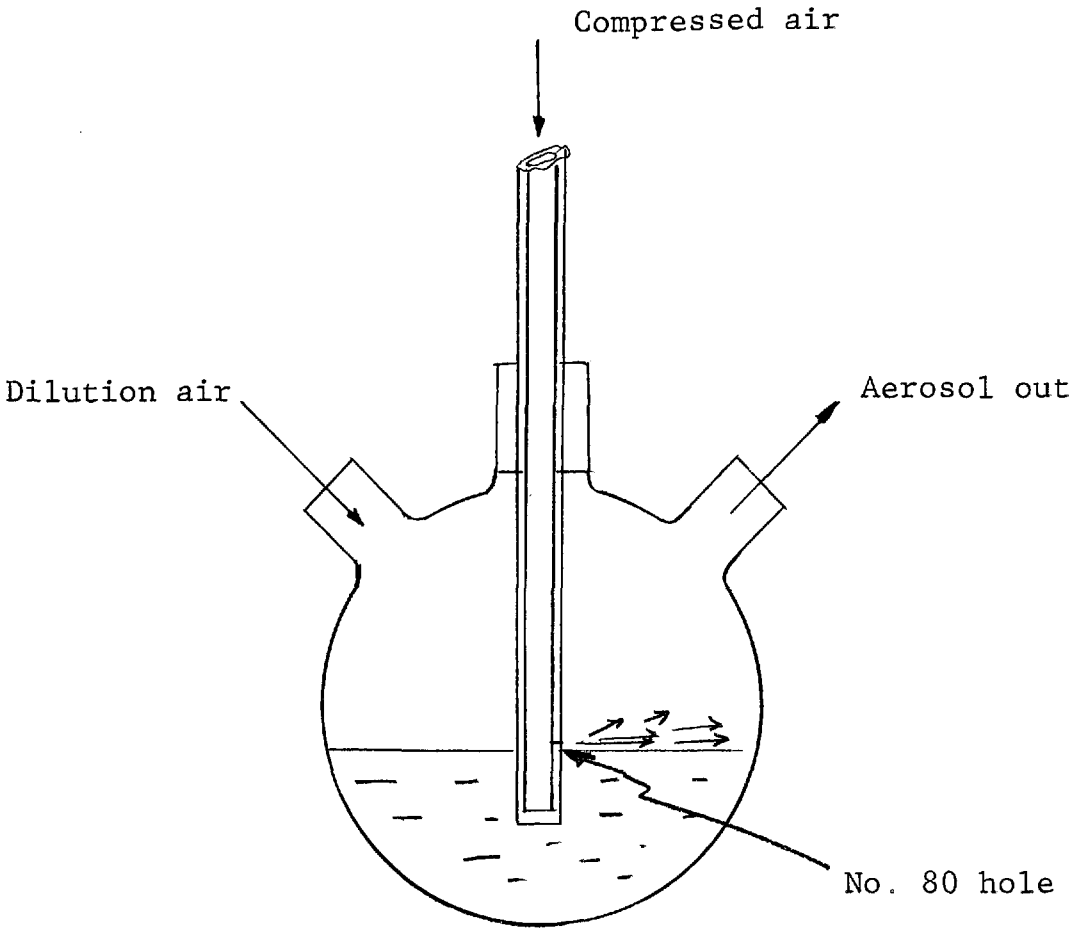

Figure 26. Nebulizer for KCl Aerosol Generation

For run #K-3, a 10% w/v solution of KCl in water was nebulized at a flow rate of 3.5 lpm (0.124 cfm) and was diluted by 3.6 lpm (0.126 cfm) of clean dry air. This was fed directly to the nozzle of the porous probe. For run #K-4, the KCl solution was nebulized at 7.1 lpm (0.25 cfm) air flow rate and was diluted by adding dry clean air to 28.3 lpm (1.0 cfm).

For run #K-5, a different nebulizer was used to cover the entire range 0.01-1.0 μm. This nebulizer is shown in Figure 27. The total sample flow rate was 7.1 lpm (0.25 cfm).

The size distributions of the KCl aerosol at the inlet and at the outlet of the porous probe, for all tests with KCl were measured by the electric mobility analyzer described in Appendix A. The data reduction is also described in Appendix A.

The data are presented in Figures 28 to 32. The Y axis represents the frequency of particles in a small differential interval of the logarithm of the particle size. This is plotted against the logarithm of particle size represented on the X-axis. The symmetrical shape of these curves (Figures 28-32) indicates that the distribution is log normal. The geometric standard deviation is obtained by dividing the GNMD by the size representing 60% of the peak value.

In Table 7, the size distribution parameters for all the KCl tests are presented. From these parameters log-normal plots were constructed for all the runs (Figures 33-37).

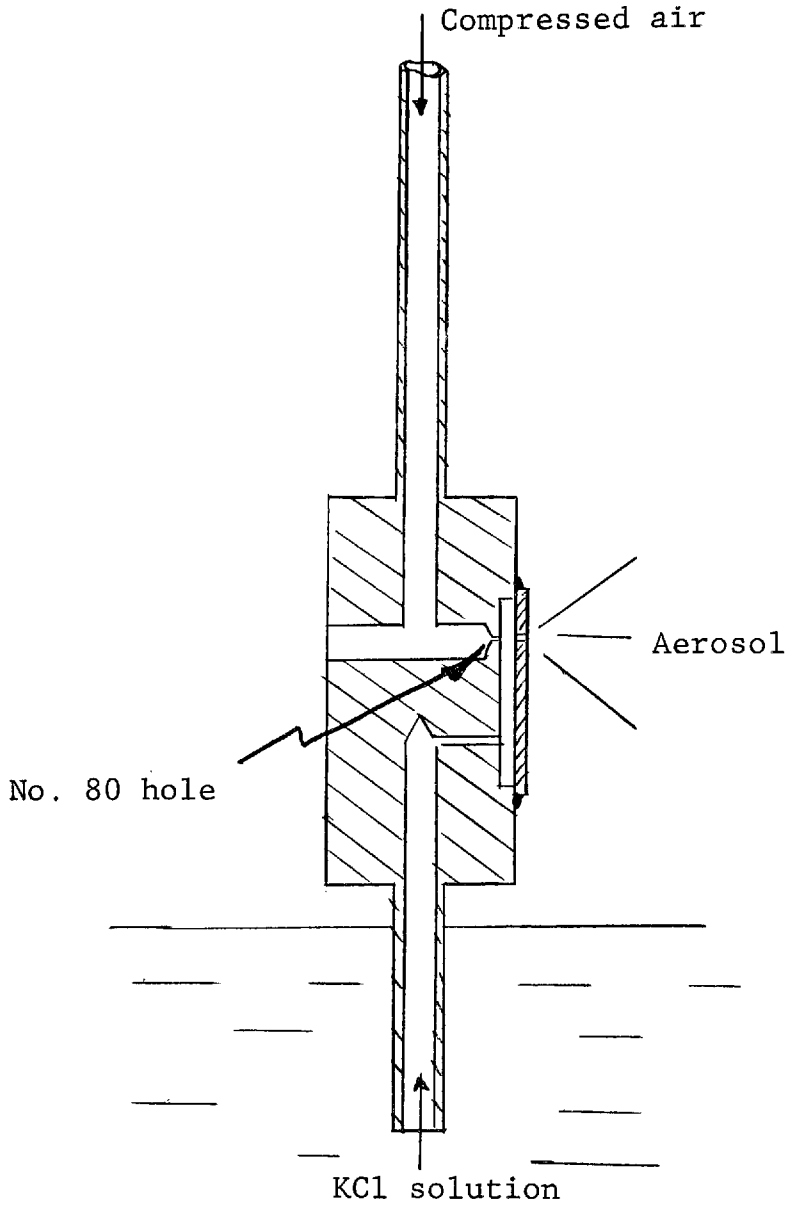

Figure 27. Nebulizer for Test K-5

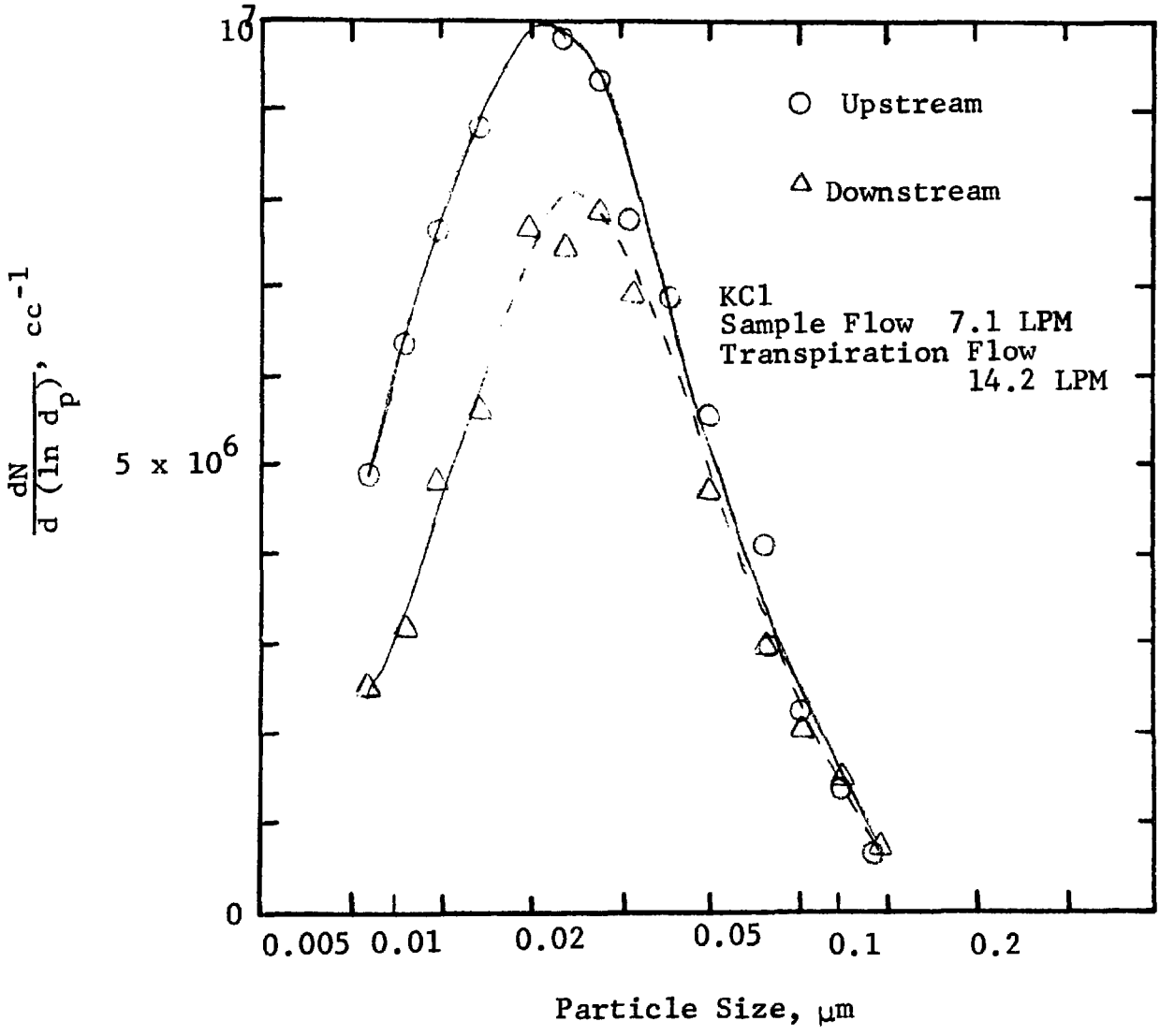

Figure 28. Size Distributions for Test K-1

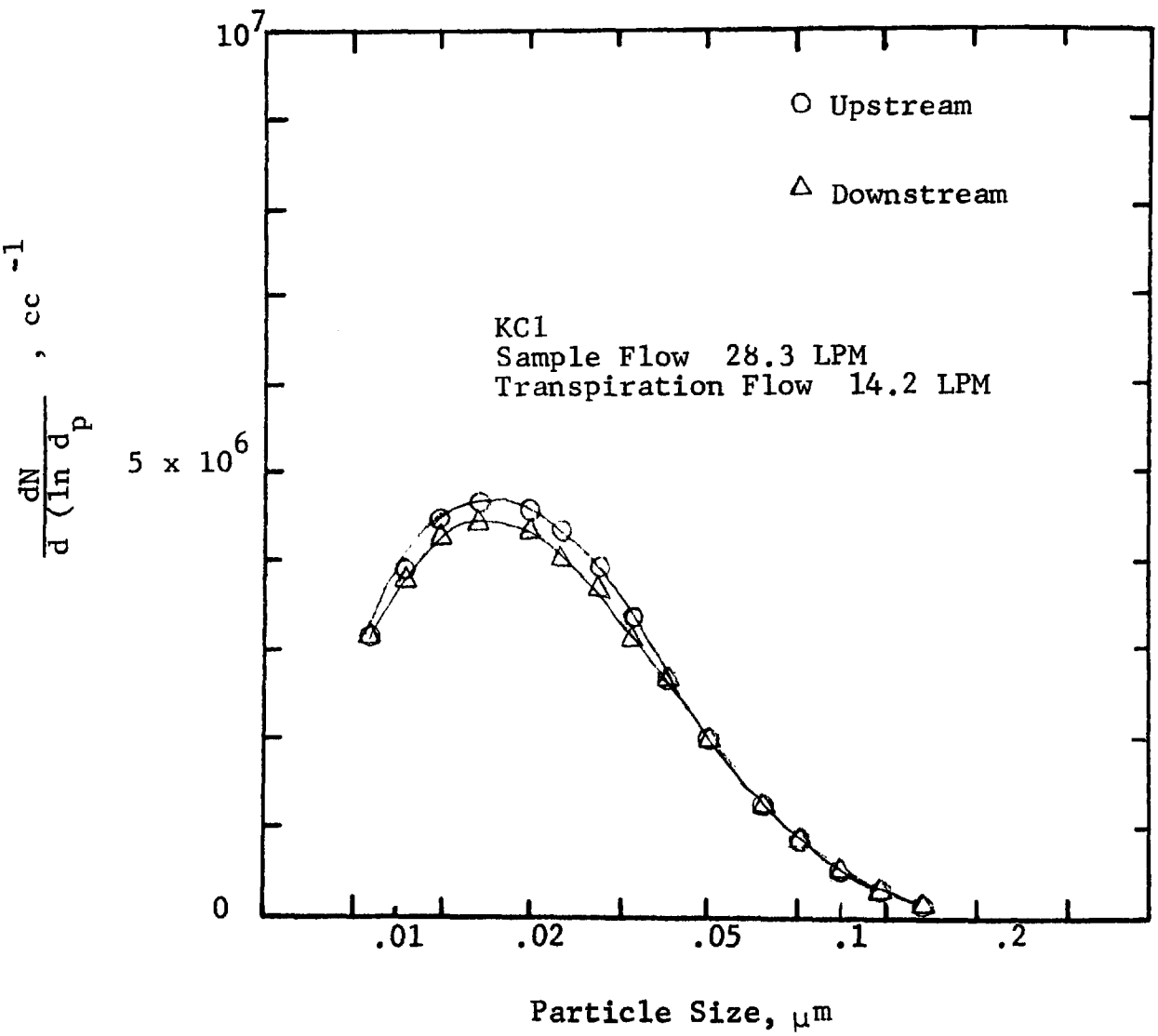

Figure 29. Size Distributions for Test K-2

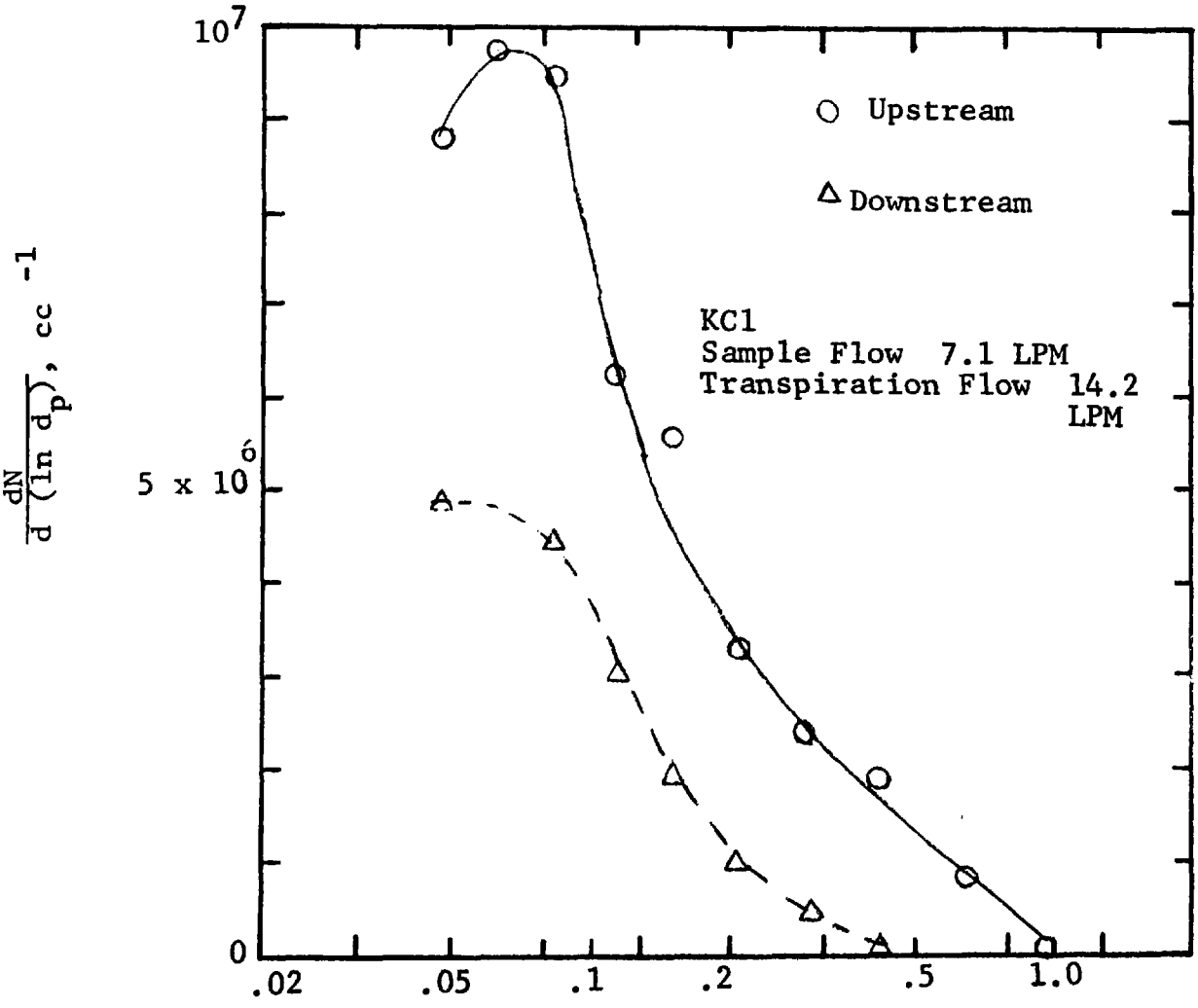

Figure 30. Size Distributions for Test K-3

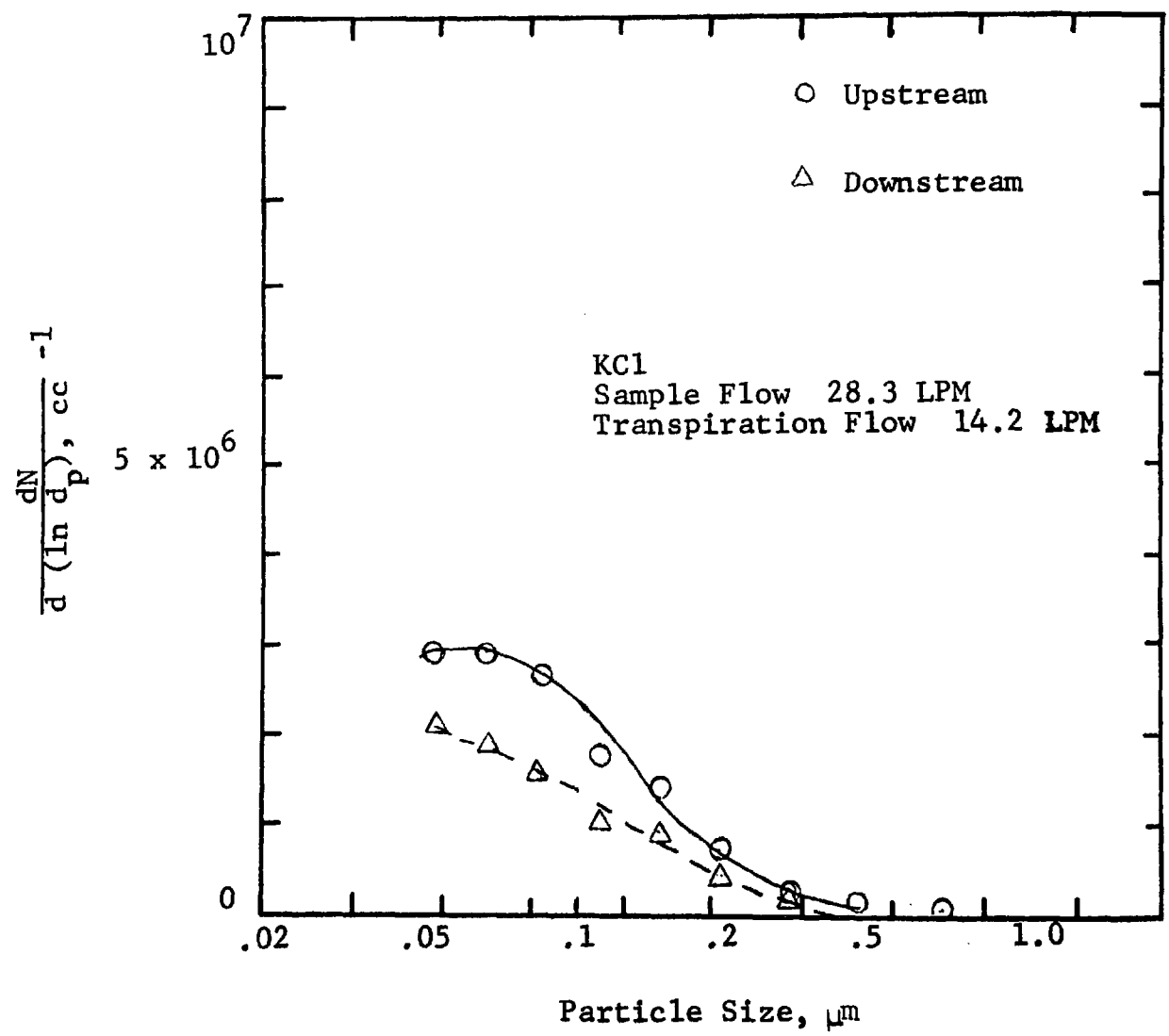

Figure 31. Size Distributions for Test K-4

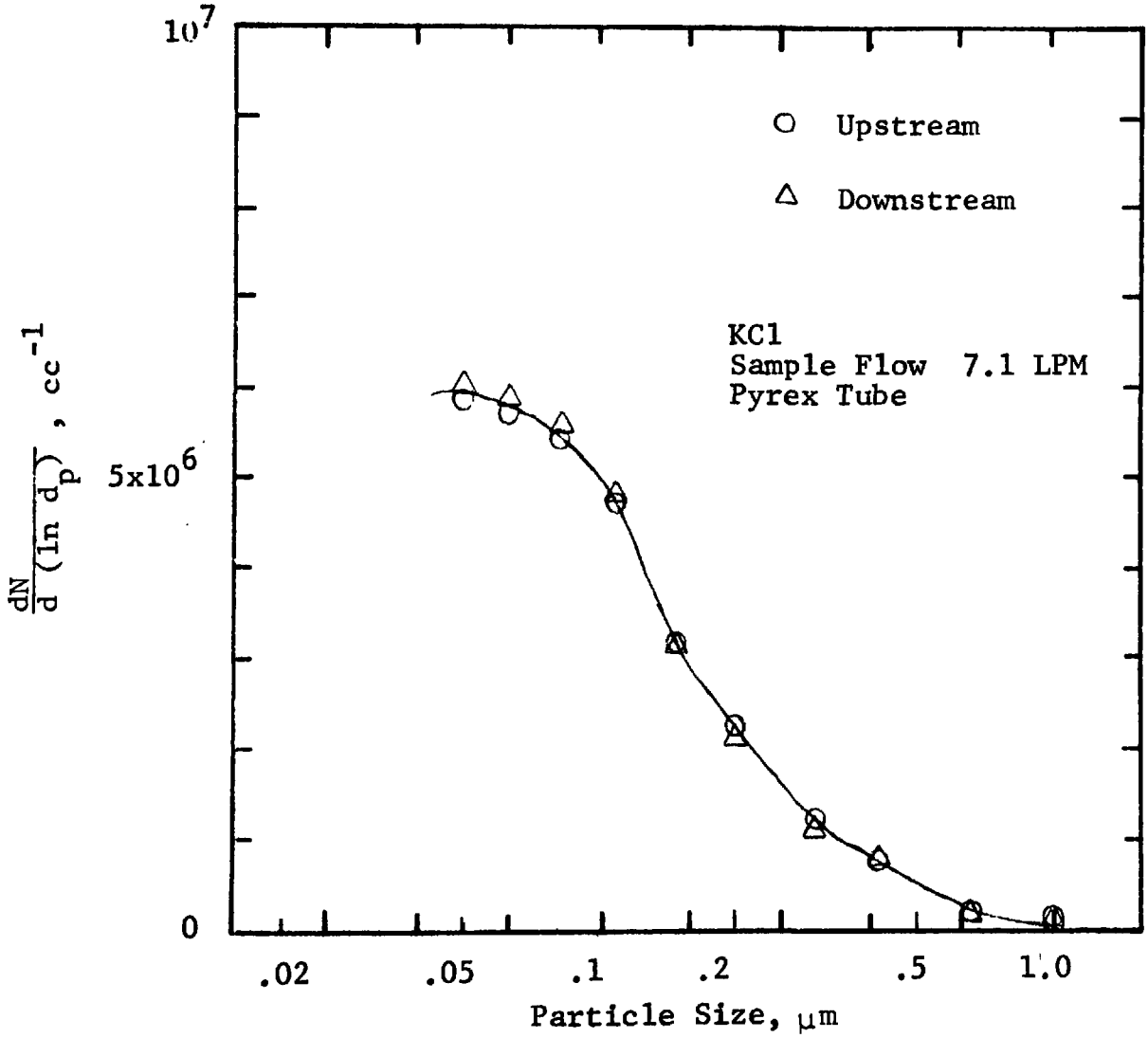

Figure 32. Size Distributions for Test K-5

Table 7. SIZE DISTRIBUTION DATA FOR TESTS WITH KCl AEROSOL

Test No.	Sample Flow Rate (lpm)	Transpiration Flow Rate (lpm)	Upstream GNMD µm	Upstream σg	Downstream GNMD µm	Downstream σg
K-5	7.1	0	0.045	2.8	0.045	2.8
K-1	7.1	14.2	0.021	2.0	0.025	2.0
K-3	7.1	14.2	0.07	1.8	0.05	2.5
K-2	28.3	14.2	0.016	2.5	0.016	2.5
K-4	28.3	14.2	0.045	2.6	0.06	2.2

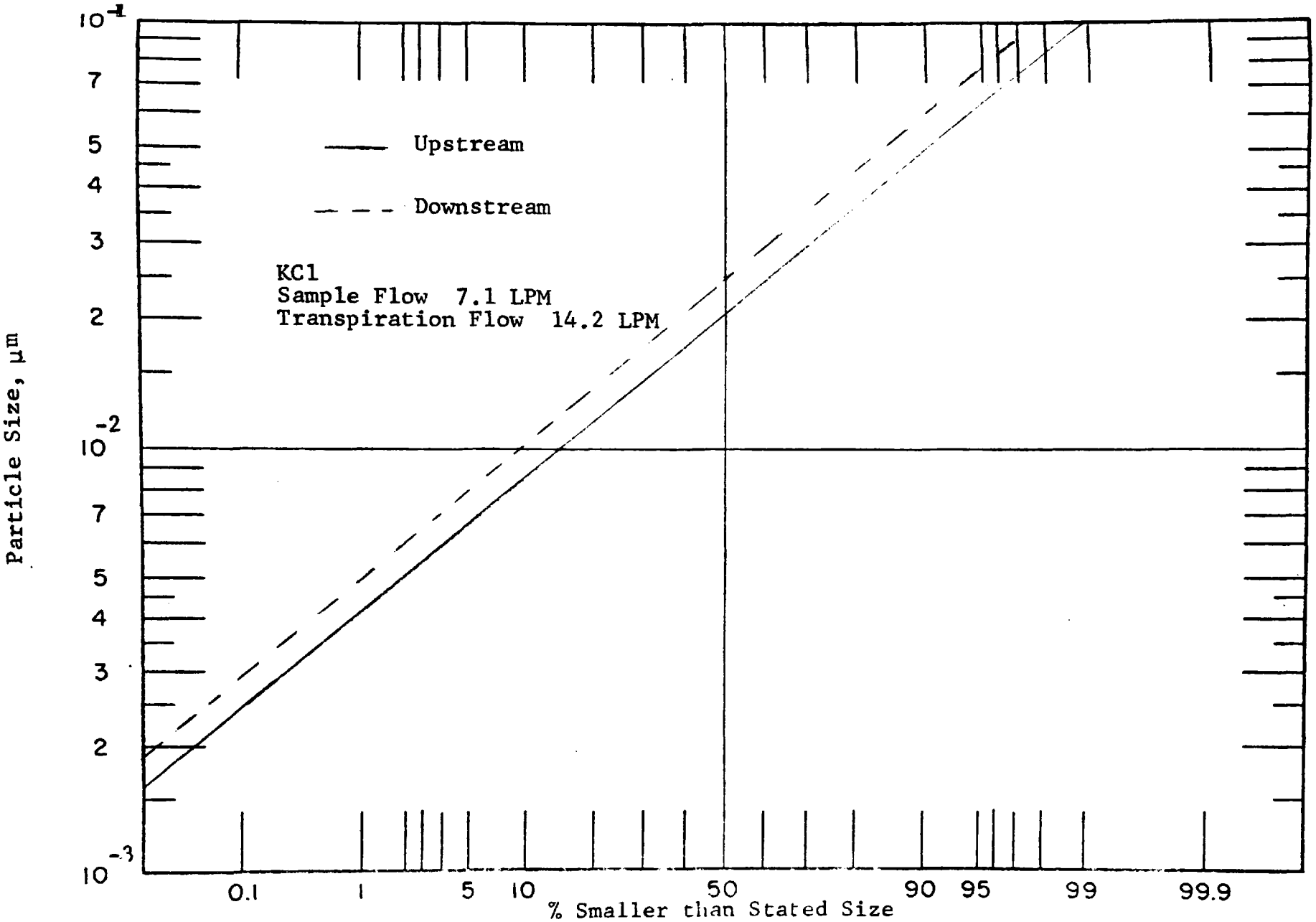

Figure 33. Log-Probability Plot of Size Distributions for Test K-1

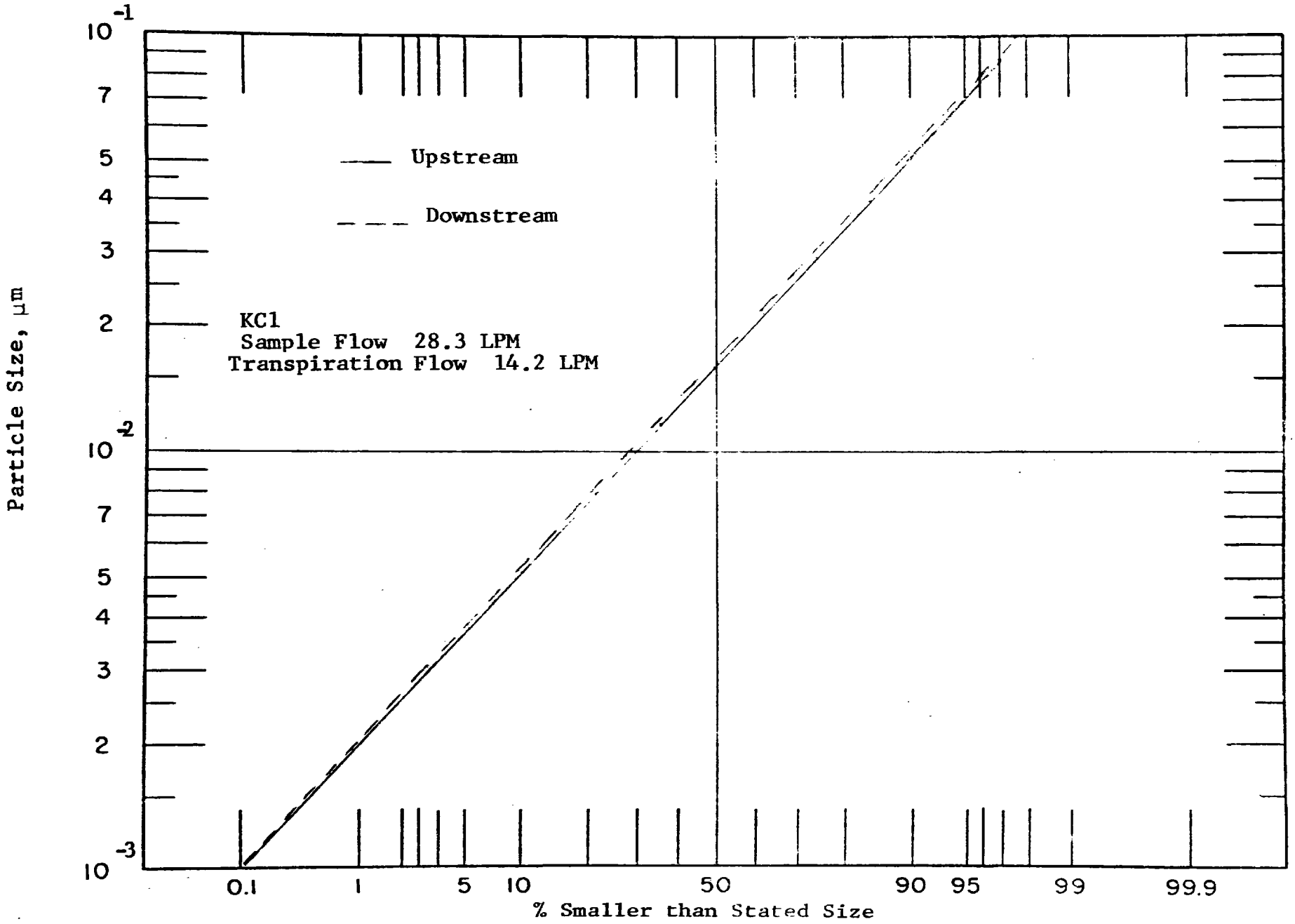

Figure 34. Log-Probability Plot of Size Distributions for Test K-2

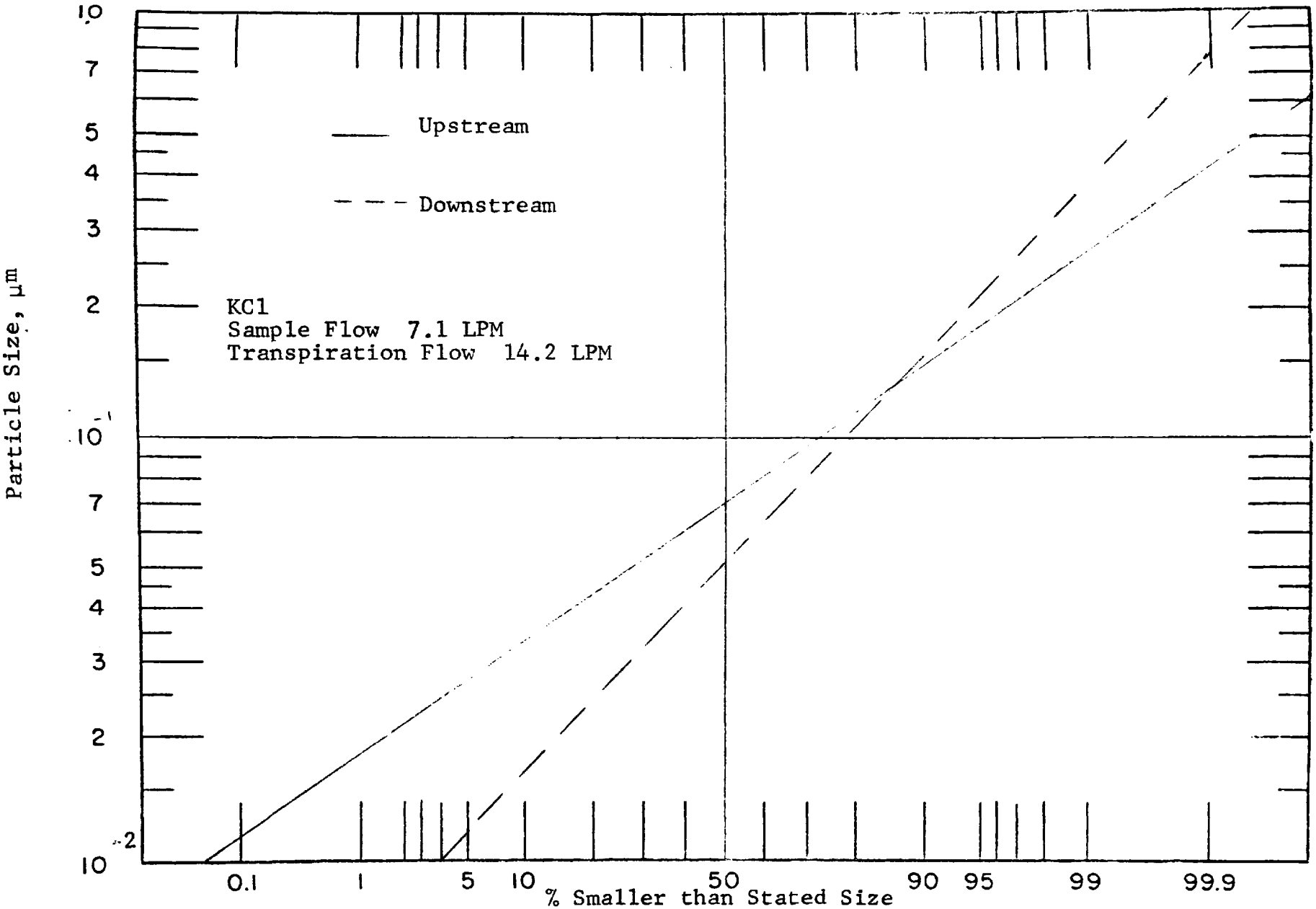

Figure 35. Log-Probability Plot of Size Distributions for Test K-3

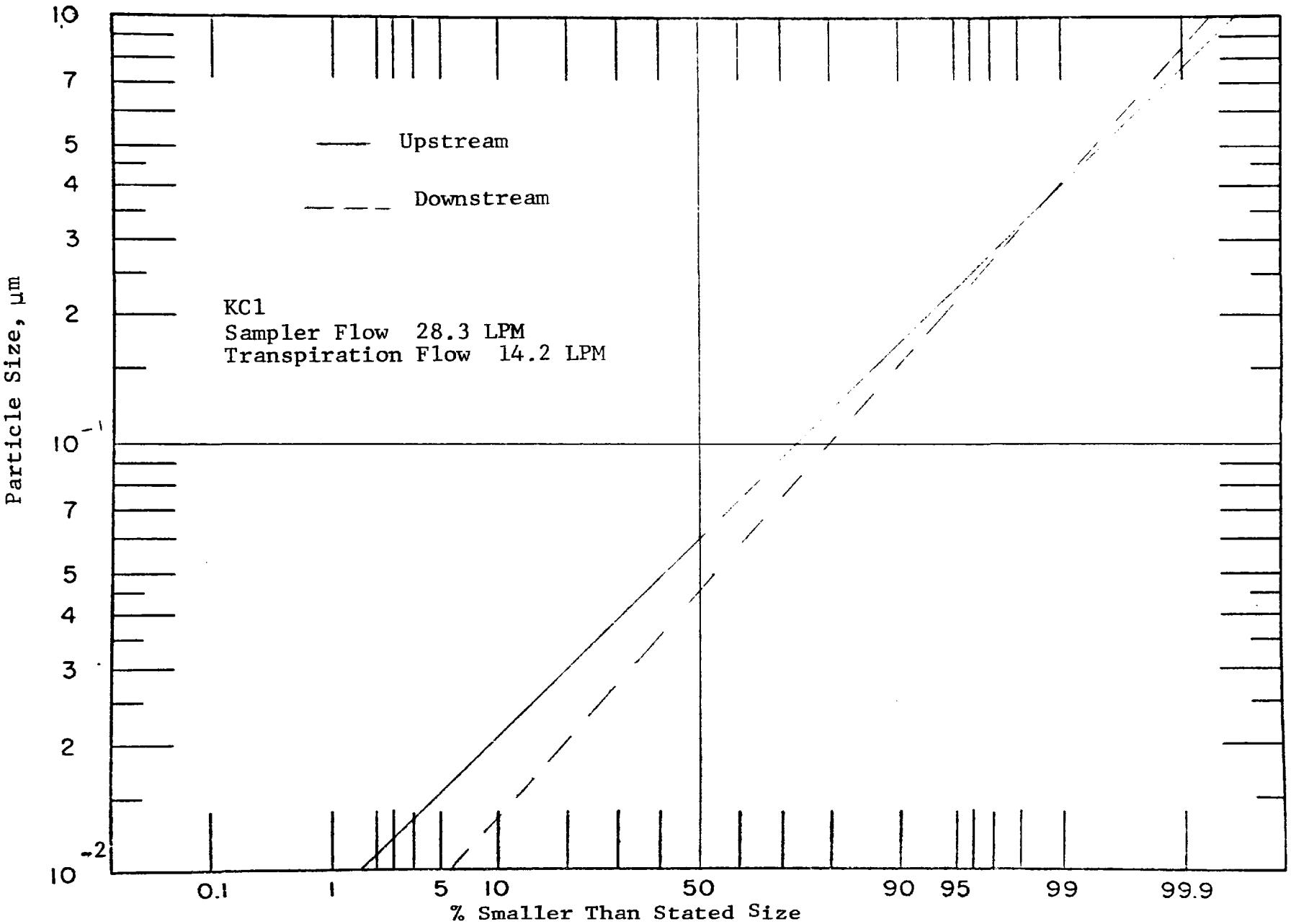
Upstream
Downstream
KCl
Sampler Flow 28.3 LPM
Transpiration Flow 14.2 LPM
Particle Size, µm
10
7
5
4
3
2
10⁻¹
7
5
4
3
2
10⁻²
0.1
1
5
10
50
90
95
99
99.9
% Smaller Than Stated Size

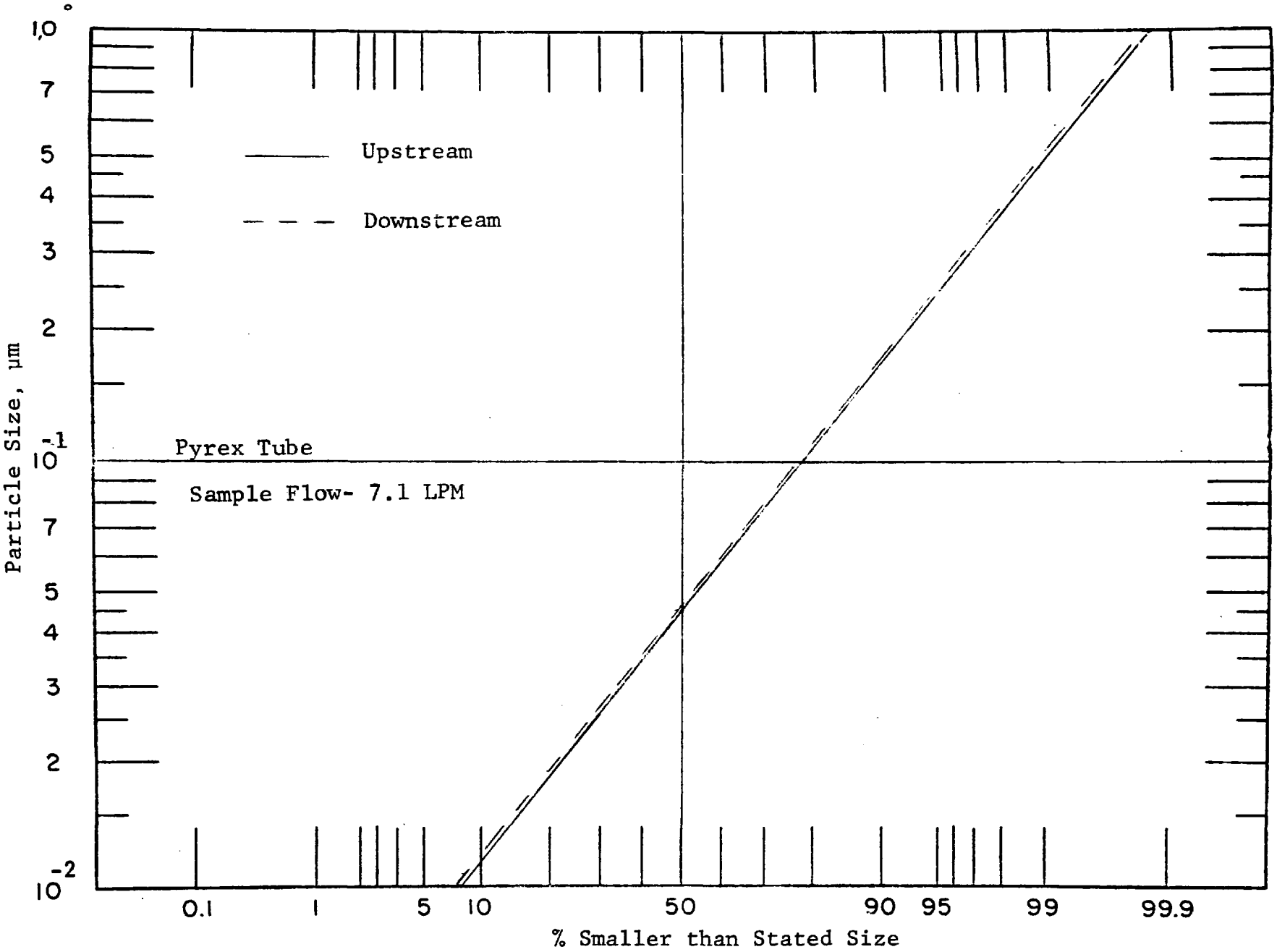

Figure 37. Log-Probability Plot of Size Distributions for Test K-4

6.2 Tests with Uranine Aerosol

The uranine for these tests was obtained by sieving the reagent grade uranine through a 270 mesh screen. The venturi dispenser used to generate the uranine aerosol in Phase I was used in these tests.

The aerosol at the inlet and the outlet of the porous probe was sampled on 47 mm dia. Nuclepore® filters with a pore size of 1 μm. The particle size distributions were measured directly from the filter, made transparent with immersion oil of refractive index 1.590, by an optical microscope interfaced with the Quantimet 720® image analyzing computer. The smallest size measured was 5 μm. The largest size was 50 μm.

The size distribution data for all the tests are presented in Table 8. Histograms and log-normal plots are also presented in Figures 38-47.

After run #U-4, qualitative information on the location of high deposition was obtained. At the end of the size distribution test, the front end of the porous probe was immersed vertically in a graduated cylinder. The graduated cylinder contained distilled water such that the level after the immersion of the porous probe was 16 cm. The uranine deposited was allowed to dissolve for five minutes. Next the probe was immersed in another cylinder filled with distilled water to a height of 60 cm. Approximately 2 mg of uranine were found on the first 16 cm, compared to 1.5 mg for the following 60 cm. This indicates that approximately 40-50% of the total deposit was in the first 16 cm.

In the test #U-5 with the pyrex tube a visible deposit in the bottom half of the tube was observed. This deposit was heaviest at the inlet to the probe and tapered off in the first 50 cm.

Table 8. SIZE DISTRIBUTION DATA FOR TESTS WITH URANINE

Particle Size	% Smaller than Stated Size									
	Test No. U-1		Test No. U-2		Test No. U-3		Test No. U-4		Test No. U-5	
	Upstream	Downstream	Upstream	Downstream	Upstream	Downstream	Upstream	Downstream	Upstream	Downstream
5-7	26.3	19.5	21.5	21.6	17.4	12.4	18.5	13.6	24.0	32.4
9	47.3	30.2	42.3	37.4	34.1	23.1	37.4	24.7	46.6	57.1
11	58.5	39.1	57.7	45.2	49.1	34.1	54.1	38.7	61.7	73.6
13	72.5	49.7	71.1	53.0	59.8	47.2	68.7	44.4	71.7	84.7
15	78.9	59.2	83.0	57.5	71.6	54.6	78.7	50.5	81.1	91.3
20	86.6	76.0	94.4	69.2	87.8	73.3	89.4	62.7	90.6	98.1
25	92.3	82.1	98.9	82.3	93.0	87.2	95.4	77.4	94.9	99.4
30	95.2	90.5	99.3	90.7	95.7	92.3	98.6	84.6	98.0	99.71
37	96.8	96.1	99.5	96.7	97.3	96.3	99.2	91.7	99.4	100.0
50	100.0	100.0	100.0	100.0	100.0	100.0	100.0	100.0	100.0	100.0

300-400 particles counted for each sample.

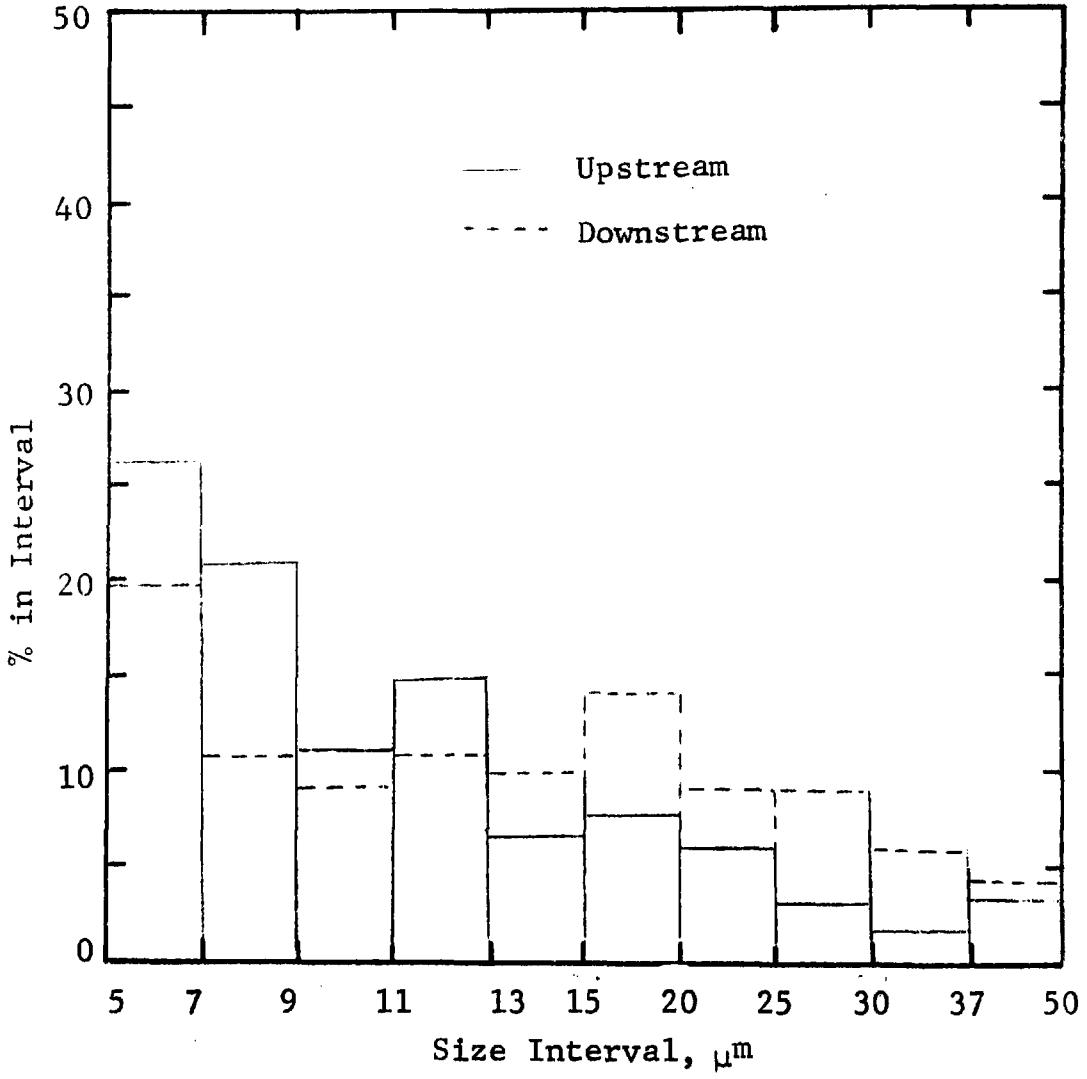

Figure 38. Histograms for Run U-1

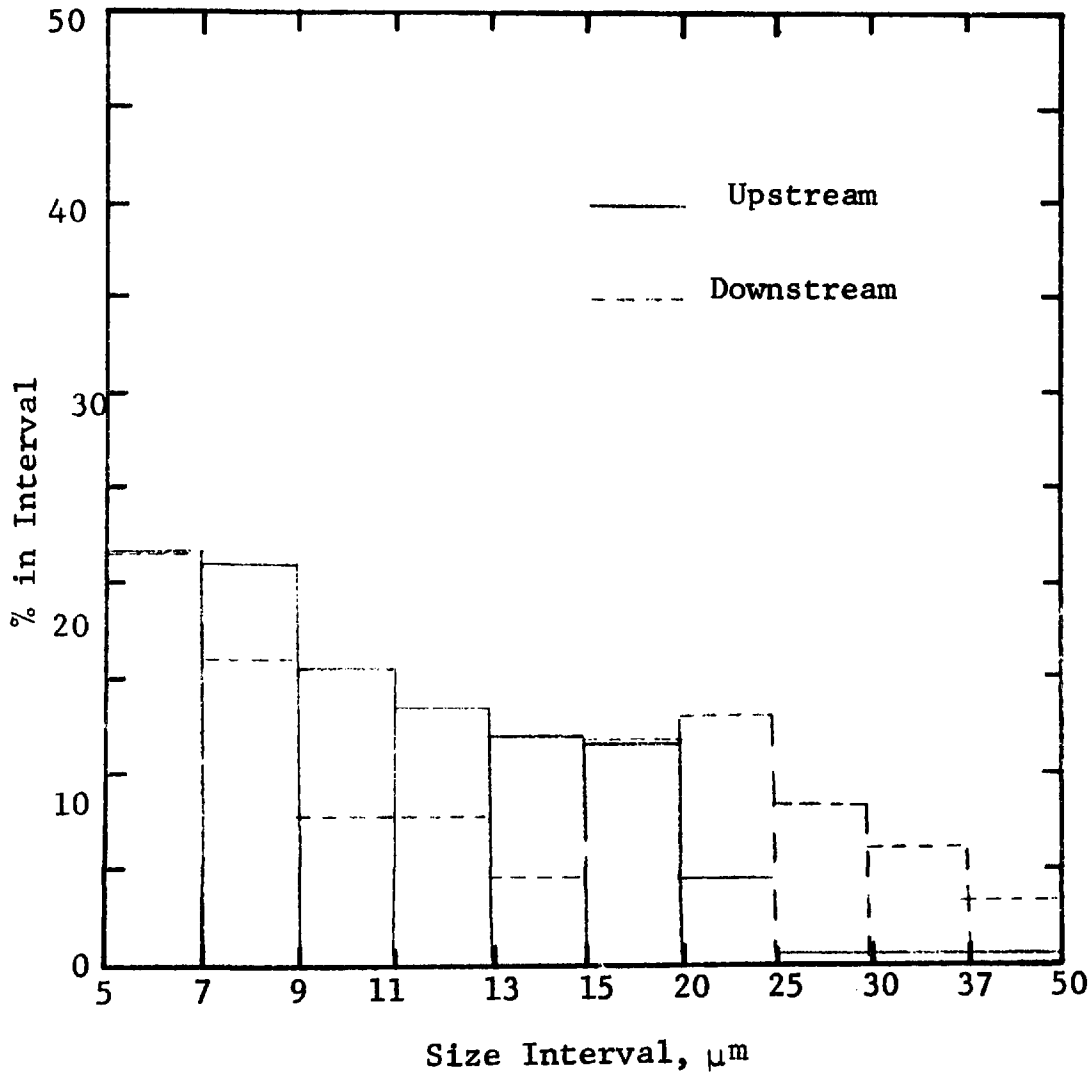

Figure 39. Histograms for Run U-2

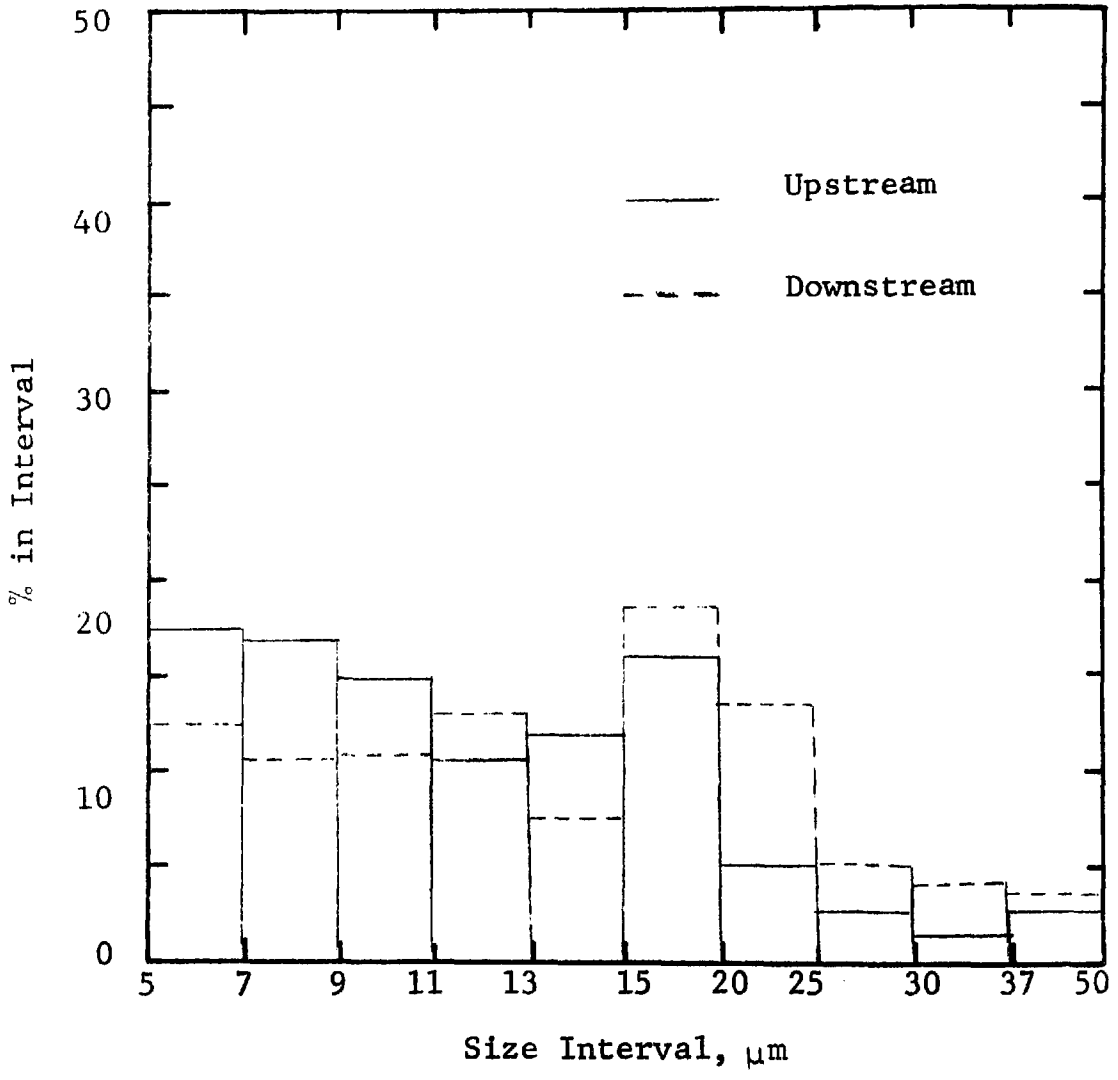

Figure 40. Histograms for Run U-3

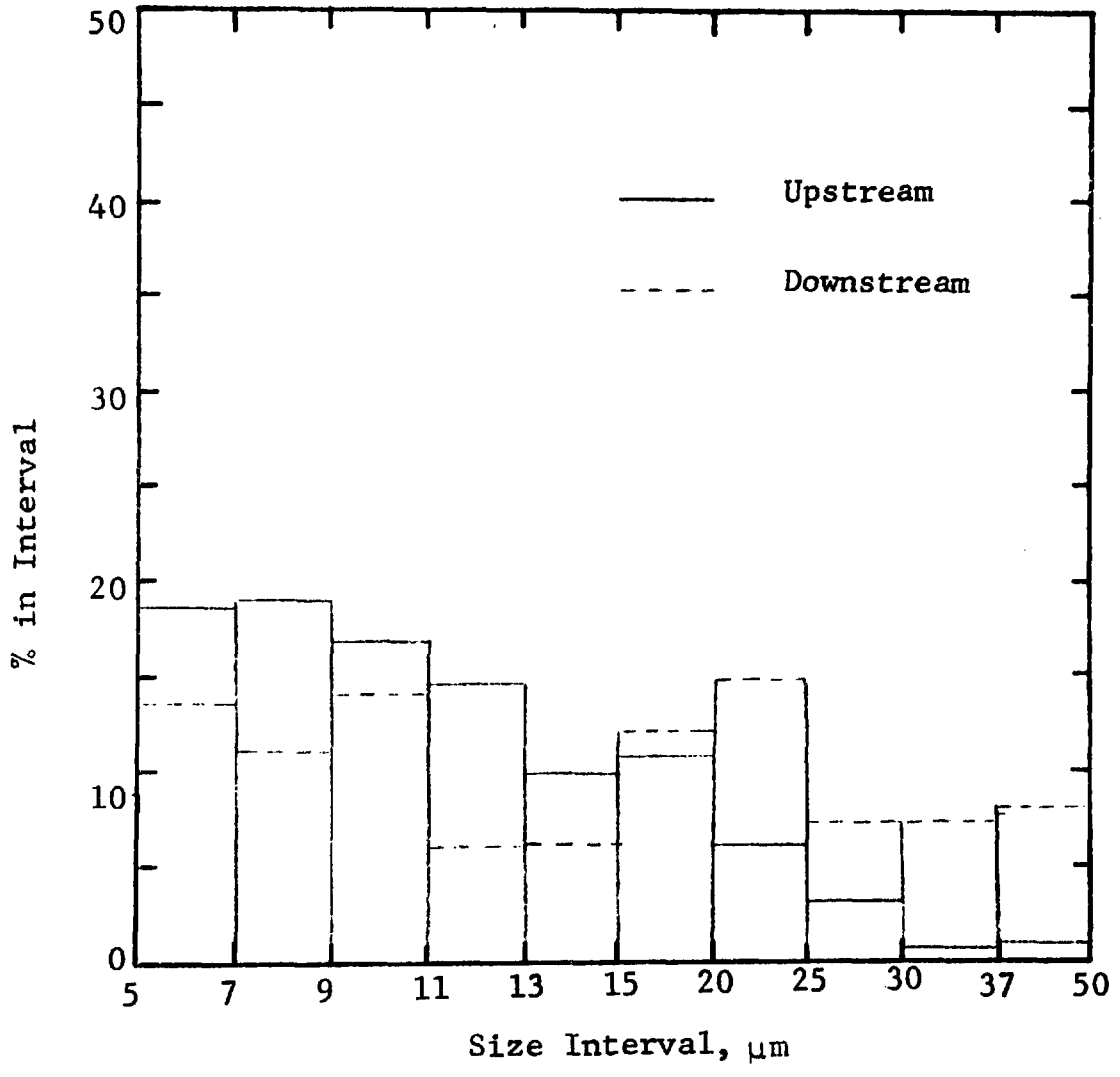

Figure 41. Histograms for Run U-4

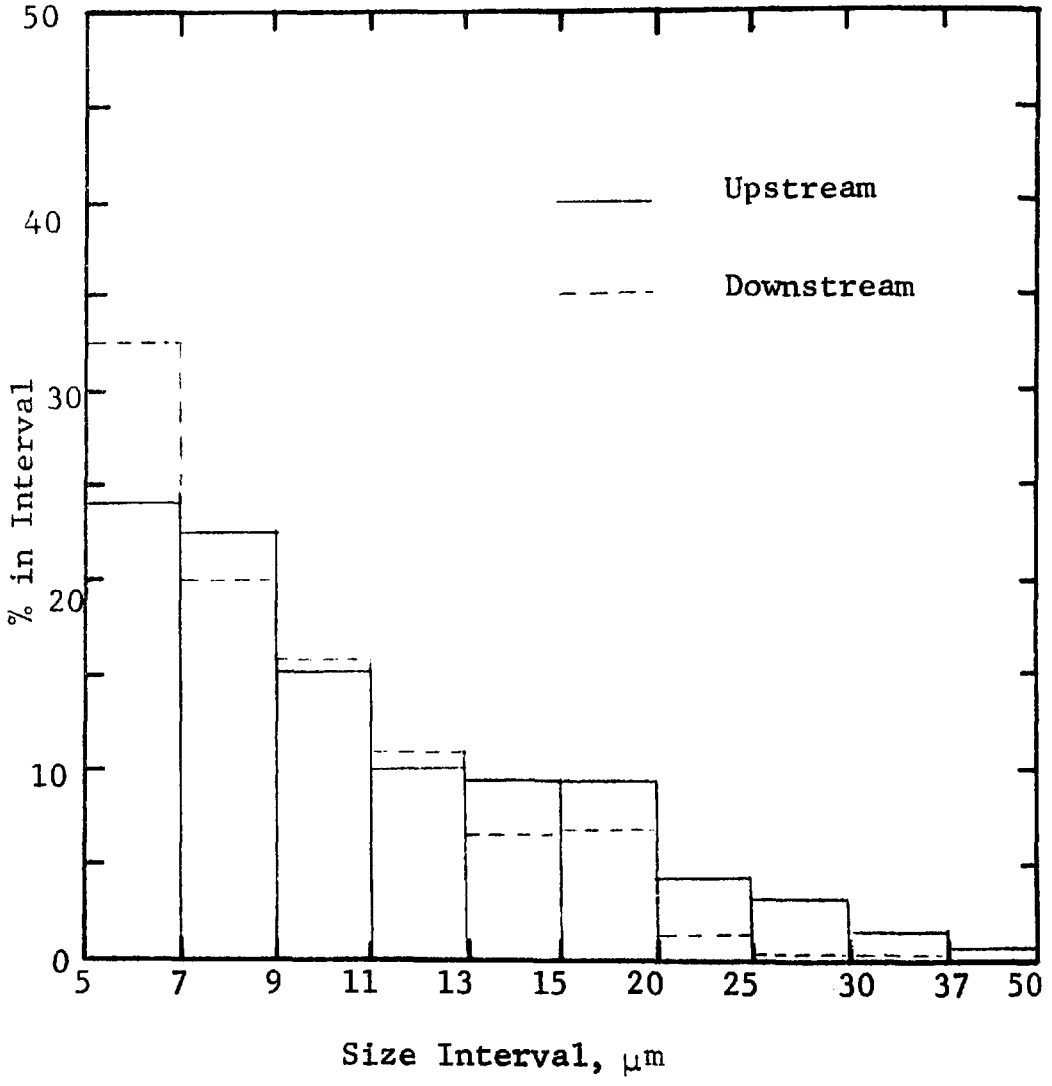

Figure 42. Histograms for Run U-5

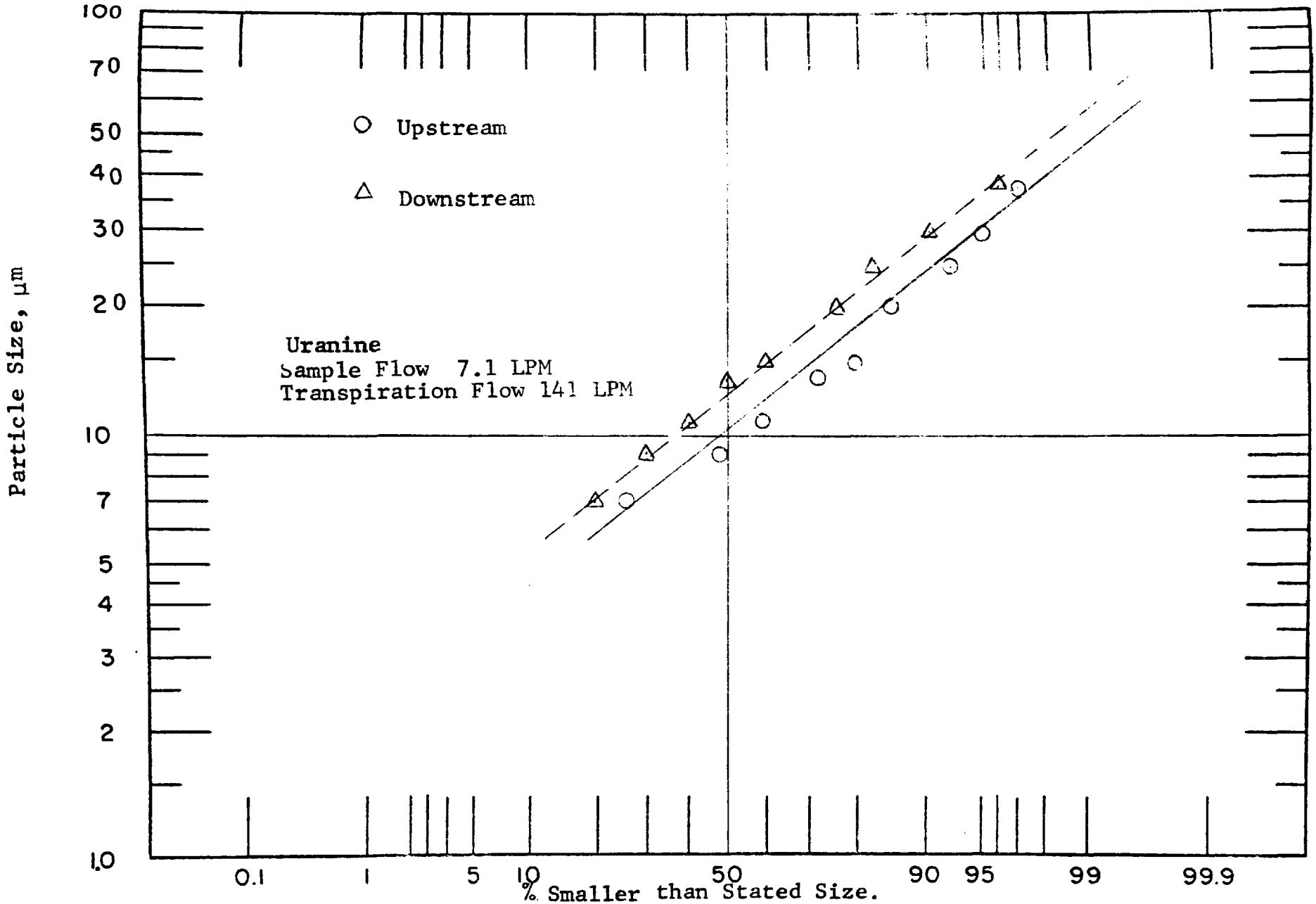

Figure 43. Size Distributions for Test U-1

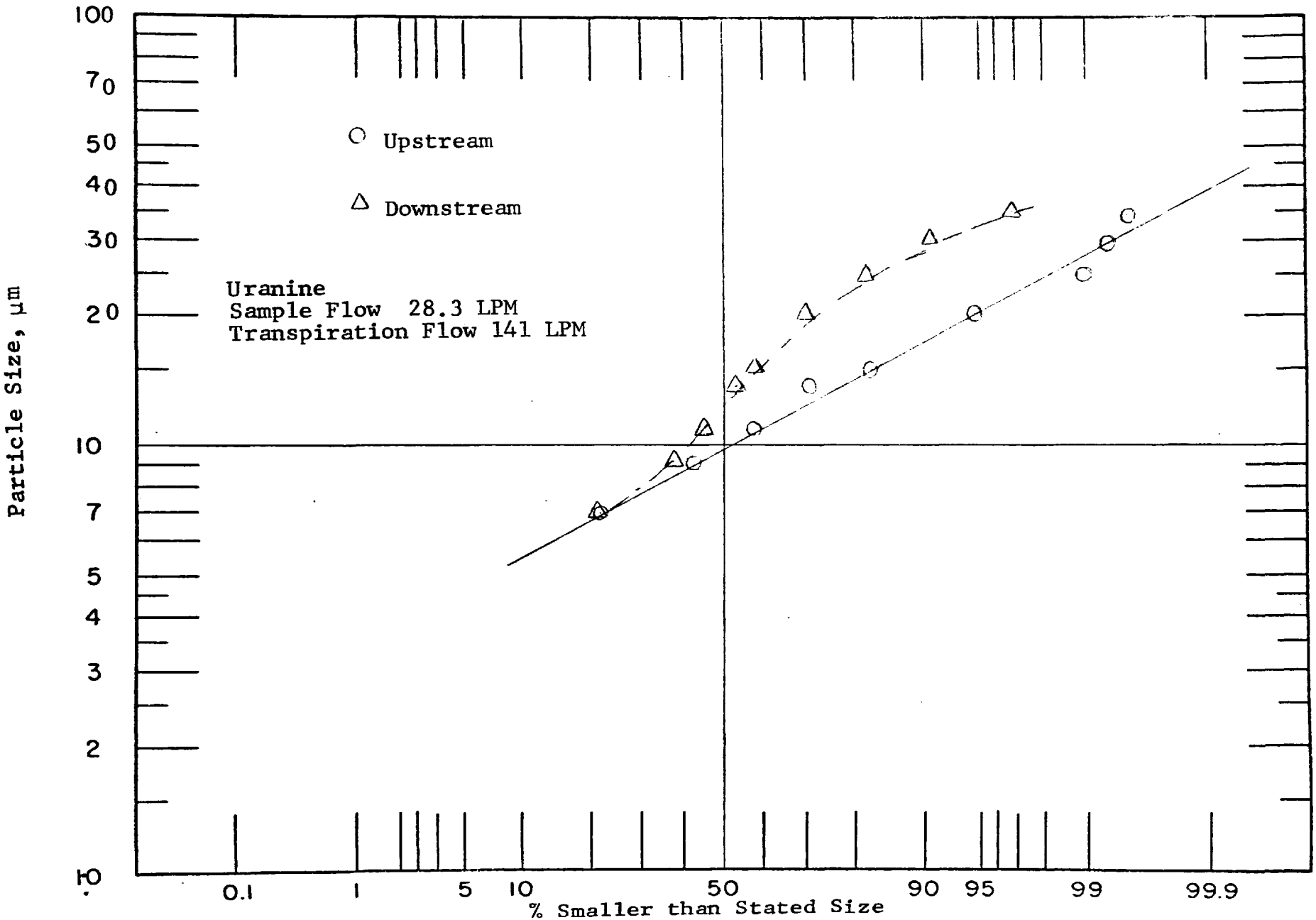
Particle Size, µm
100
70
50
40
30
20
10
7
5
4
3
2
1.0
Upstream
Downstream
Uranine
Sample Flow 28.3 LPM
Transpiration Flow 141 LPM
0.1
1
5
10
50
90
95
99
99.9
% Smaller than Stated Size

06

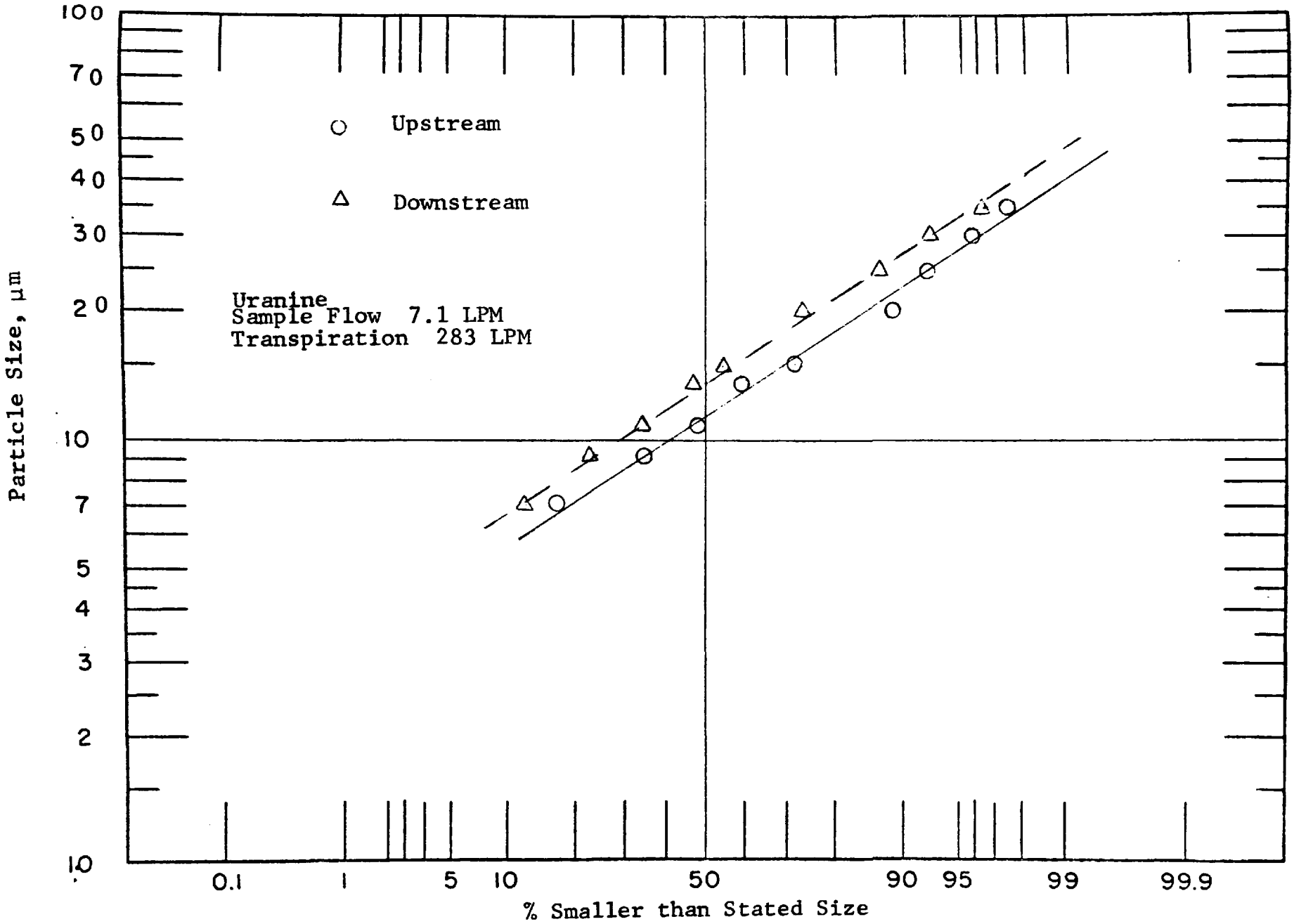

Figure 45. Size Distributions for Test U-3

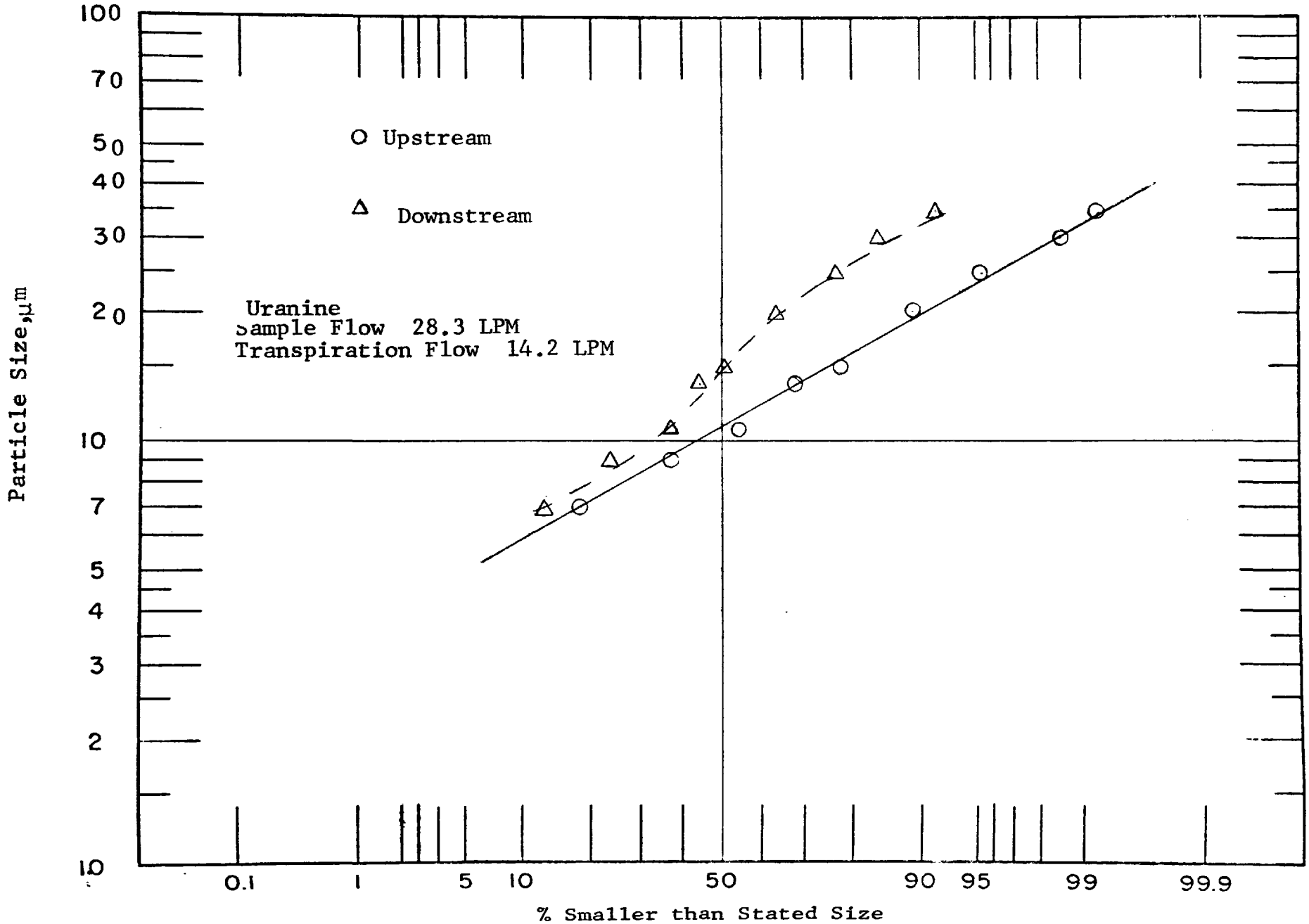
100
70
50
40
30
20
10
7
5
4
3
2
1.0
Particle Size, µm
O Upstream
Δ Downstream
Uranine
Sample Flow 28.3 LPM
Transpiration Flow 14.2 LPM
0.1
1
5
10
50
90
95
99
99.9
% Smaller than Stated Size

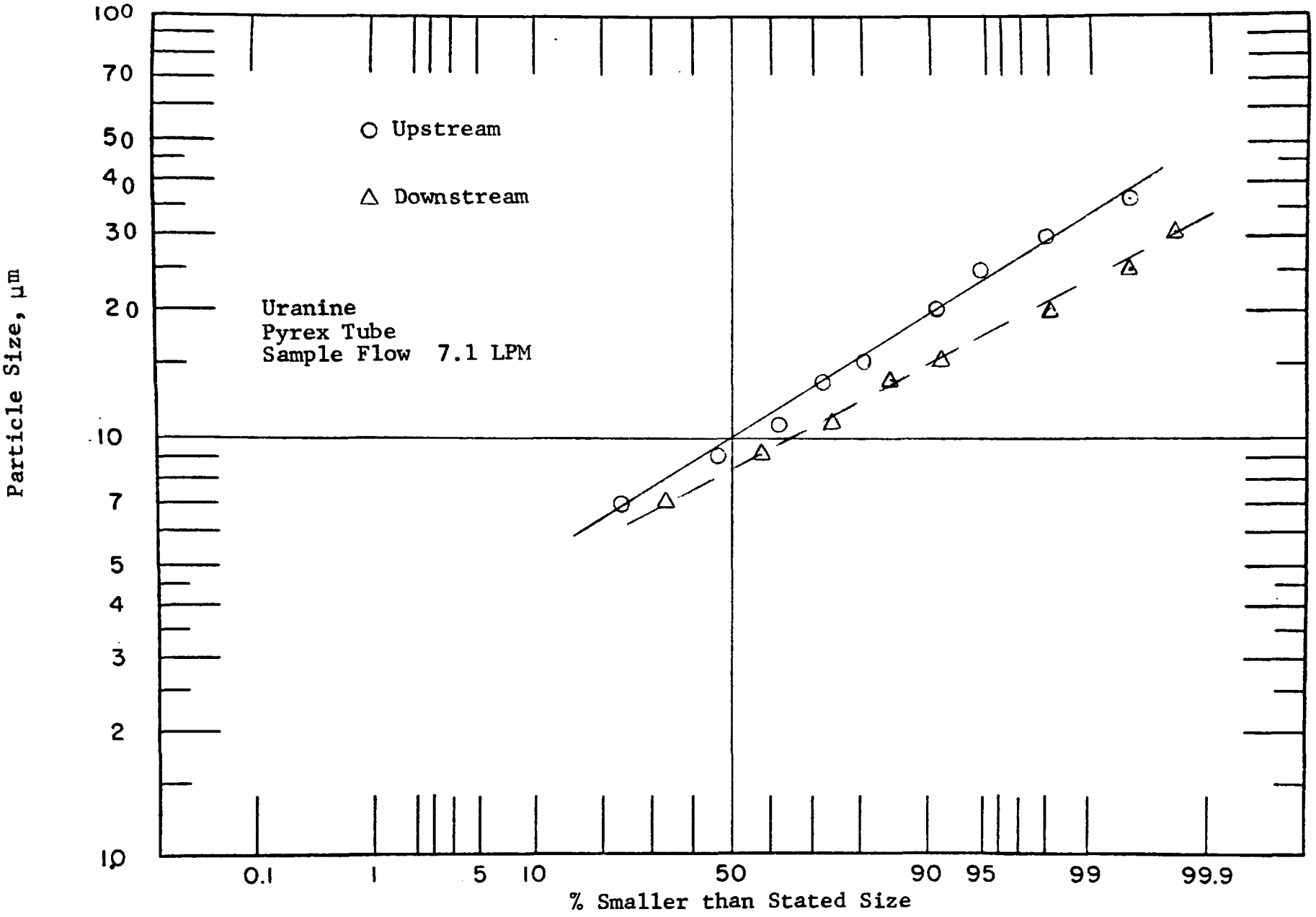

Figure 47. Size Distributions for Test U-5

6.3 Tests with Flyash

The flyash was prepared by sieving it through a 270 mesh screen. The same venturi dispenser used with the uranine aerosol was used to generate the flyash aerosol. The samples, as in the tests with uranine, were taken on a nuclepore filter.

The immersion oil used with uranine could not be used for the flyash since the oil dissolved the particles. Therefore, the deposit was transfered to a glass slide by washing the filter with isopropyl alcohol and placing a drop of the suspension on the glass slide. After drying the slide, a drop of Aerochlor® was used instead of an immersion oil.

We had hoped to measure the size distribution on the Quantimet 720 image analyzer, but the wide variation of the grey levels of the flyash particles coupled with the wide size distribution was too much for the image analyzer to handle. The counting had to be done manually with an optical microscope. The same size categories as uranine were used. The size distribution data are presented in Table 9 and Figures 48-57 in the same form as for uranine.

In test No. F-5 with the pyrex tube, a deposition pattern similar to the corresponding uranine test U-5 was observed.

6.4 Tests with 1-MAAQ Aerosol

The aerosol for these tests was generated with the generator used in Phase I except no KCl nuclei were used. This resulted in a wider size distribution much more meaningful for the Phase II tests than the nearly monodisperse 1.6 μm (Geometric mass mean diameter) aerosol. The aerosol had an GNMD (count basis) of approximately 0.7 μm.

The aerosol was generated at a flow rate of 7.1 lpm (0.25 cfm). When required, it was diluted with clean dry air. The samples at the inlet and the outlet of probe were collected with

Table 9. SIZE DISTRIBUTION DATA FOR TESTS WITH FLYASH AEROSOL

Particle Size	% Smaller than Stated Size									
	Test No. F-1		Test No. F-2		Test No. F-3		Test No. F-4		Test No. F-5	
	Upstream	Downstream	Upstream	Downstream	Upstream	Downstream	Upstream	Downstream	Upstream	Downstream
5-7	33.1	28.6	33.9	23.0	28.7	29.1	27.0	37.2	32.0	55.4
9	63.0	46.9	65.8	45.8	74.3	44.9	40.3	59.4	60.2	79.7
11	75.4	57.8	81.1	61.9	88.4	47.1	64.9	68.3	76.2	89.7
13	83.1	67.3	90.6	70.9	91.6	65.0	76.7	72.9	83.7	94.3
15	88.7	74.9	93.6	77.5	94.6	71.2	84.5	76.1	87.8	96.0
20	95.0	87.2	97.5	83.9	96.8	81.1	93.0	82.4	92.0	97.1
25	97.8	90.2	98.9	87.8	98.4	86.7	98.0	85.6	93.9	98.3
30	98.9	93.2	99.4	91.5	99.2	90.4	99.2	88.5	95.3	99.1
37	99.2	95.6	99.7	95.0	99.5	93.2	99.4	92.5	97.0	99.4
>37	100.0	100.0	100.0	100.0	100.0	100.0	100.0	100.0	100.0	100.0

300-400 Particles counted for each sample.

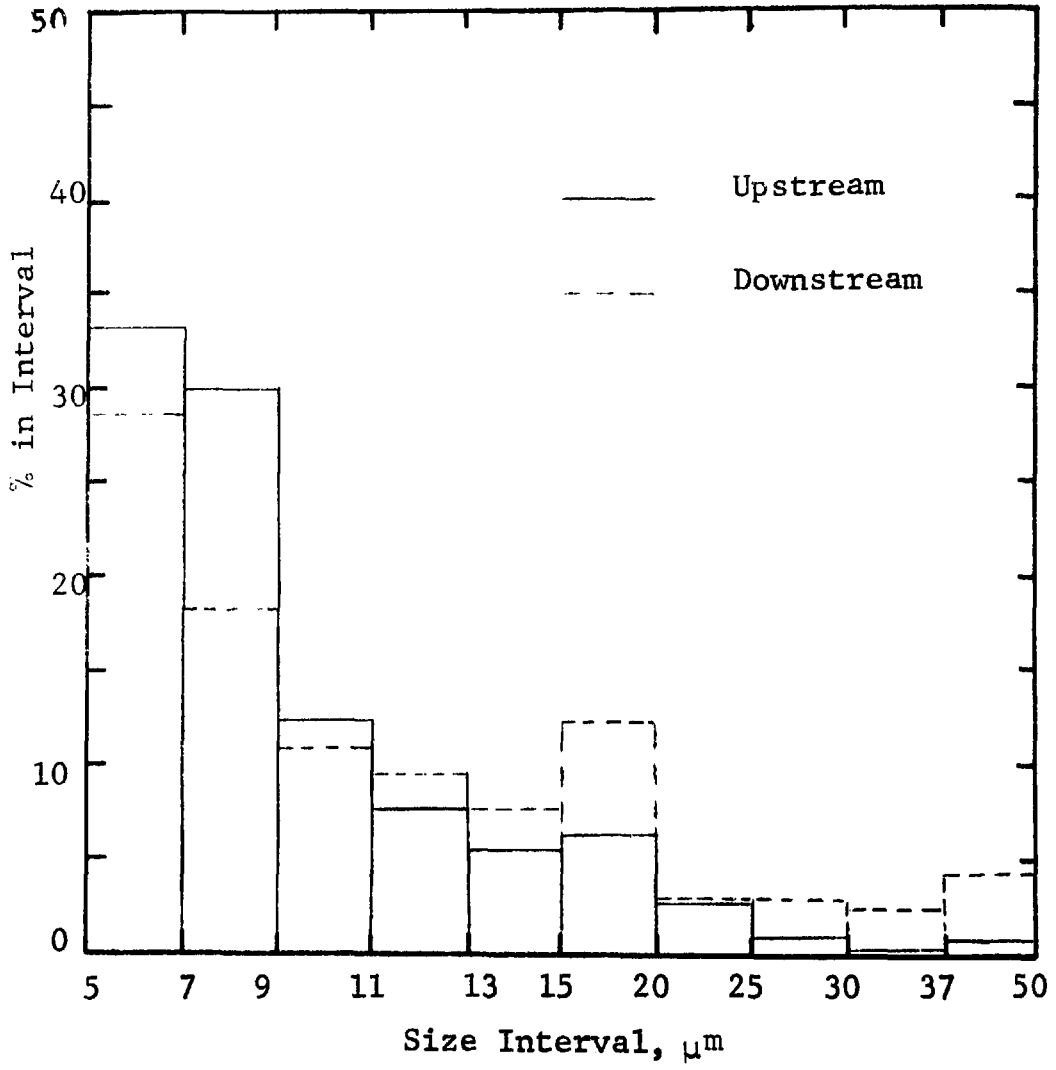

Figure 48. Histograms for Run F-1

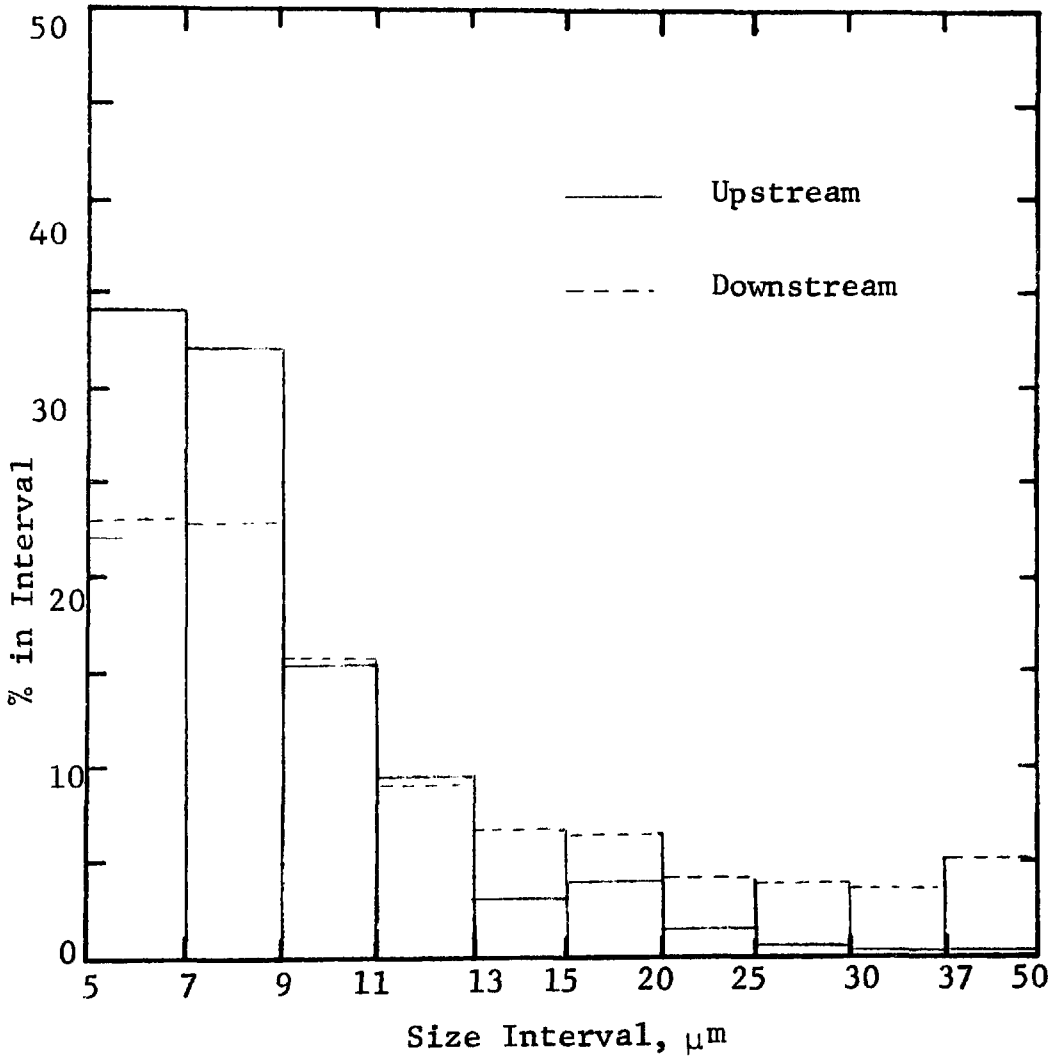

Figure 49. Histograms for Run F-2

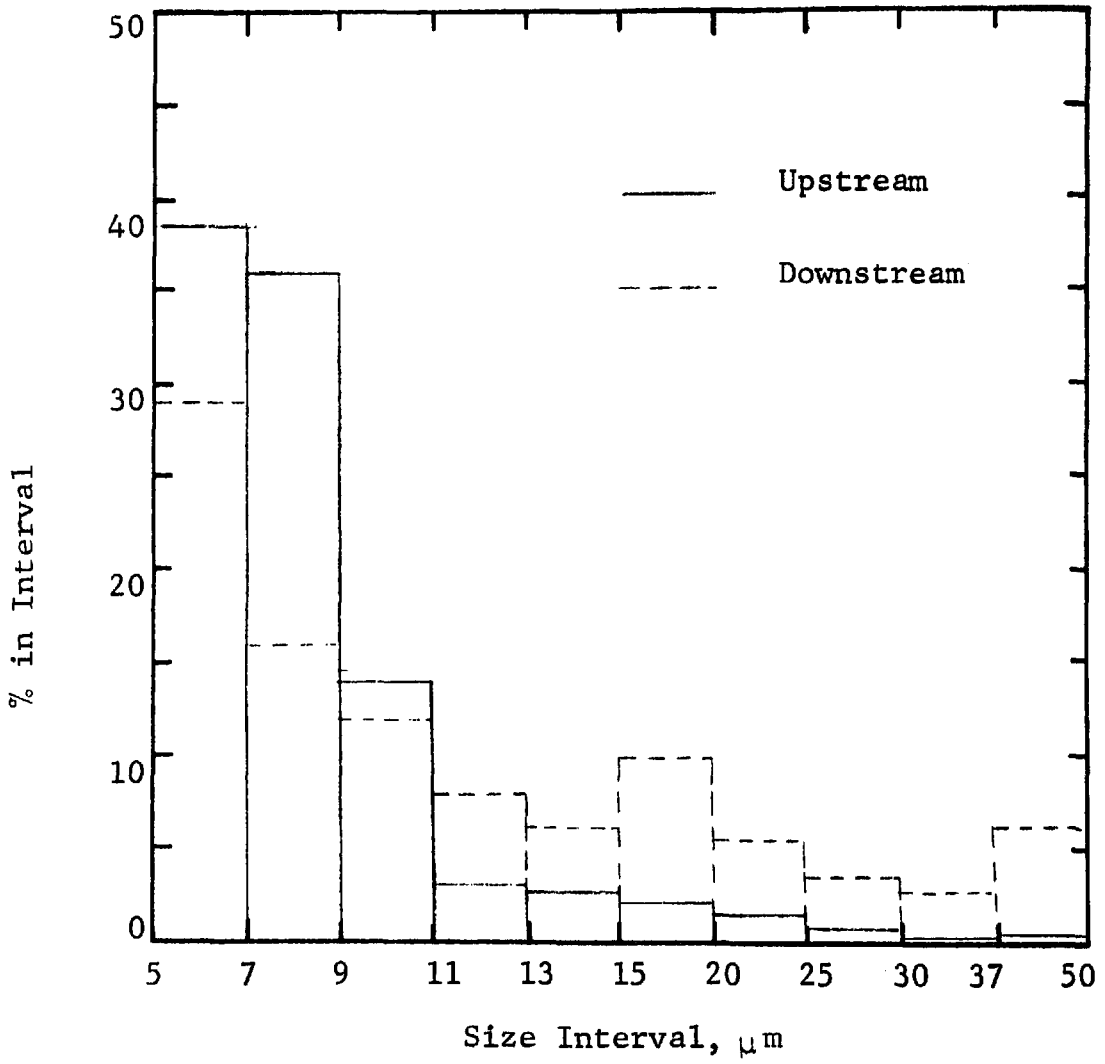

Figure 50. Histograms for Run F-3

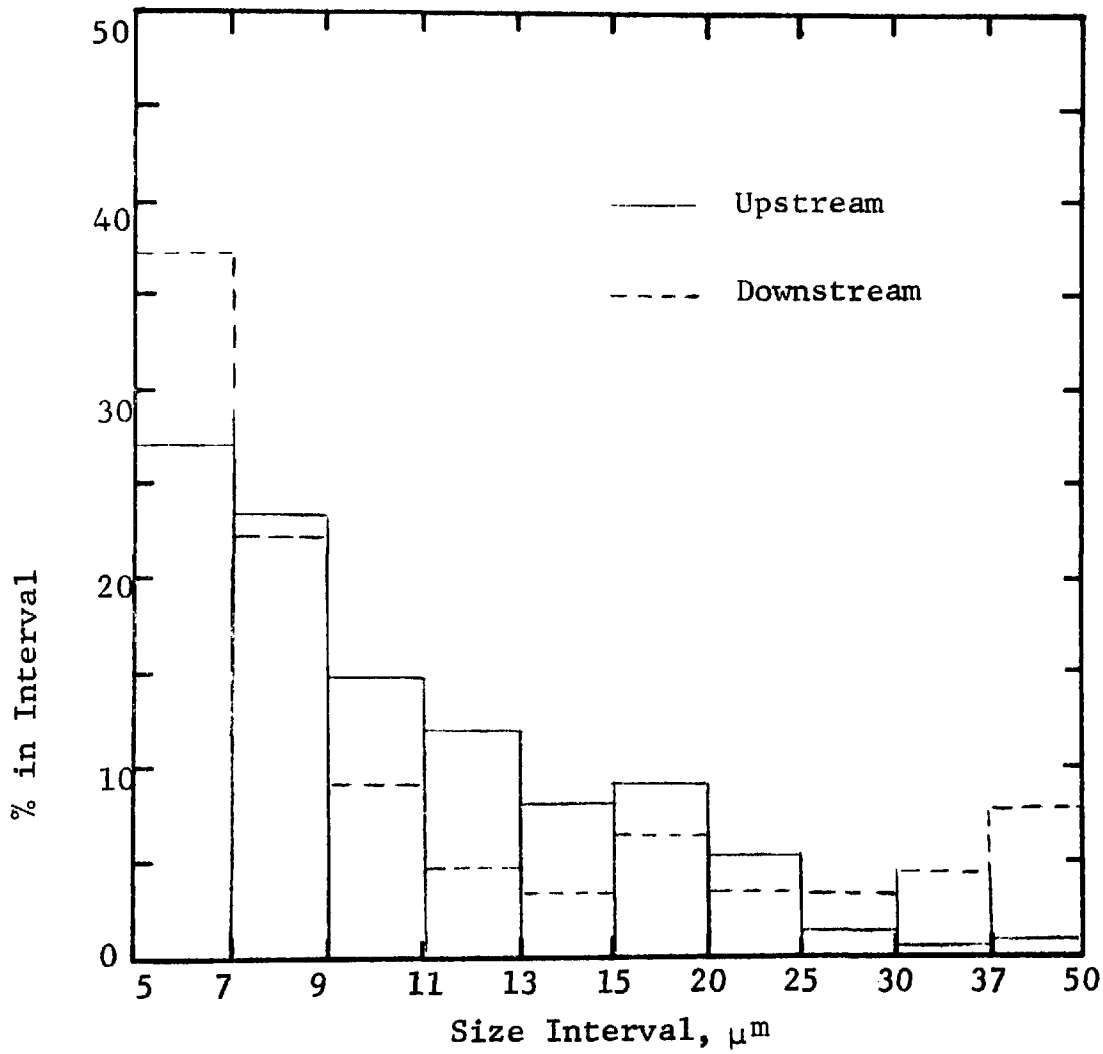

Figure 51. Histograms for Run F-4

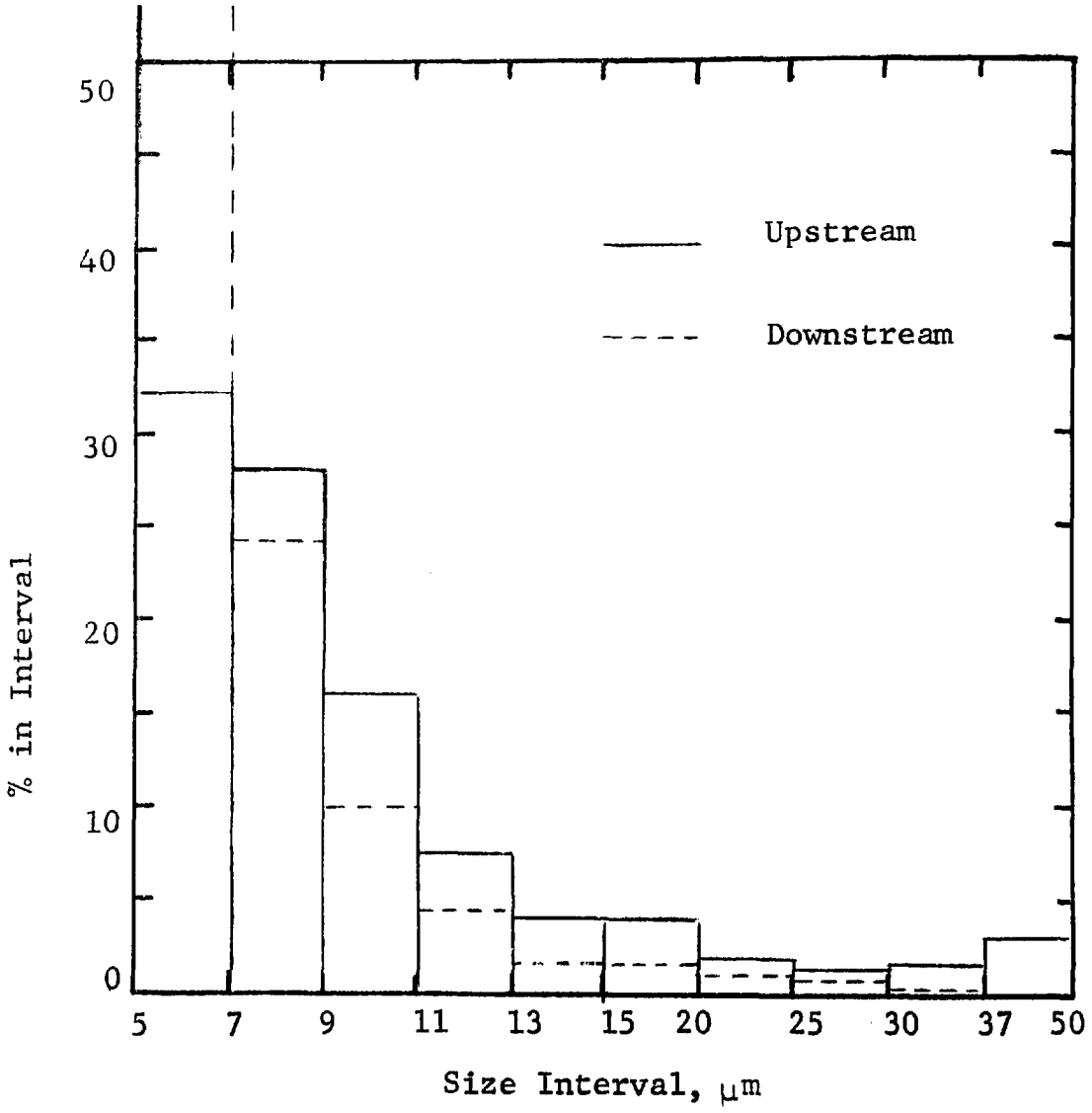

Figure 52. Histograms for Run F-5

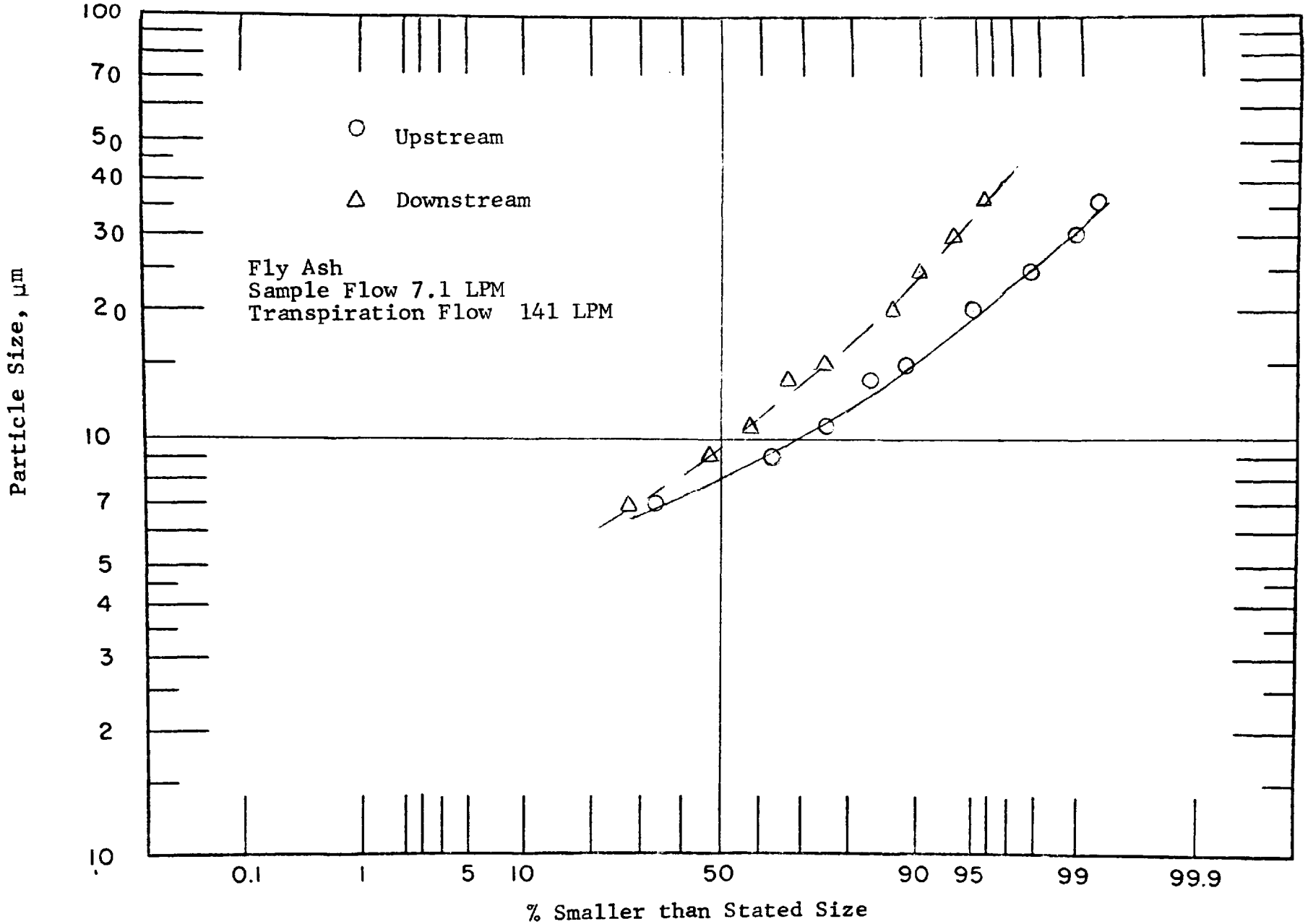

Figure 53. Size Distributions for Test F-1

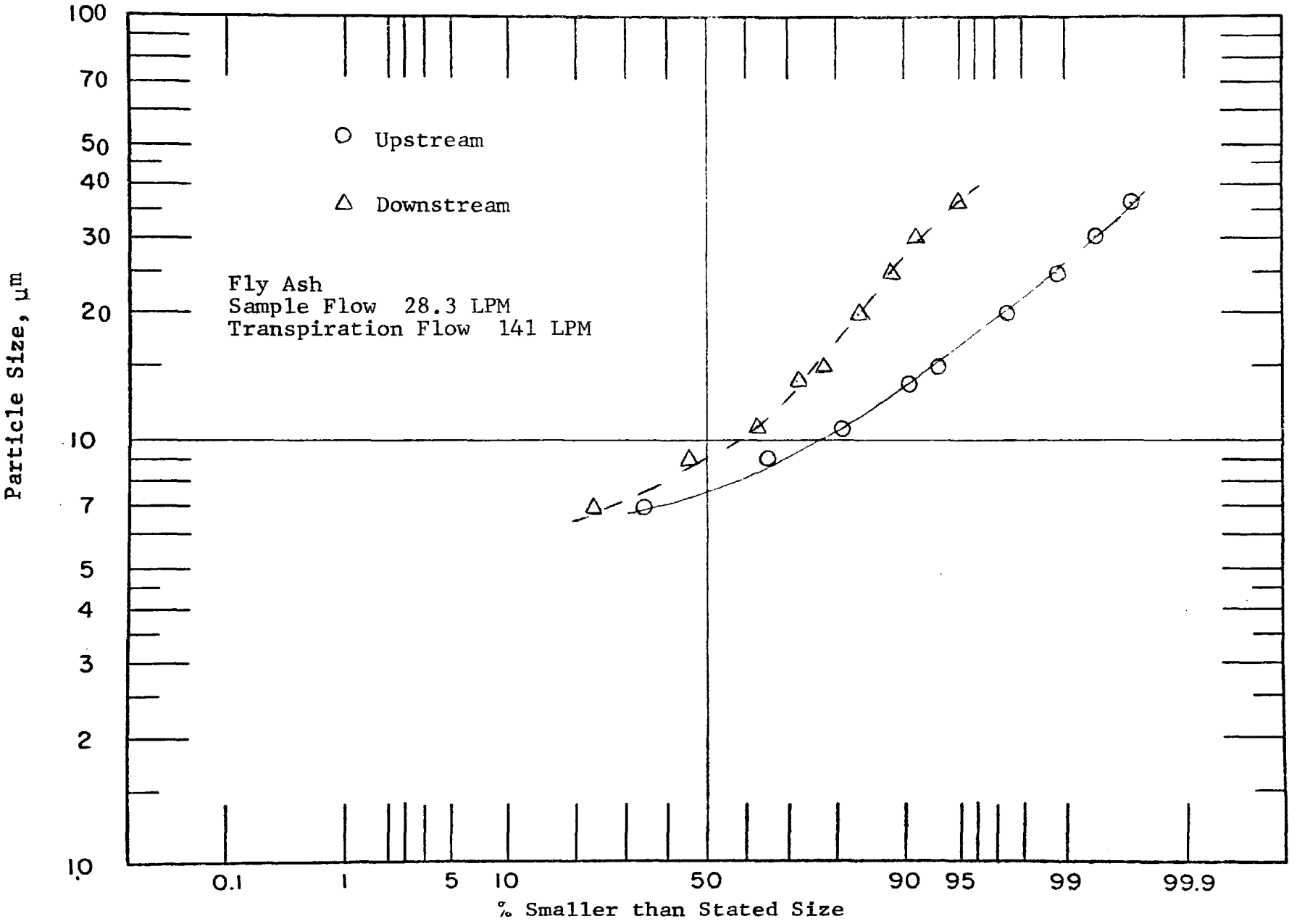

Figure 54. Size Distributions for Test F-2

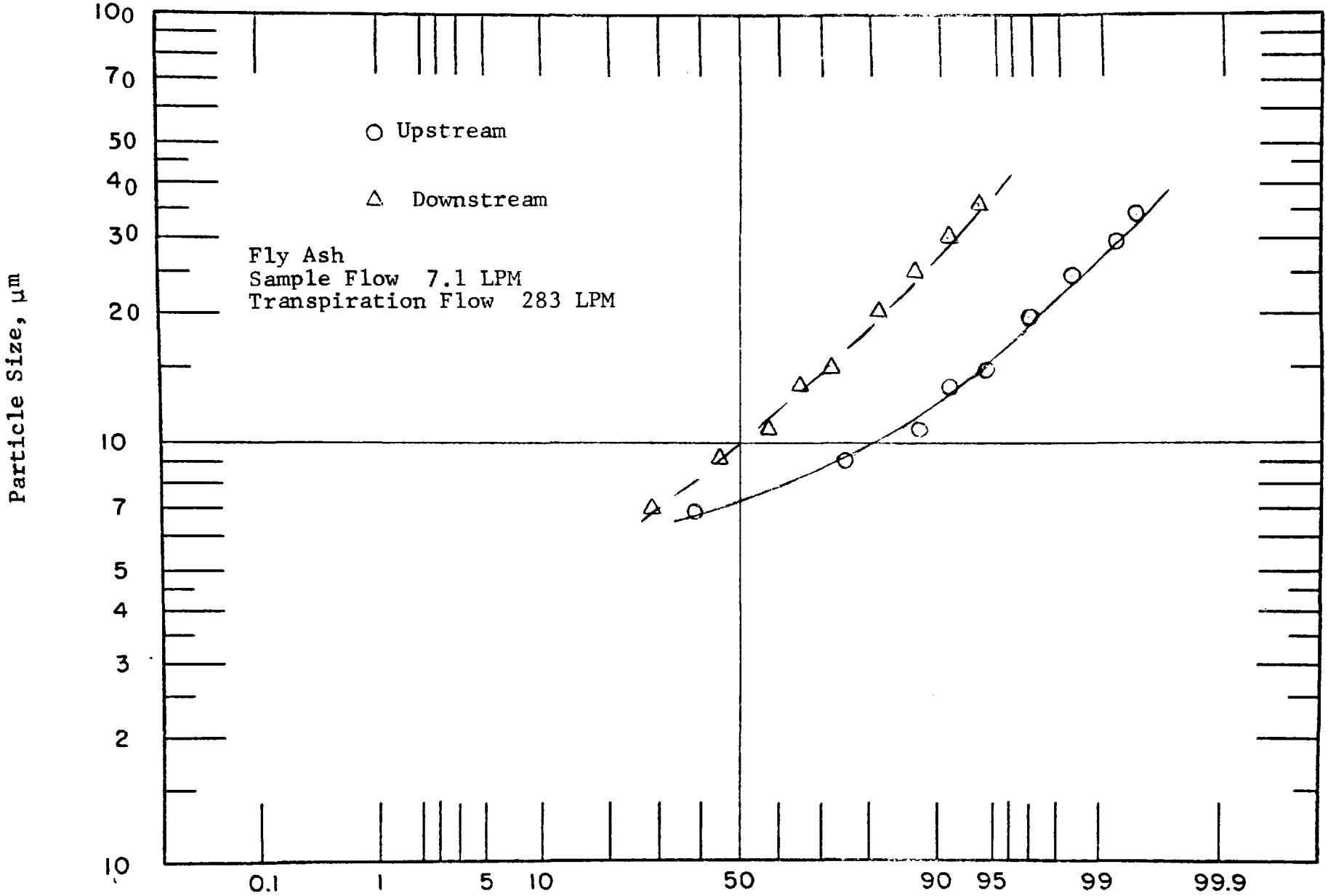

Figure 55. Size Distributions for Test F-3

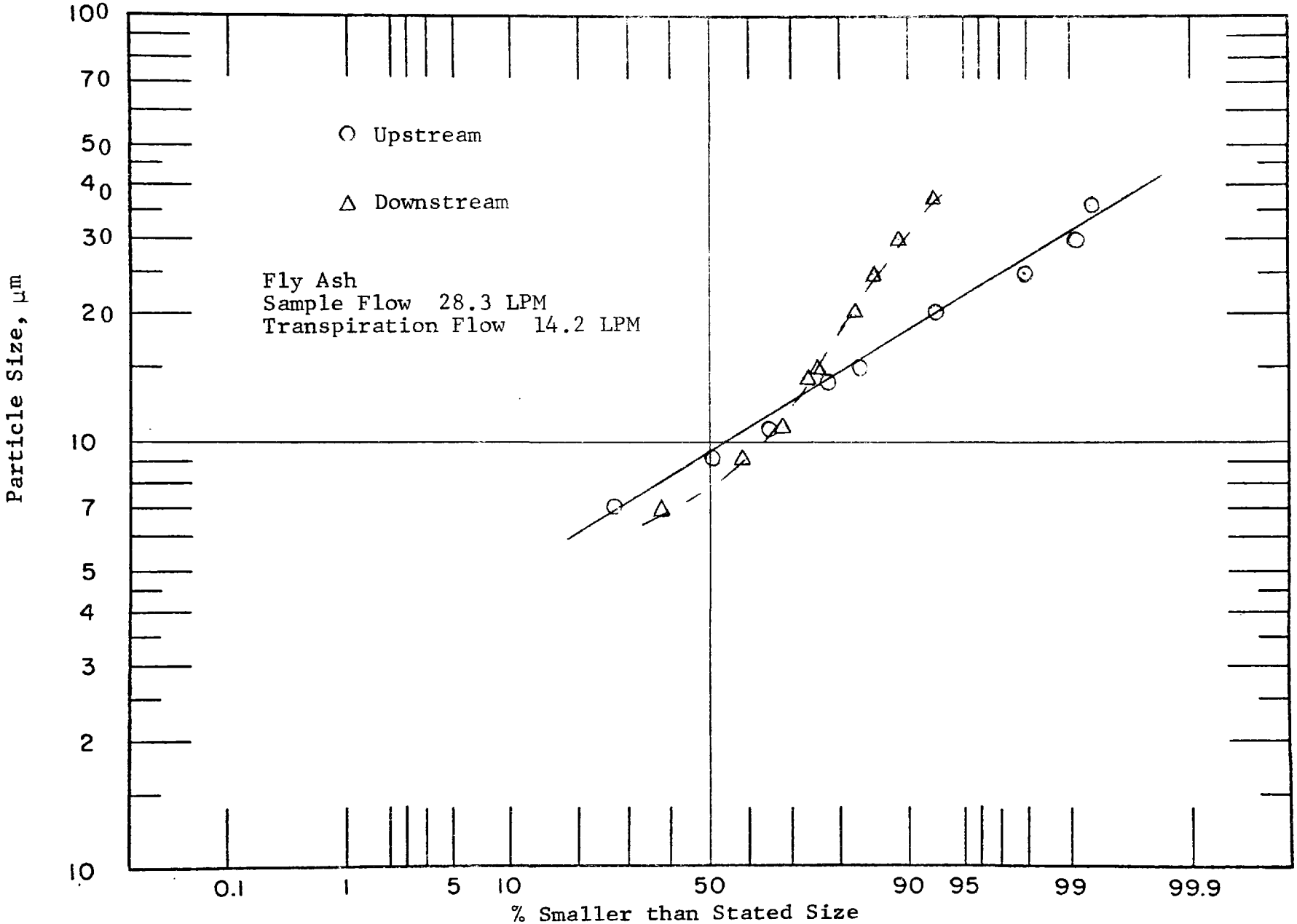

Figure 56. Size Distributions for Test F-4

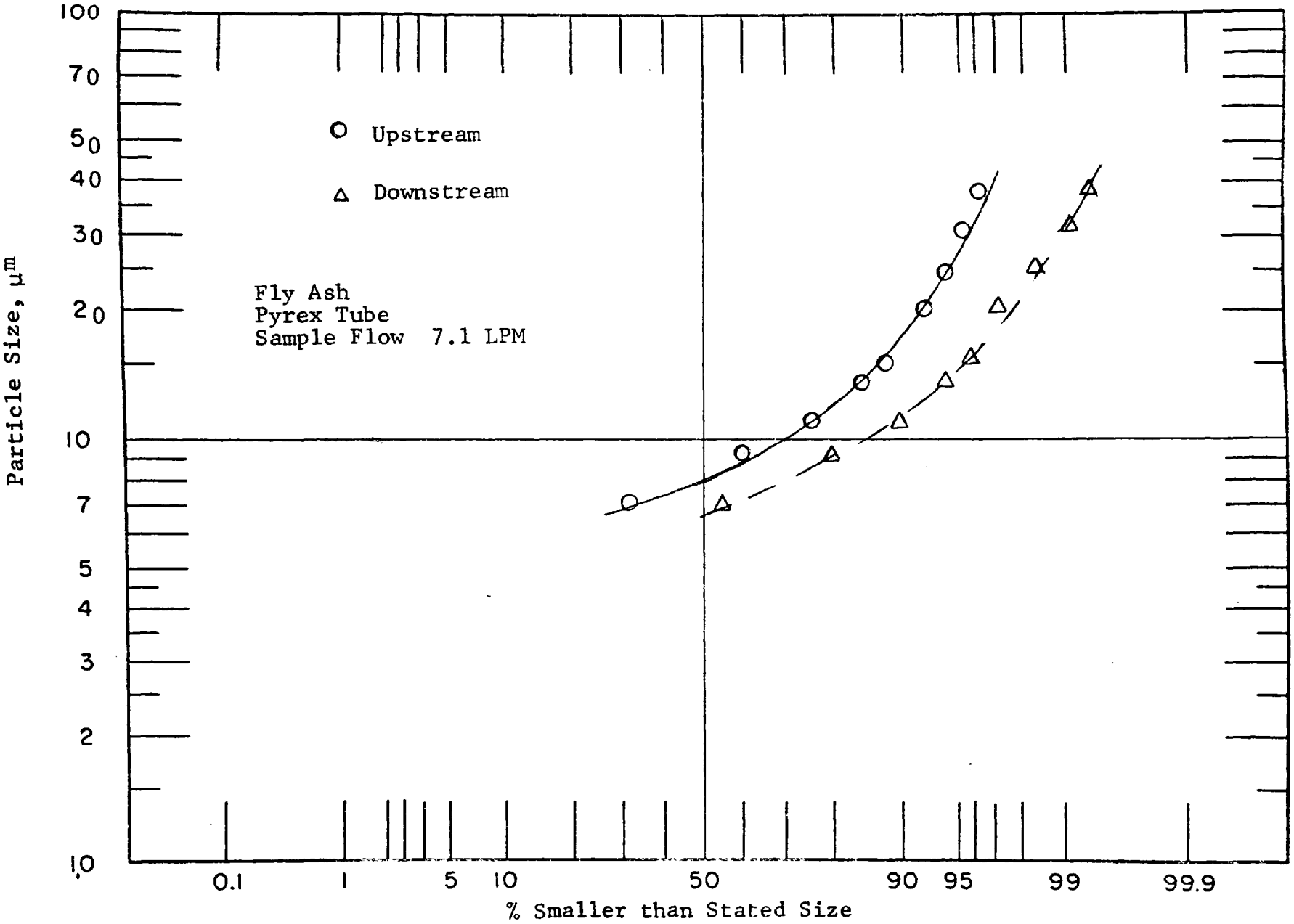

Figure 57. Size Distributions for Test F-5

the IITRI moving slide impactor on microscope slides. The size distribution was determined by counting manually on an optical microscope.

The size distribution data are presented in Table 10 and Figures 58-62.

7. RESULTS

7.1 Tests with KCl Aerosol

In Table 11, the size distribution parameters for tests with KCl aerosol are presented in the ascending order of transpiration flow rates, and the ratios of the transpiration velocity to the sample velocity at the inlet to the porous probe. The size distribution changed very little in all the tests. For runs K-5, K-1, K-2 the agreement is excellent. For runs K-3 and K-4, the agreement is not as good. However, this scatter is believed to be due to the nebulizer (Figure 26) used for the generation aerosols. The size parameters of the aerosol are very sensitive to the level of the solution in the flask, and are subject to change with time.

The results indicate that for particles below 1 μm, the pyrex tube and the porous sampling interface are both effective in the preservation of the size distribution. These results are consistent with the Phase I results which indicate that the maximum deposition for KCl aerosol with 0.05 μm nominal diameter is less than 3% on mass basis for all of the above conditions.

7.2 Tests with 1-MAAQ Aerosol

As with KCl, the size parameters are grouped in Table 12 for 1-MAAQ. The agreement between the upstream and downstream size distribution is excellent. Even for the pyrex tube, the size distribution is well preserved. Examination of Figure

Table 10. SIZE DISTRIBUTION DATA FOR TESTS WITH 1-MAAQ AEROSOL

Particle Size (μm)	% Smaller than Stated Size									
	Test No. M-1		Test No. M-2		Test No. M-3		Test No. M-4		Test No. M-5	
	Upstream	Downstream	Upstream	Downstream	Upstream	Downstream	Upstream	Downstream	Upstream	Downstream
0.5	23.7	17.9	24.8	28.9	21.0	21.7	15.0	36.5	21.2	25.4
1.0	79.0	60.7	71.8	70.4	72.7	73.4	67.9	82.5	72.9	73.9
1.5	95.8	85.7	92.6	88.9	95.1	96.5	93.6	97.8	94.3	94.9
2.0	99.3	95.7	98.0	97.0	97.9	99.3	98.6	99.3	98.4	100.0
2.5	100.0	98.6	99.3	99.3	99.3	100.0	99.3	100.0	99.5	100.0
>2.5	100.0	100.0	100.0	100.0	100.0	100.0	100.0	100.0	100.0	100.0

150-250 Particles counted for each sample.

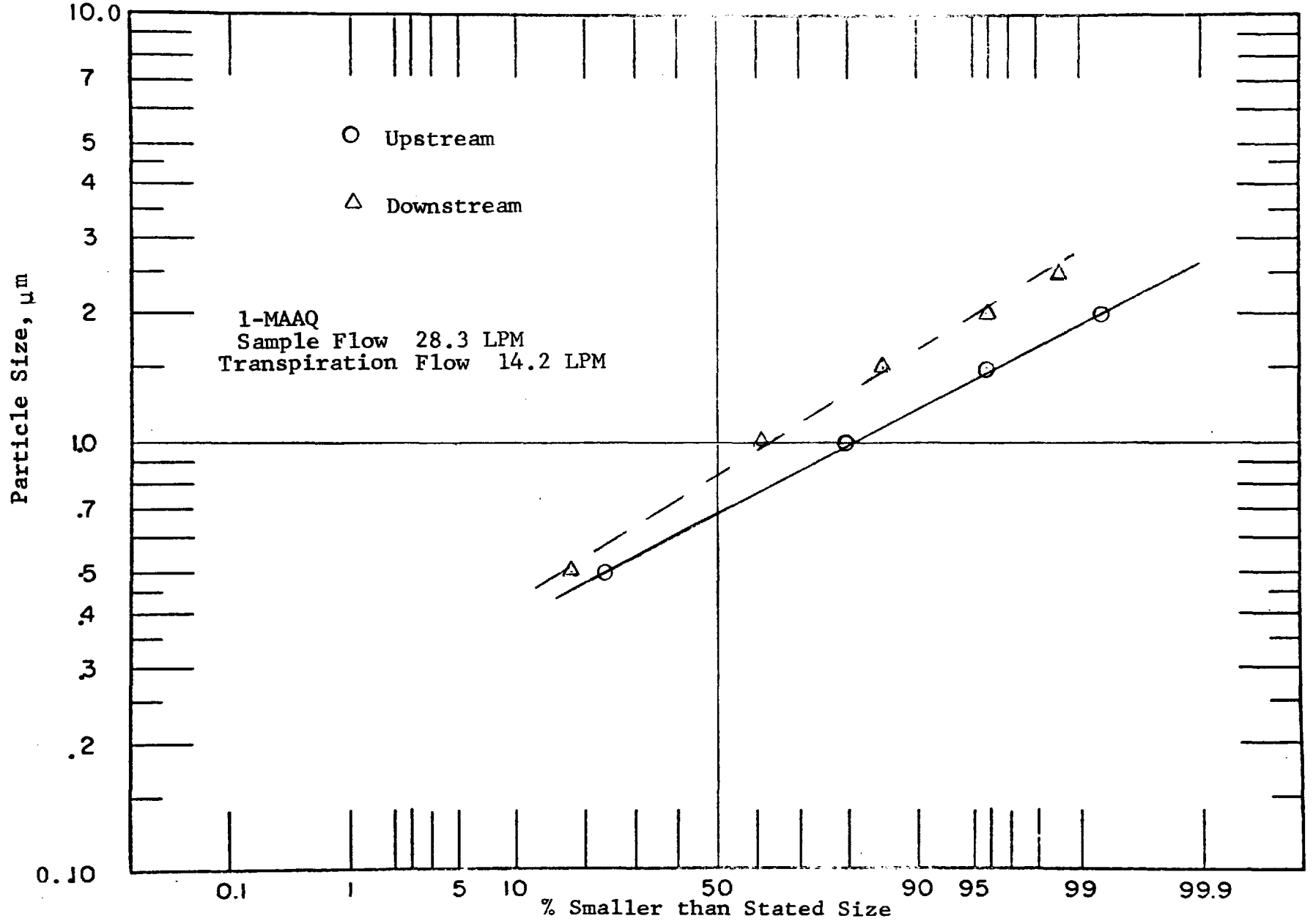

Figure 58. Size Distributions for Test M-1

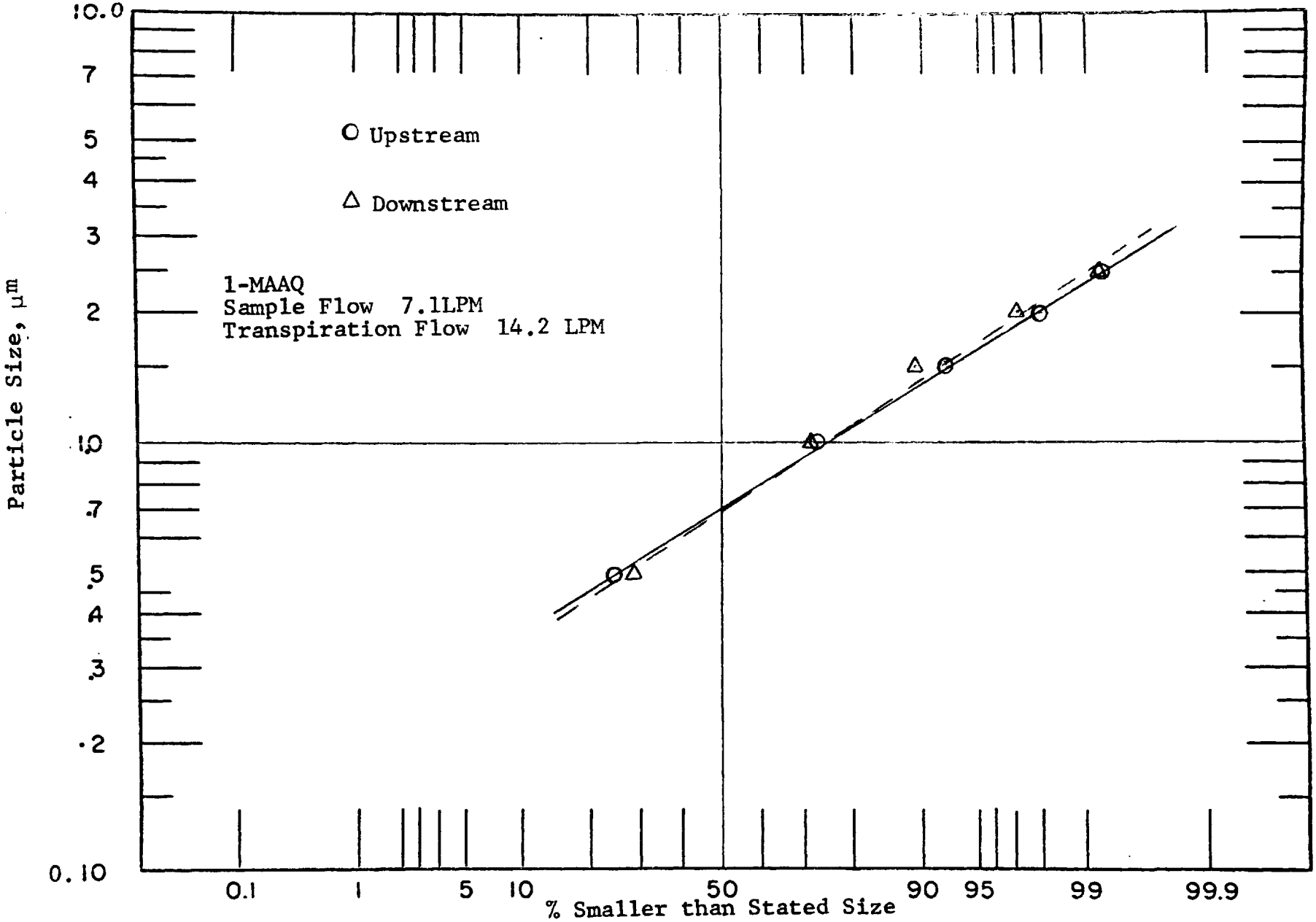

Figure 59. Size Distributions for Test M-2

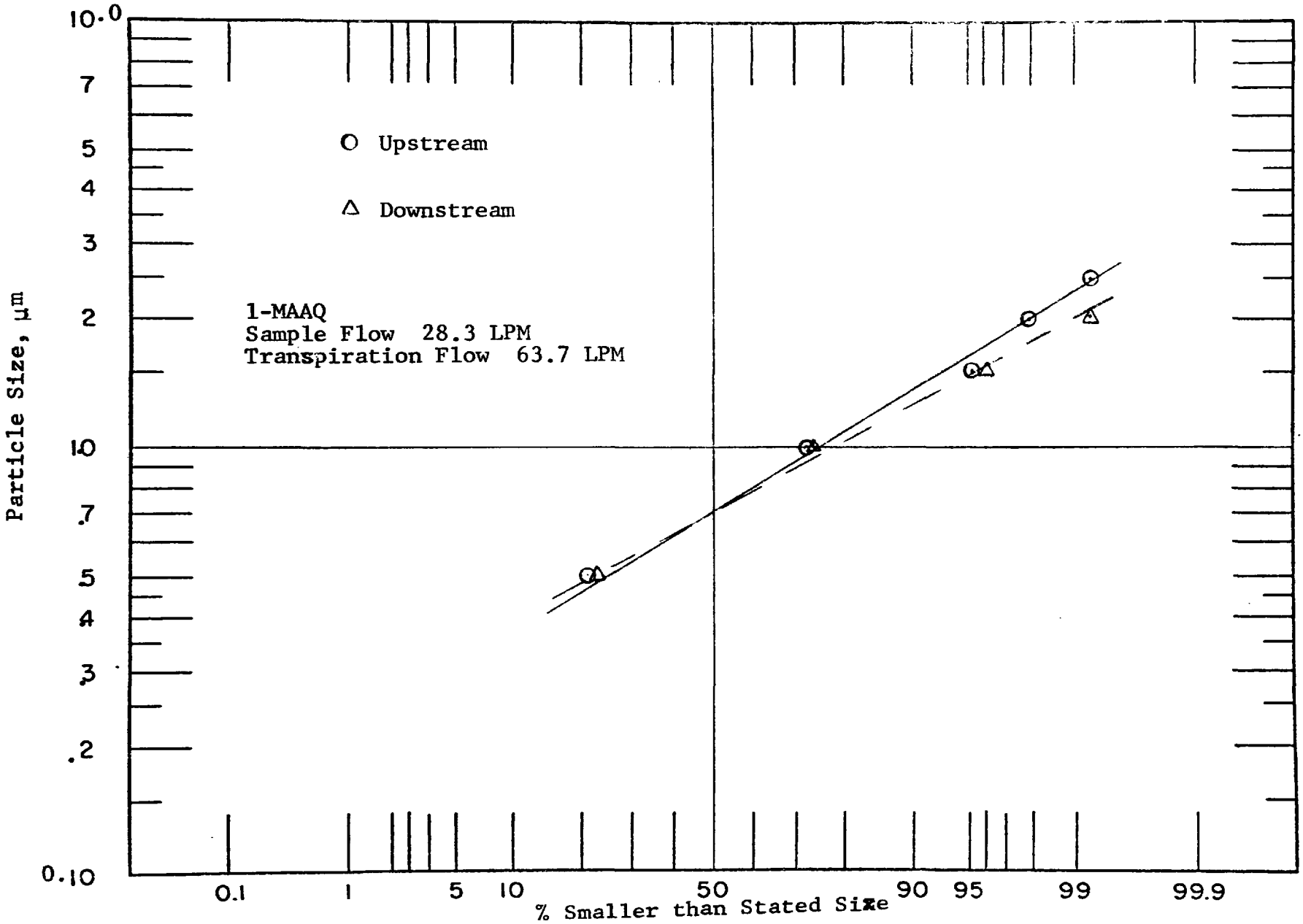

Figure 60 Size Distributions for Test M-3

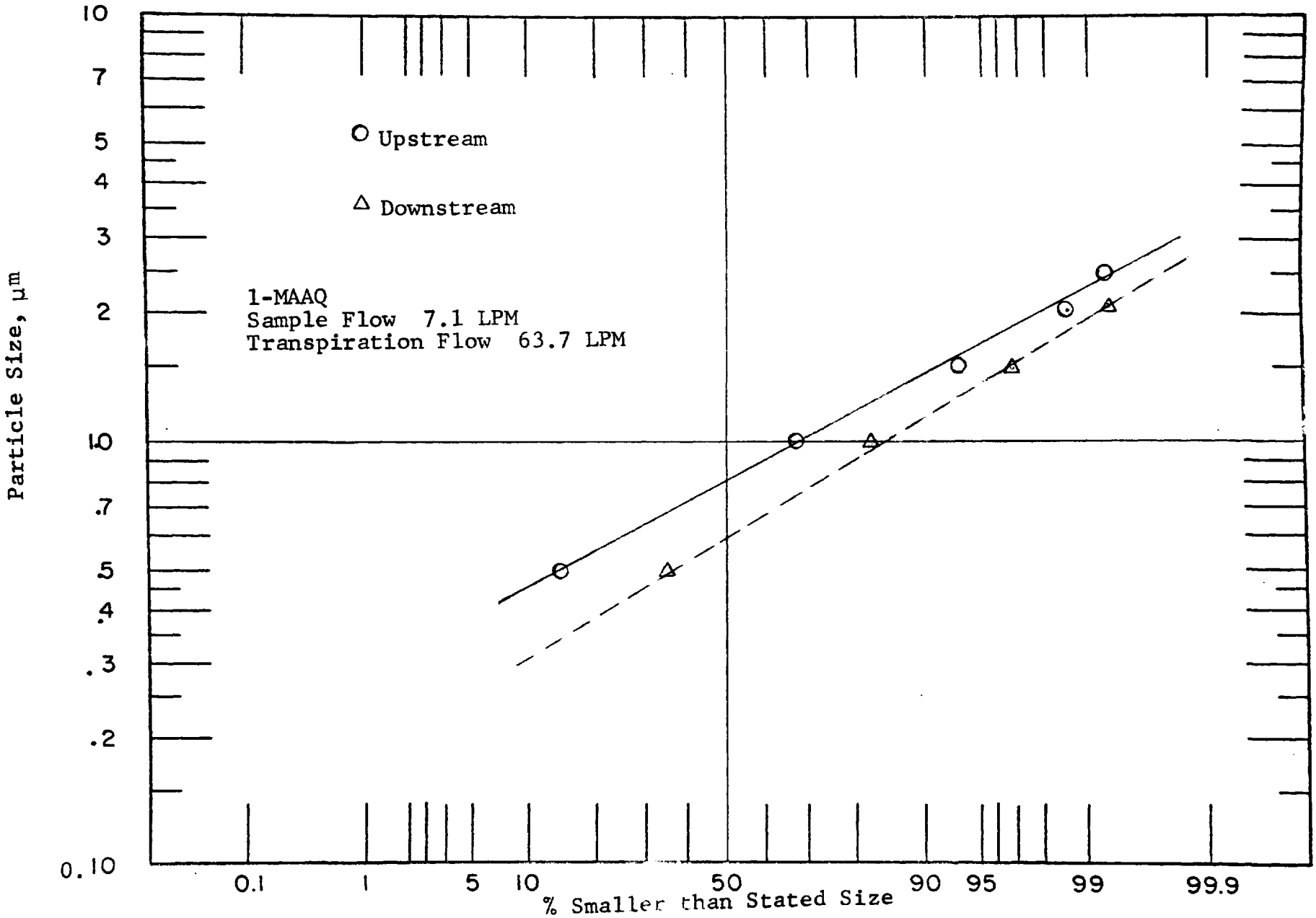

Figure 61. Size Distributions for Test M-4

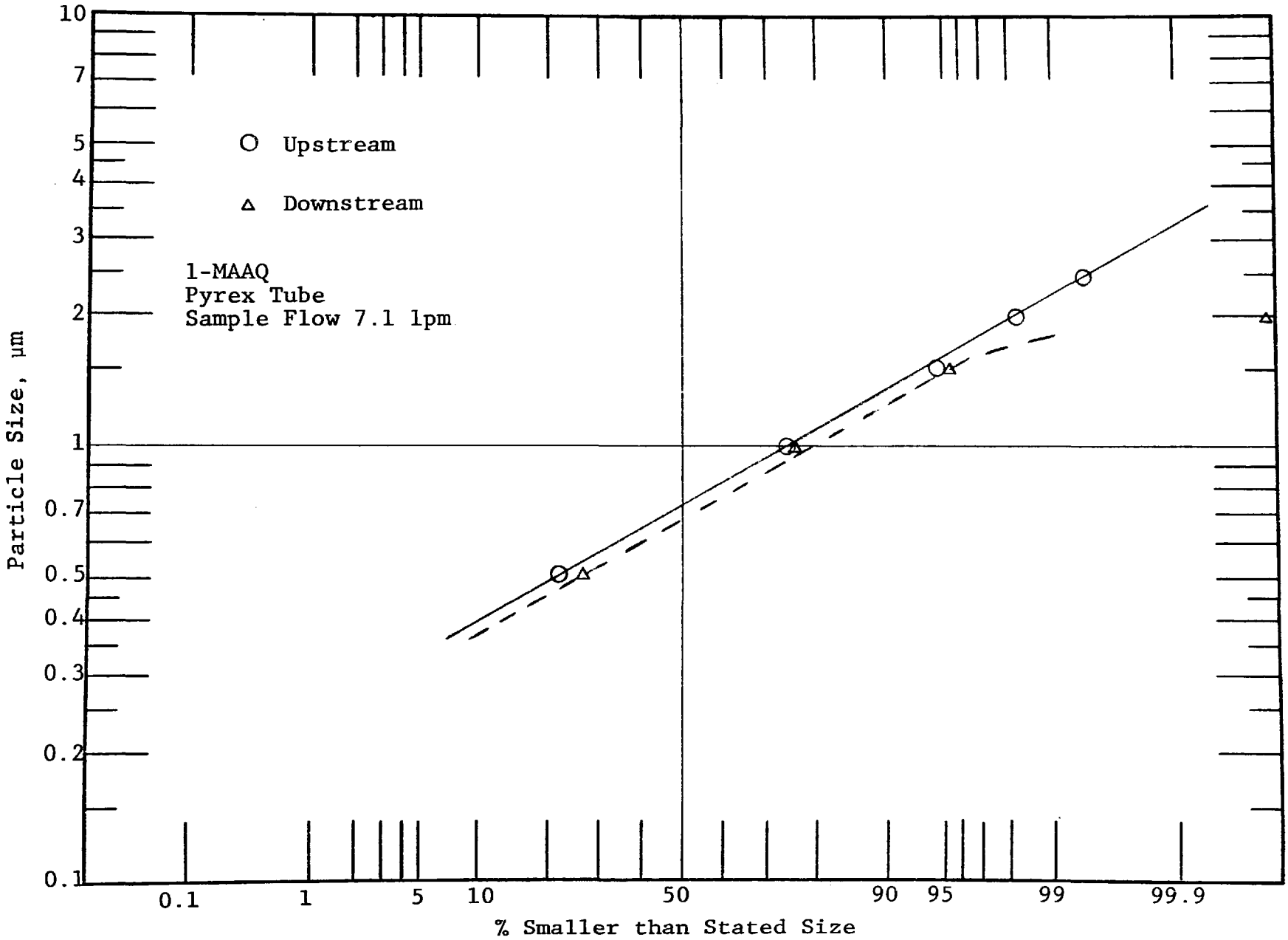
10
7
5
4
3
2
1
0.7
0.5
0.4
0.3
0.2
0.1
Particle Size, µm
O Upstream
Δ Downstream
1-MAAQ
Pyrex Tube
Sample Flow 7.1 lpm
0.1
1
5
10
50
90
95
99
99.9
% Smaller than Stated Size

Table 11. SIZE DISTRIBUTION PARAMETERS FOR KCl AEROSOL

Test No.	Nominal Size Range Covered (μm)	Sample Flow Rate (lpm)	Transpiration Flow Rate (lpm)	V Transp / V Sample	Upstream GNMD μm	Upstream σ_g	Downstream GNMD μm	Downstream σ_g
K-5	0.01-1.0	7.1	0	0	0.045	2.8	0.045	2.8
K-1	0.01-0.1	7.1	14.2	0.0034	0.021	2.0	0.025	2.0
K-3	0.01-1.0	7.1	14.2	0.0034	0.016	2.5	0.016	2.5
K-2	0.01-1.0	28.3	14.2	0.0009	0.045	2.6	0.06	2.2
K-4	0.01-1.0	28.3	14.2	0.0009	0.045	2.6	0.06	2.2

Table 12. SIZE DISTRIBUTION PARAMETERS FOR 1-MAAQ AEROSOL

Test No.	Nominal Size Range Covered (μm)	Sample Flow Rate (lpm)	Transpiration Flow Rate (lpm)	$\frac{V\ Transp}{V\ Sample}$	Upstream GNMD μm	Upstream σ_g	Downstream GNMD μm	Downstream σ_g
M-5	0.5-2.25	7.1	0	0	0.7	1.7	0.7	1.7
M-2	0.5-2.25	7.1	14.2	0.0034	0.72	1.8	6.72	1.8
M-4	0.5-2.25	7.1	63.7	0.016	0.8	1.6	0.6	1.6
M-1	0.5-2.25	28.3	14.2	0.0009	0.63	1.6	0.82	1.7
M-3	0.5-2.25	28.3	63.7	0.0039	0.72	1.7	0.72	1.7

62 shows that the particles above 2 μm were lost. Even though this end of the plot represents a very small number, absence of the particles larger than 2 μm was obvious during the microscopic examination.

This suggests that particles above 2.0 μm size are deposited by gravity at the downstream end of the pyrex tube.

These tests indicate that for particles below 2 μm, the pyrex tube and the porous sampling interface are both effective. These results are consistent with the Phase I results which show that the maximum deposition of 1.6 μm 1-MAAQ on the mass basis is less than 3% in all the cases.

7.3 Tests with Uranine and Flyash Aerosols

The size parameters for uranine and flyash are presented together in Table 13 as the nominal size range and test conditions were identical.

The effect of gravitational deposition on the particle size distribution during the transport through the pyrex probe (Test U-5, F-5) is seen from Figures 42, 47, and 55. The mean particle size has decreased. The standard deviation, σ_g, is not significantly affected. As expected, the deposition of larger particles is more severe for the heavier flyash. In tests U-1 and F-1, the standard deviation has not changed significantly and the shape of the upstream and downstream curves are similar. The mean particle size has increased downstream. In tests U-3 and F-3, the same trend is observed. However, the standard deviation for F-3 has gone up significantly. In Test U-4, the mean particle size has increased, and the shape of the distribution has been significantly changed (Figures 41 and 46). At the two ends of the distribution, the curves are parallel, but in the midsection a skewness is observed in the curve for the downstream sample.

Table 13. SIZE DISTRIBUTION PARAMETERS FOR TESTS WITH URANINE AND FLYASH AEROSOLS

Test No.	Nominal Size Range Covered (μm)	Sample Flow Rate (lpm)	Transpiration Flow Rate (lpm)	V Transp. / V Sample	Upstream GNMD μm	Upstream σ_g	Downstream GNMD μm	Downstream σ_g
U-5	Uranine; 5-50	7.1	0	0	9.5	1.8	8.5	1.6
U-1	Uranine; 5-50	7.1	141.5	0.034	10.0	1.9	12.0	2.1
U-3	Uranine; 5-50	7.1	283.0	0.069	11.0	1.8	13.0	1.8
U-4	Uranine; 5-50	28.3	14.2	0.0009	10.5	1.7	14.5	2.0
U-2	Uranine; 5-50	28.3	141.5	0.009	10.0	1.6	12.5	1.8
F-5	Flyash; 5-50	7.1	0	0	8.0	1.7	6.6	1.5
F-1	Flyash; 5-50	7.1	141.5	0.034	8.0	1.8	9.6	2.0
F-3	Flyash; 5-50	7.1	283.0	0.069	7.4	1.4	9.3	2.4
F-4	Flyash; 5-50	28.3	14.2	0.0009	9.0	1.7	8.3	2.5
F-2	Flyash; 5-50	28.3	141.5	0.009	8.0	1.4	9.1	2.2

For the flyash, in the corresponding test F-4, the skewness is even more marked. Particles around 10 μm are being lost in the flow through the porous sampling interface at a higher rate than the very large particles. This trend is observed for tests U-2 and F-2. The sample flow rate is high in all those tests which showed the skewness. The transpiration flow rates were moderate to moderately high. This effect is believed to be due to the microturbulence at the inlet of the porous probe where the sample and transpiration flow meet. A qualitative justification of this reasoning was obtained in test U-3. In a crude test, the amount of deposit in the first 16 cm of the porous probe was found to be approximately 40-50% of the total deposit in the tube.

Large particles, once they are entrained, are disturbed least by the microturbulence while the smaller particles are carried by the eddies and are probably deposited on the walls.

8. CONCLUSIONS

In Phase I, the quantitative mass transport of the aerosols was investigated. The following conclusions were reached.

(1) Of the four factors investigated, particle concentration has the least effect on particle deposition. There was a slight increase in deposition with an increase in concentration, but this effect is marginally significant statistically.

(2) Deposition depends strongly on particle size. Deposition was quite low for both 0.05 μm and 1.6 μm particles, but 50 μm particles have a substantially higher deposition rate at intermediate levels of transpiration flow rate, sample flow rate, and particle concentration: between 5 and 10% as contrasted with the range 0.1 to 0.5% for the smaller particles.

(3) Sample flow rate and transpiration flow rate have a degree of parallelism in their general effect on reduction of deposition with increase in flow. There is an interaction between the two terms and an interaction of each with particle size.

(4) The simple effect of increasing sample flow rate, holding other factors at intermediate settings, is to decrease the deposition.

(5) The main effect of increasing sample flow rate, holding other factors at intermediate levels, is to reduce the fraction of the aerosol particle mass that is deposited on the walls of the sampling probe. At all levels of sample flow rate tested deposition of large particles (~ 50 μm) is reduced when the transpiration flow rate is increased; and the reduction is greatest at the low sample flow rate. For example, deposition of 50 μm particles from a high

concentration aerosol sample at 7.1 lpm (0.25 cfm) is sharply reduced with 283 lpm (10 cfm) of transpiration air from more than 99.9% to about 5%. At the higher levels of sample flow rate the percentage deposition of large particles is brought considerably lower than at low sample flow rate as the transpiration flow rate increases from zero to 283 lpm (10 cfm), but the reference values at zero transpiration flow rate are also much lower. At the low sample flow rate the porous tube with increasing rates of transpiration flow reduces deposition for all particle sizes tested. At the intermediate sample flow rate, transpiration air continued to reduce deposition of medium sized particles (~ 0.05 μm); this reduced effect is of little practical importance due to the low percentage deposition of the small and intermediate particles. At the high sample flow rate, the range of variation of deposition is much reduced with a slight increase in deposition of the intermediate, and especially small, particles with increasing transpiration air, but, again, the magnitude of deposition is only of the order of 0.1 to 5%.

(6) Tests with the 0.05 and 1.6 μm aerosols indicate that only 14.2 lpm (0.5 cfm) of transpiration air is needed to reduce deposition to virtually insignificant levels on the order of 0.2% or less.

(7) The porous probe experiments were clearly definitive in demonstrating the significant reduction in loss of aerosol mass through the use of transpiration air. At 7.1-14.2 lpm (0.25-0.50 cfm) of sample volume deposition of 50 μm particles ranged from close to 100% at 0-14.2 lpm (0-0.5 cfm) of transpiration air to less than 0.1% a5 283 lpm (10 cfm) of transpiration air.

(8) A redesign of the probe inlet is recommended to make the porous sampling probe even more effective for large particles at reduced transpiration air flow rates. If more of the transpiration air is introduced at the very

inlet of the porous probe, deposition of large particles near the entrance, at the 7.1-14.2 lpm (0.25-0.50 cfm) sample flow rates, will be greatly reduced at modest transpiration air flow rates. Such a design should establish a clean air sheath in a shorter distance and should also reduce deposition of the less problematical intermediate and small aerosol particles.

The conditions for Phase II were chosen on the basis of results of Phase I experiments. Changes in the size distribution of aerosols transported through the sampling interface ranging from 0.01-50 μm were investigated using conditions that gave good transport efficiencies on the mass basis. For comparison, a set of tests with a 1.25 cm (½ in.) diameter, pyrex tube was also conducted. The following conclusions were reached.

(1) For the particles below 2 μm, the pyrex tube and the porous sampling interface were equally effective.

(2) For particles around 2-2.5 μm, the porous tube was more effective than the pyrex tube.

(3) For the 5-50 μm particles, the pyrex tube data showed that the mean particle size decreased. With the porous tube the mean size generally increased.

(4) At low sample flow rate (7.1 lpm) the size distribution was similar in shape. At the higher sample rate (28.3 lpm) the size distribution of the aerosol transported through the porous probe was skewed. Particles around 10 μm in size were deposited to a greater extent than larger particles. This was believed to be due to the microturbulence at the entrance to the porous probe.

(5) The porous probe was found to be effective in preserving the size distribution of the aerosol during transport in addition to the capability of preserving mass as

demonstrated in Phase I. For particles up to a few micrometers in size the flow rates had little effect on the size distribution. For the particles such as flyash in the range of 5-50 μm, low sample flow rate and a transpiration flow rate high enough to preserve mass are most effective for their total quantitative transport.

(6) The feasibility of the porous probe concept has been established under this contract. Design of a quantitative sampling interface is now possible due to the information generated under this program. Factors such as exposures to high temperatures and corrosive substance expected in the actual stack sampling in fuel must be considered for the design of the sampling interface prototype.

Appendix A

AN ELECTRIC MOBILITY METHOD OF SIZING 0.01 to 1.0 μm POLYDISPERSE AEROSOLS

AN ELECTRIC MOBILITY METHOD OF SIZING 0.01 to 1.0 μm POLYDISPERSE AEROSOLS

Of the indirect methods for aerosol size analysis, Whitby and Clark's (A1) electric mobility analysis method with unipolar charging has poor resolution above 0.3 μm. Knutson's electric mobility method (A2), with bipolar charging, is limited to near monodisperse aerosols. Kudo and Takahashi (A3) have explored another mobility analysis method with bipolar charging, but its potential resolving power seems limited.

In the following, another variation of the electric mobility method for aerosol size analysis is described. Bipolar charging is used. This method applies to polydisperse aerosols, i.e., geometric standard deviation ≥ 1.2. It is suited for automation, since no manual microscopy is required. No empirical calibration is necessary. As a penalty, the method requires a complicated and lengthy calculation to recover the size distribution from the raw data. These are best carried out on a remote computer terminal.

APPARATUS

The apparatus required for this method of aerosol size determination are:

1. A concentric cylinder electric mobility analyzer described by Knutson (A2). This type has two inlet air streams and two outlet air streams.

2. A bipolar charging device (charge neutralizer).

3. A suitable aerosol sensing device. This device must give a response proportional to either the number concentration charge, concentration or mass concentration.

4. A precision high voltage power supply. A sketch of the mobility analyzer is given in Figure A1. Condensation nuclei counter (number measurement) was used as the aerosol sensing device.

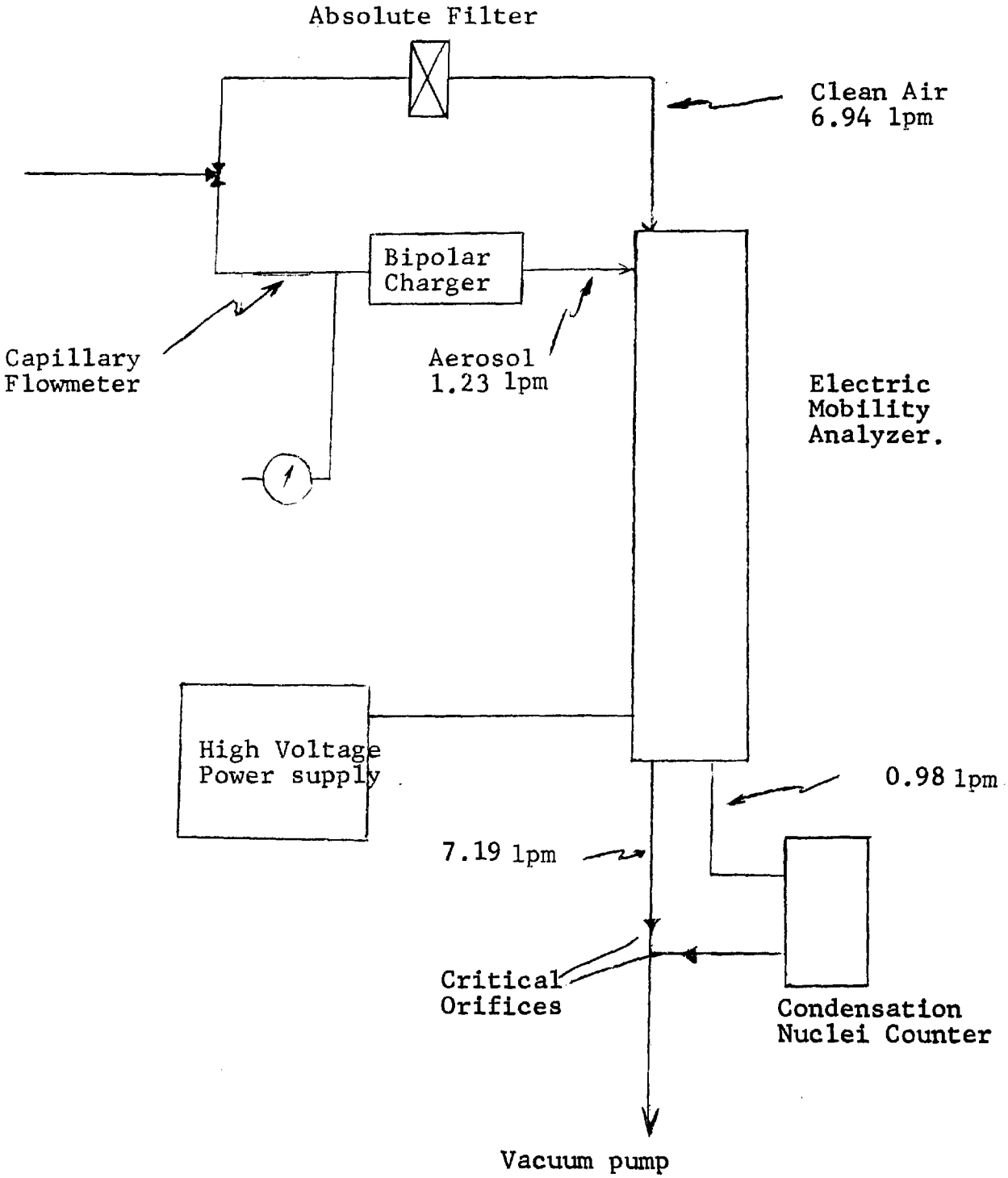

Figure A-1: System for Measuring Aerosol Size in the Range 0.01-1.0 Microns

OPERATING PROCEDURE

The aerosol sample is continuously drawn through the analyzer by the vacuum pump (Figure A1). The sample is split into two streams. One stream flows through a capillary flow meter and a bipolar charger for neutralization of charges on the aerosol.. The other part of the sample stream is passed through a glass fiber filter. This acts as a sheath for the first sample stream in the annulus between the two coaxial cylinders. A voltage differential between the two cylinders is maintained with the help of the high voltage power supply. At a given voltage setting, a stream of aerosol particles having equal electric mobility is removed through a series of holes at the other end of the analyzer. The particle concentration of this stream is measured by the nuclei counter (Gardner Associates; Schenectady, N.Y.). This procedure is repeated at various voltage settings ranging from 0-10,000 volts.

THEORY AND DATA REDUCTION

The starting point for the theory of this method of aerosol size determination is the transfer function, Ω, for the mobility analyzer. This has been given by Knutson (A3). The transfer function is most conveniently presented in graphical form, with the product Z_pV as absissa and Ω, as ordinate, as in Figure A2. Ω is the probability that a particle with electric mobility Z_p will reach the mobility analyzer sampling outlet flow, given that the voltage applied to the center rod is V. Values for certain flow rates are also needed, as are certain geometric dimensions. These are indicated in Figure A2.

The number of particles entering the mobility analyzer in unit time is C_aq_a, where C_a is the aerosol concentration rate. Of these, a fraction $f(d_p)dd_p$ have size in the range d_p to $d_p + dd_p$. f is the unknown size distribution function.

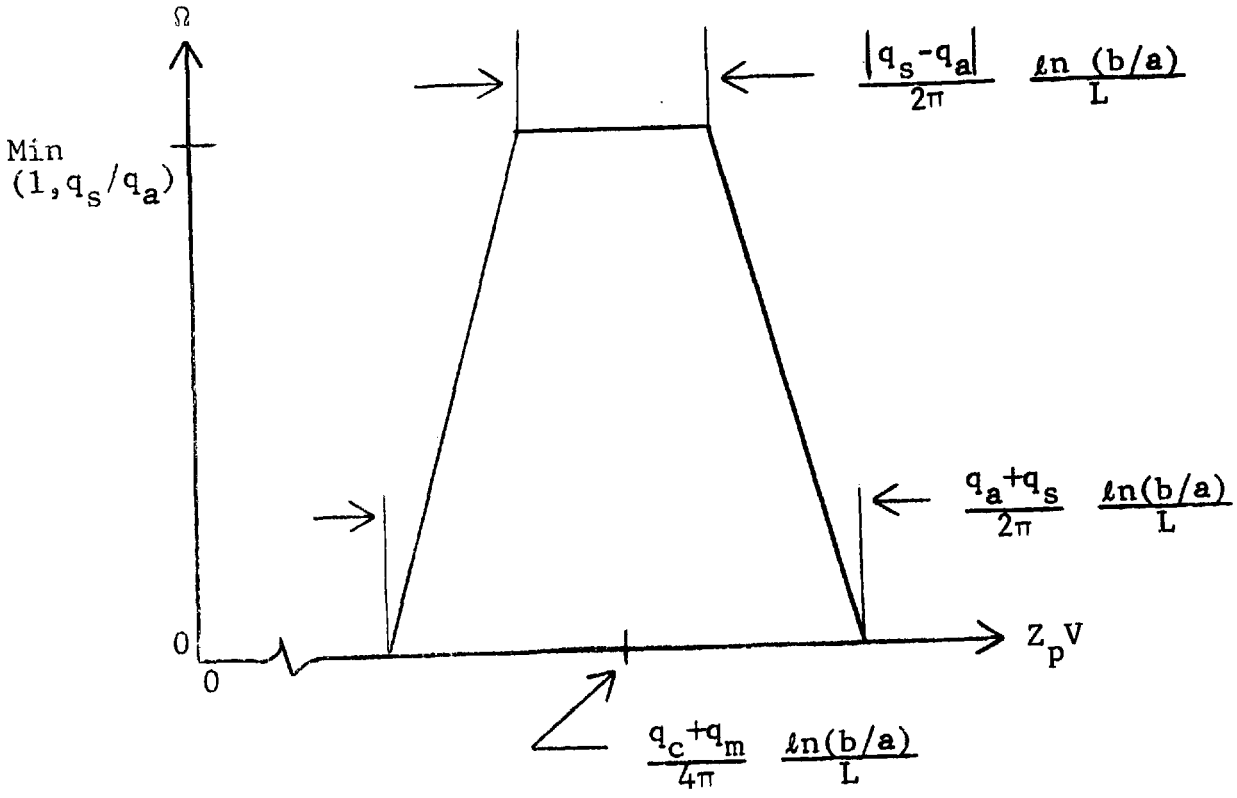

Mobility Analyzer Flow Rates:

q_c = clean air inlet

q_a = aerosol inlet

q_m = main outlet

q_s = sampling outlet

Mobility Analyzer Dimensions:

b = I.D. of outer cylinder

a = O.D. of inner cylinder

L = distance between aerosol inlet and sampling outlet

Figure A2

TRANSFER FUNCTION FOR THE MOBILITY ANALYZER

In turn, the fraction carrying k elementary charges is $p(k;d_p)$, which is assumed known. Thus,

$$\begin{pmatrix}\text{Number of particle of size } d_p \text{ to } d_p + dd_p, \text{ with charge } k, \text{ entering in unit time}\end{pmatrix} = \left(C_a q_a\right)\left(p(k;d_p)\right) f(d_p)dd_p \quad \text{(A1)}$$

The electric mobility of these particles is $k \cdot Z_1(d_p)$, where $Z_1(d_p)$ is the mobility of a singly charged particle of diameter d_p.

Of the number of particles defined in Equation A1, a fraction, $\Omega(k \cdot Z_1 \cdot V)$ reaches the sample outlet of the mobility analyzer and is carried out with the sample outlet flow. The total number which reach the sample outlet in unit time is found by integrating over d_p and summing over k. Thus,

$$C_s(V)q_s = C_a q_a \sum_{k=1}^{\infty} \int_0^{\infty} \Omega(k \cdot Z_1 \cdot V)p(k;d_p)f(d_p)dd_p \quad \text{(A2)}$$

where $C_s(V)$ is the concentration of the sampling outlet stream (volumetric flow = q_s) for a voltage setting V. The k-sum is taken over the positive k values only, on the assumption that V is negative. The opposite case is handled similarly.

The quantities q_s, q_a, Ω, and p in Equation A2 are known. In addition, $C_s(V)$ may be determined by experiment, i.e., by measuring C_s for several discrete values of V. The quantity C_a serves only as a normalizing factor. Hence, in principle, Equation A2 can be solved for the size distribution f. A convenient way of obtaining this solution is described next.

For each integral in Equation A2, change variable from d_p to x, where $x = k \cdot Z_1 \cdot V$ and k and V are held constant.

$$Z_1(d_p) = \frac{x}{kV}$$

$$dd_p = \frac{dx}{kVZ_1'(d_p)} \tag{A3}$$

The first of Equations A3 implicitly defines d_p in terms of x. The second, in which Z_1' is the derivative of Z_1, gives the relationship between dd_p and dx. The integrals in Equation A2 become

$$\int_0^\infty \Omega(x)p(k;d_p)f(d_p)\ \frac{dx}{kVZ_1'} \tag{A4}$$

Figure A2 shows that if q_s and q_a are small in comparison with q_c and q_m, the function Ω is non-zero only near $x = x^* = (q_c + q_m) \cdot \ell n(b/a)/4\pi L$. Hence, by the mean value theorem for integrals, integral A4 may be approximated by

$$\frac{p(k;d_p^*)}{kVZ_1^*}f(d_p^*)\int_0^\infty \Omega(x)dx = \frac{p(k;d_p^*)}{dVZ_1'^*}\ f(d_p^*)\ \frac{q_s}{2\pi} =$$

$$\frac{p(k;d_p^*)}{p(1;d_p^*)}\ \frac{g(d_p^*)}{C_a q_a} \tag{A5}$$

In Equation A5, d_p^* is the particle size defined implicitly by Equation A3, i.e. by

$$Z_1(d_p^*) = \frac{x^*}{kV} = \frac{(q_m + q_c)\ell n(b/a)}{4\pi kVL} \tag{A6}$$

$Z_1'^*$ is the corresponding value of Z_1'. The function $g(d_p^*)$,

$$g(d_p^*) = C_a q_a q_s\ \frac{p(1;d_p^*)f(d_p^*)}{2\pi kZ_1'^* V} \tag{A7}$$

has been introduced for later notational convenience.

With the approximation in Equation A5, Equation A2 becomes

$$C_s(V)q_s = \sum_{k=1}^{\infty} \frac{p(k;d_p^*)}{p(1;d_p^*)}\, g(d_p^*) \qquad \text{(A8)}$$

where d_p^* depends on both k and V. For a given V, the concentration C_s receives contributions from several discrete particle sizes, the size increasing with k. The key to solving Equation A8 for the corresponding discrete values of g lies in a particular choice of the sequence of voltage settings, V, for which C_s is measured. The first setting, V_1, must be so large that only singly charged particles contribute significantly to C_s. The remaining members of the sequence (V_2, V_3, V_4, ...) must form a descending geometric progression:

$$V_{i+1} = V_i/r$$
$$\text{with } r = \sqrt[23]{10} \qquad \text{(A9)}$$

This sequence has the property that

$$kV_i = \begin{cases} 0.9925\ V_{i-7} & \text{for } k = 2 \\ 0.9997\ V_{i-11} & \text{for } k = 3 \\ 0.9847\ V_{i-14} & \text{for } k = 4 \\ 1.0077\ V_{i-16} & \text{for } k = 5 \\ 0.9898\ V_{i-18} & \text{for } k = 6 \end{cases}$$

To good approximation, the numerical coefficients of the V's on the right may be set equal to unity. Thus, the sequence $2V_i$ duplicates the sequence V_i, except that it is shifted by seven places. Similar remarks apply to the sequences $3V_i$, $4V_i$, $5V_i$, and $6V_i$.

Equation A8 may now be solved for $g(d_p^*)$ as follows. Let $d_p^*(1)$, $d_p^*(2)$, $d_p^*(3)$, ... be the sequence of values

generated from the sequence V_1, V_2, V_3, ... by Equation A6 with k = 1. Truncate the sum in Equation A8 after the sixth term. Then

$$C_s(V_i)q_s = g\{d_p^*(i-18)\} + \frac{p\{2;d_p^*(i-7)\}}{p\{1;d_p^*(i-7)\}} g\{d_p^*(i-7)\} + \ldots + \frac{p\{6;d_p^*(i-18)\}}{p\{1;d_p^*(i-18)\}} g\{d_p^*(i-18)\} \qquad \text{(A11)}$$

This equation may be solved recursively for the $g\{d_p^*(i)\}$, recalling that $g\{d_p^*(i)\} = 0$ for $i < 1$, by the choice of the first voltage setting, V_1. With these values for the g's, the values $C_a f\{d_p^*(i)\}$ may be recovered from Equation A7. Finally, C_a is determined by normalizing $f(d_p^*)$.

This discussion of the theory of the method has assumed that the aerosol sensor measures number concentration. If a mass sensor is used, it is only necessary to interpret C_a and $f(d_p)$ as the mass-by-diameter distribution. If a charge sensor is used, it is necessary to insert the factor Ke, where e is the elementary unit of charge, within the summation sign in Equation A2 and carry it through the analysis. The quantity $C_s(V)q_s$ should then be interpreted as the electric current due to the sampling outlet flow.

A computer program for the size distribution calculations was developed. The output is plotted in terms of the derivative of the number concentration of particles with respect to the log of particle size. The symmetrical nature of the curve represents a log-normal distribution. The GNMD is given by the value corresponding to the peak of the curve. The geometric standard derivative is given by ratio of the size corresponding to the 60% of the peak value and the GNMD.

REFERENCES

A1. K.T. Whitby and W.E. Clark, "Electric Aerosol Particle Counting and Size Distribution Measuring System for the 0.015 to 1 μ Size Range, Tellus XVIII, 573-86 (1966).

A2. E.O. Knutson, The Distribution of Electric Charge Among the Particles of an Artificially Charged Aerosol, Ph.D. Thesis, University of Minnesota, Minneapolis, Minn. (1971).

A3. A. Kudo and K. Takahashi, "A Method of Determining Aerosol Particle Size Applying Boltzmann's Law," Atmos. Envir., 6 (8), 543-50 (1972).

TECHNICAL REPORT DATA
(Please read Instructions on the reverse before completing)

1. REPORT NO.	2.	3. RECIPIENT'S ACCESSION NO.
EPA-650/2-74-016		

4. TITLE AND SUBTITLE
Sampling Interface for Quantitative Transport of Aerosols

5. REPORT DATE
December, 1973

6. PERFORMING ORGANIZATION CODE

7. AUTHOR(S)
Madhav B. Ranade

8. PERFORMING ORGANIZATION REPORT NO.

9. PERFORMING ORGANIZATION NAME AND ADDRESS
IIT Research Institute
10 West 35th Street
Chicago, Illinois 60617

10. PROGRAM ELEMENT NO.
1AA010

11. CONTRACT/GRANT NO.
68-02-05-79

12. SPONSORING AGENCY NAME AND ADDRESS
EPA, Chemistry & Physics Laboratory
National Environmental Research Center
Research Triangle Park, N.C. 27711

13. TYPE OF REPORT AND PERIOD COVERED
Final Report

14. SPONSORING AGENCY CODE

15. SUPPLEMENTARY NOTES

16. ABSTRACT

A sampling probe was designed, fabricated, and evaluated for quantitative transport of aerosols through a conduit from a source to a sensor. The probe consists of a porous metal tube encased in a manifold through which transpiration air was passed inward to provide a moving clean air sheath that minimized particle deposition on the walls. In Phase I, the quantitative mass transport of aerosols was investigated, and in Phase II, the preservation of size distribution of the transported aerosol was studied. The 178 cm. (70 in.) long by 1.27 cm (1/2 in.) ID probe required only 14.2 lpm (0.5cfm) of transpiration air to virtually eliminate deposition of particles in the 0.05 to 15 μm size range. Particles as large as 70 μm required as much as 283 lpm (10 cfm) to prevent deposition losses at low sample flow rates. A statistical analysis of the data conclusively demonstrates the effectiveness of the porous probe sampling concept. Tests at selected conditions show that the porous probe is effective in the preservation of size distribution.

Optimization of the sample and transpiration flow ration is necessary for a given size range to obtain the most effective use of the porous probe concept.

17. KEY WORDS AND DOCUMENT ANALYSIS

a. DESCRIPTORS	b. IDENTIFIERS/OPEN ENDED TERMS	c. COSATI Field/Group
Sampling Probe Sampling Interface Aerosol Transport Quantitative Transport of Aerosol Boundary layer probe	Pollution Monitoring Sampling Aerosols Stack Monitoring Stationary Source Sampling	

18. DISTRIBUTION STATEMENT	19. SECURITY CLASS *(This Report)*	21. NO. OF PAGES
Release Unlimited	Unclassified	141
	20. SECURITY CLASS *(This page)*	22. PRICE
	Unclassified	

EPA Form 2220-1 (9-73)